Universität Hamburg
DER FORSCHUNG | DER LEHRE | DER BILDUNG

BNITM
Bernhard-Nocht-Institut für Tropenmedizin

Molecular characterization of interactions between bunyavirus L protein and host proteins

Dissertation

zur
Erlangung des akademischen Grades
Doktorin der Naturwissenschaften (Dr. rer. nat.)

Vorgelegt dem Fachbereich Biologie
der Universität Hamburg

Angefertigt in der Abteilung für Virologie des
Bernhard-Nocht-Instituts für Tropenmedizin, Hamburg

von

Selina Karoline Krüger

Hamburg, Mai 2025

Die vorliegende Arbeit wurde im Zeitraum von Februar 2022 bis Mai 2025 in der Abteilung für Virologie des Bernhard-Nocht-Instituts für Tropenmedizin in Hamburg unter der Leitung von Prof. Dr. med. Stephan Günther in der Arbeitsgruppe von Dr. Maria Rosenthal angefertigt.

Erste Gutachterin:

Prof. Dr. Esther Schnettler
Fachbereich Biologie
Universität Hamburg

Zweite Gutachterin:

Dr. Maria Rosenthal
Abteilung Virologie
Bernhard-Nocht-Institut für Tropenmedizin, Hamburg

Vorsitzender der Prüfungskommission:

Prof. Dr. Tobias Lenz
Fachbereich Biologie
Universität Hamburg

Disputation abgehalten am 11.07.2025

ABSTRACT

The class of *Bunyaviricetes* is a diverse group of viruses with worldwide distribution, including several important human pathogens such as the Lassa virus (LASV), Rift Valley fever Virus, Hantaan virus, and Andes virus. To date, there are no FDA- or EMA-approved vaccines or antiviral treatments available for human use, highlighting the urgent need for effective therapeutic strategies. Despite differences in host tropism, viral transmission, and replication cycle among bunyaviruses, conserved strategies likely include the viral transcription and genome replication in the cytoplasm. These processes are catalyzed by the L protein, which contains the viral polymerase. Bunyavirus L proteins share many similarities regarding their modes of function and overall protein architecture. Although essential for the viral replication cycle, the interactions between the L protein and host proteins remain poorly understood. In this work, potential interactions of the LASV L protein and host proteins were investigated, with a focus on proteins of the DEAD-box (DDX) family. DDX proteins are ATP-dependent RNA helicases that play important roles in both host RNA metabolism and innate immune responses. The results revealed interactions between the LASV L protein and host proteins DDX17, DDX19, DDX24, DDX5, and CCNT1 within the cellular context. DDX17 was identified as a conserved interaction partner of bunyavirus L proteins across several families. Studies with purified proteins revealed the capability of DDX24 and, to some extent, DDX17 to form complexes with the LASV L protein *in vitro*. Viral infection, as well as minireplicon experiments in combination with host factor overexpression, knockdown, and knockout, yielded ambiguous results, though. Therefore, the exact roles of these interactions in the bunyavirus replication cycle remain unclear. This work identified host proteins interacting with the bunyavirus L protein. The established experimental procedures provide an important platform for further studies of the bunyavirus replication cycle and will contribute to the identification of new targets for potentially broad-spectrum antiviral strategies in the future.

KURZZUSAMMENFASSUNG

Die Klasse der *Bunyaviricetes* stellt eine vielfältige Gruppe von Viren mit globaler Verbreitung dar, zu der mehrere bedeutende menschliche Krankheitserreger wie das Lassa-Virus (LASV), das Rifttal-Fieber-Virus, das Hantaan-Virus und das Anden-Virus gehören. Bis heute gibt es keine von der FDA oder EMA zugelassenen Impfstoffe oder antiviralen Medikamente für den Menschen, was den dringenden Bedarf an wirksamen therapeutischen Strategien verdeutlicht. Trotz der Unterschiede im Wirtsspektrum, in den viralen Übertragungswegen und im Replikationszyklus zwischen Bunyaviren sind die virale Transkription und Genomreplikation im Zytoplasma vermutlich konserviert. Diese Prozesse werden durch das L-Protein katalysiert, welches die virale Polymerase enthält. Die L-Proteine der Bunyaviren zeigen viele Gemeinsamkeiten in Bezug auf ihre Funktionsweise und die generelle Proteinarchitektur. Obwohl sie für den viralen Replikationszyklus von essenzieller Bedeutung sind, sind die Interaktionen zwischen dem L-Protein und den Wirtsproteinen bisher nur unzureichend erforscht. In dieser Arbeit wurden mögliche Interaktionen des LASV-L-Proteins mit Wirtsproteinen untersucht, wobei der Schwerpunkt auf Proteinen der DEAD-Box (DDX)-Familie lag. DDX-Proteine sind ATP-abhängige RNA-Helikasen, die sowohl im RNA-Stoffwechsel der Wirtszelle, als auch bei der unspezifischen Immunantwort wichtige Rollen spielen. Die Ergebnisse zeigten Interaktionen zwischen dem LASV-L-Protein und den Wirtsproteinen DDX17, DDX19, DDX24, DDX5 und CCNT1 im zellulären Kontext. DDX17 wurde als konservierter Interaktionspartner von L-Proteinen aus mehreren Bunyavirusfamilien identifiziert. Untersuchungen mit gereinigten Proteinen zeigten, dass DDX24 und in gewissem Umfang auch DDX17 *in vitro* Komplexe mit dem LASV-L-Protein bilden können. Experimente mit Virusinfektionen und Minireplikonsystemen in Kombination mit Überexpression, Knock-down und Knock-out von Wirtsfaktoren ergaben jedoch keine eindeutigen Ergebnisse. Die genauen Rollen dieser Interaktionen im Replikationszyklus der Bunyaviren bleiben daher unklar. In dieser Arbeit wurden Wirtsproteine identifiziert, die mit dem Bunyavirus-L-Protein interagieren. Die etablierten experimentellen Verfahren bilden eine wichtige Grundlage für weitere Studien zum Replikationszyklus der Bunyaviren und werden zur künftigen Identifizierung neuer Angriffspunkte für potenzielle antivirale Breitbandstrategien beitragen.

TABLE OF CONTENT

1 INTRODUCTION

1.1 The class of *Bunyaviricetes*

Bunyaviruses are a highly diverse group of predominantly insect- or rodent-borne viruses with worldwide distribution. The first bunyavirus was isolated from *Aedes* mosquitoes in western Uganda in 1943. It was named Bunyamwera virus (BUNV) after the town in which it was found (1). The discovery of numerous serologically and morphologically similar viruses to BUNV led to the establishment of the family *Bunyaviridae* in 1975 (2). In the following years, the family expanded, and viruses isolated from various hosts were included. To adequately reflect this diversity, the *Bunyaviridae* family was promoted to the order of *Bunyavirales* in 2017 and then to the class *Bunyaviricetes* in 2024 (3,4). The phylogenetic classification of the bunyaviruses based on their RNA-dependent RNA polymerases (RdRps) allowed a division into the orders *Elliovirales* and *Hareavirales*. The class of *Bunyaviricetes* currently consists of two orders, 18 families, 80 genera, and a total of 638 species (5).

Bunyaviruses can infect a wide range of hosts, including mammals, reptiles, arthropods, and plants. The families *Arenaviridae*, *Hantaviridae*, *Nairoviridae*, *Peribunyaviridae*, and *Phenuiviridae* contain pathogenic viruses that can cause severe human disease. Bunyavirus infections are typically zoonoses that are transmitted directly from an animal reservoir to humans or via arthropod vectors. However, human-to-human transmission is possible for many of these viruses.

There are currently no FDA- or EMA-approved vaccines or treatments available for humans against any bunyaviruses or diseases caused by bunyaviruses. Therefore, the WHO R&D Blueprint for Pathogen Prioritization of 2024 highlights the families *Arenaviridae*, *Hantaviridae*, *Nairoviridae*, and *Phenuiviridae* as high risk for public health emergencies of international concern (6).

The families *Arenaviridae*, *Phenuiviridae*, and *Hantaviridae* will be introduced in the following sections. They include some of the most important human pathogenic bunyaviruses in terms of the extent of their geographic distribution, disease severity, and outbreak potential. Representative viruses from each family are described in more detail: Lassa virus (LASV), Tacaribe virus (TCRV), Rift Valley fever virus (RVFV), Hantaan virus (HTNV), and Andes virus (ANDV).

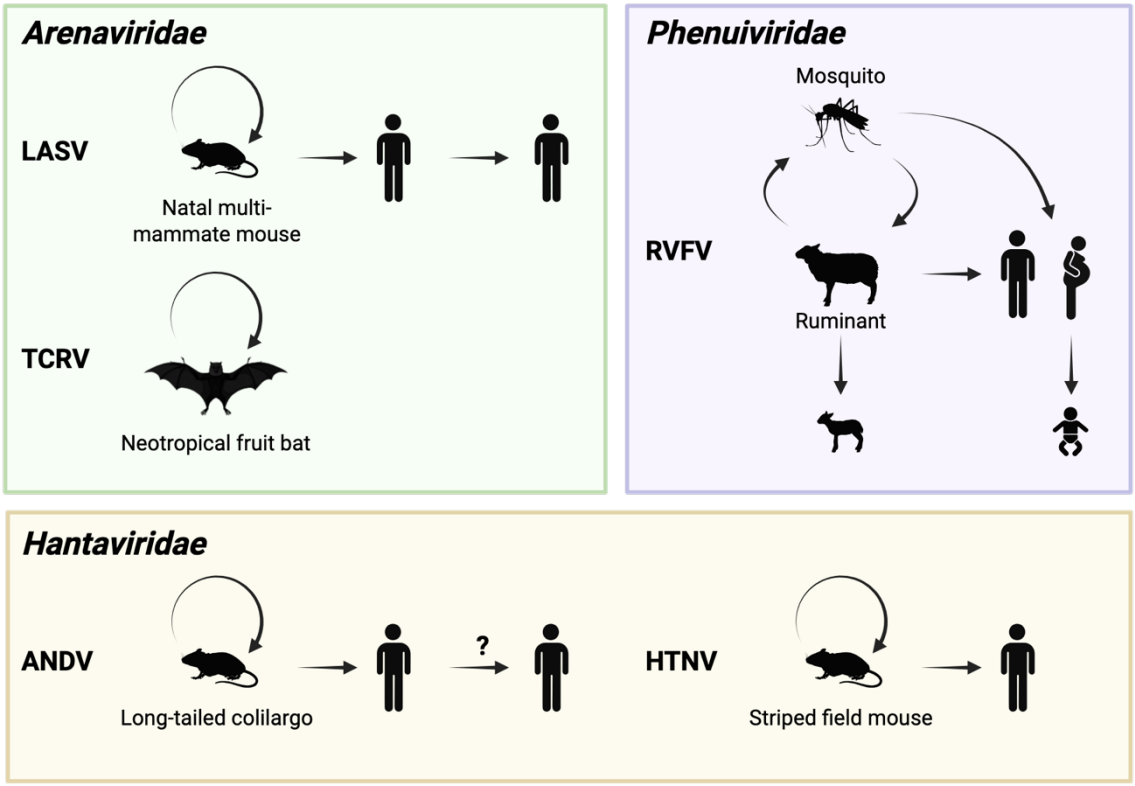

Figure 1: Overview of natural reservoirs, vectors, and transmission routes of selected bunyaviruses. ***Arenaviridae***: LASV: The main natural reservoir is the natal multimammate mouse. Zoonotic spillover leads to human infection. Direct human-to-human transmission, including vertical transmission, has been reported. TCRV: The natural reservoirs are neotropical fruit bats. Natural human infection has not been reported. ***Phenuiviridae***: RVFV circulates between ruminants and mosquitoes. Infection of humans is possible through mosquitoes, but primarily occurs via contact with infected ruminants. Vertical transmission has been reported for humans, ruminants, and mosquitoes. ***Hantaviridae***: ANDV: The natural reservoir is the long-tailed colilargo. Zoonotic spillover leads to human infection. Human-to-human transmission has been reported in rare cases. HTNV: The natural reservoir is the striped field mouse. Zoonotic spillover leads to human infection. Human-to-human transmission has not been reported. Created with BioRender.com.

1.1.1 The *Arenaviridae* family

Viruses of the family *Arenaviridae* belong to the order *Hareavirales* and are distributed worldwide. They infect rodents, bats, shrews, snakes, fish, and humans (7). Arenaviruses that infect mammals, primarily rodents, are classified in the genus *Mammarenavirus*, which is divided geographically, serologically, and phylogenetically into the Old World and New World arenaviruses. Old World arenaviruses are found in Africa, Europe, and Asia, while New World arenaviruses are found in North and South America. An exception is the Old World arenavirus lymphocytic choriomeningitis virus (LCMV), which is distributed worldwide.

Most arenaviruses are not associated with human disease, but some can cause life-threatening viral hemorrhagic fevers, such as the Old World arenaviruses LASV and Lujo virus, and the New World arenaviruses Junín virus (JUNV), Machupo virus (MACV), Guanarito virus, Chapare virus, Whitewater Arroyo virus, and Sabiá virus (8–12). Human infection usually occurs through contact

with infected rodents or their contaminated excretions, but human-to-human transmission has also been documented, mainly for LASV in the nosocomial setting (11,13–15).

LASV is endemic to West Africa, especially Nigeria and the Mano River Union countries (Guinea, Liberia, and Sierra Leone). It is primarily transmitted by its main natural reservoir, the natal multimammate mouse (*Mastomys natalensis*) (16–18). The exact number of annual LASV infections is unknown, but in the past, it has been estimated that 300,000 humans are infected annually, with a mortality rate of 1 – 2 % (9,19). Recent studies based on computer-assisted modeling have estimated nearly 900,000 infections per year (20). The majority of LASV infections cause mild disease and remain undiagnosed (21). However, in up to 20 % of cases, the infection progresses to Lassa fever, an acute viral hemorrhagic fever with symptoms including mucosal hemorrhage, pleural effusion, encephalopathy, organ failure, and terminal shock (22–24).

TCRV was originally isolated from neotropical fruit bats (*Artibeus species*) in Trinidad and Tobago, in contrast to other New World arenaviruses that infect rodents (25,26). To date, no natural human infections with TCRV have been reported. Because of its high phylogenetic and serological similarity to JUNV and MACV, TCRV serves as a model virus for its highly pathogenic relatives (10,27).

1.1.2 The *Phenuiviridae* family

Viruses of the family *Phenuiviridae* belong to the order *Hareavirales* and are distributed worldwide. Phenuiviruses infect a variety of hosts, including arthropods, mammals, birds, crustaceans, and plants (28). Phenuiviruses that infect humans are mostly arthropod-borne viruses, transmitted by ticks, sandflies, or mosquitoes (29). Important human pathogens include the tick-borne severe fever with thrombocytopenia syndrome virus (SFTSV) and Heartland virus, as well as the Toscana virus, which is transmitted by sandflies (30–32).

Another virus of the *Phenuiviridae* family that causes severe disease in humans and animals is the mosquito-borne RVFV. It is endemic in several countries in Africa and the Arabian Peninsula (33). RVFV is transmitted to ruminants such as sheep, goats, and cattle, primarily by mosquitoes of the *Aedes* and *Culex* species (34,35). Infection of humans by mosquitoes is possible, but primarily occurs through contact with infected tissues and fluids from infected livestock (36). Direct human-to-human transmission has not been reported (37). Similarly, direct transmission between animals appears to be rare or non-existent (38). However, vertical transmission has been reported for both humans and animals (39,40). Outbreaks of RVFV in ruminants are associated with numerous deaths and abortions, resulting in significant economic losses (37). Infections in humans mainly result in a self-limiting febrile illness, but in an estimated 1 – 2 % of cases, the infection progresses to severe

disease with symptoms including liver damage, bleeding tendencies, and encephalitis, associated with high mortality (37). Different vaccines are available for the immunization of livestock, but vaccination strategies need further improvement as vaccines are inconsistently used in endemic regions (41).

1.1.3 The *Hantaviridae* family

Viruses of the family *Hantaviridae* belong to the order *Elliovirales*. These viruses are rodent-borne and have a global distribution. Hantaviruses are classified as Old World and New World hantaviruses based on their geographic distribution and the disease they cause in humans (42). Old World hantaviruses, such as HTNV, Puumala virus, and Dobrava-Belgrade virus, are found primarily in Europe and Asia and can cause hemorrhagic fever with renal syndrome (HFRS). An exception is the Old World hantavirus Seoul virus, which is found worldwide. New World hantaviruses, such as ANDV and Sin Nombre virus, are found in North and South America and can cause hantavirus cardiopulmonary syndrome (HCPS) (43). Nearly 200,000 humans are infected with hantaviruses annually. Mortality rates for HCPS and HFRS vary widely and can be as high as 60 % and 12 %, respectively (44,45).

The natural reservoirs of hantaviruses are distinct rodent species, in which they cause persistent infection. They are transmitted to humans through aerosols of rodent urine, feces, or saliva, and through direct contact or bites (46,47).

HTNV was first isolated in 1978 in South Korea from its natural reservoir, the striped field mouse (*Apodemus agrarius*) (48). It is distributed in China, South Korea, Vietnam, and Russia (49) and can cause HFRS in humans. Symptoms of HFRS include fever, bleeding tendencies, and renal failure (50). More than 90 % of the HFRS cases worldwide are reported in China, with the majority being caused by HTNV. In China, HFRS affects up to 20,000 people annually, with a mortality rate of 1 – 2 % (51).

ANDV is found in Argentina and Chile in its natural reservoir, the long-tailed colilargo (*Oligoryzomys longicaudatus*) (43). Infection in humans can cause HCPS, which is the most severe manifestation of hantavirus infection. It is characterized by pneumonia and cardiopulmonary dysfunction, with mortality rates as high as 60 % (45,52). Human-to-human transmission of hantaviruses has only been reported for ANDV so far, but a recent systematic review did not support this claim (53,54).

1.2 The structure of the bunyavirus particle

Bunyaviruses are segmented, negative-sense, single-stranded RNA viruses. The virions of some families, such as *Arenaviridae* or *Phenuiviridae,* are spherical, whereas the virions of *Hantaviridae* are pleomorphic in shape, ranging from spherical to tubular (55–57). The size of the bunyavirus virions ranges from 70 – 160 nm in diameter. They are enveloped by a lipid bilayer derived from the host cell.

The RNA genome of bunyaviruses is generally of negative polarity, but some also employ ambisense coding strategies. Most bunyaviruses are tri-segmented, with the genome being divided into three segments. However, the number of segments ranges from two segments for arenaviruses to up to eight segments for some phenuiviruses (28). The segments of tri-segmented bunyaviruses are named according to their size and encode four structural proteins. The small segment encodes the nucleoprotein (NP), the medium segment encodes the glycoprotein precursor (GPC), which is co-translationally cleaved into the glycoproteins Gn and Gc, and the large segment encodes the large protein (L), which includes the RdRp (58).

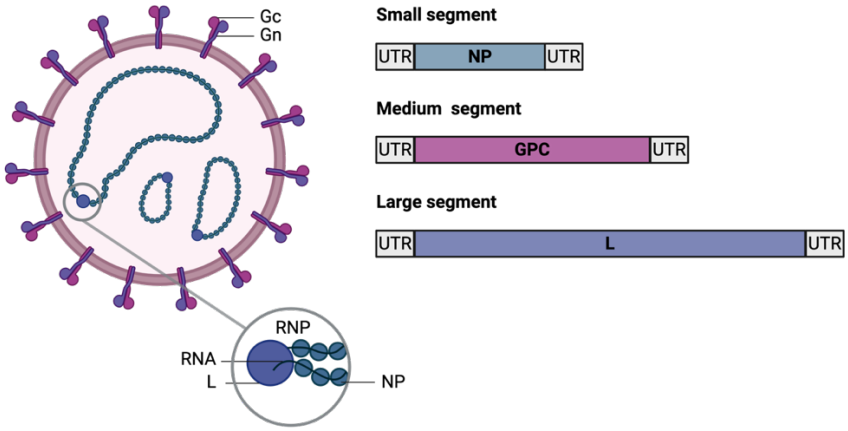

Figure 2: Molecular composition and genome organization of tri-segmented bunyaviruses. Schematic structure of a tri-segmented bunyavirus particle and genome organization. The glycoproteins Gc and Gn form spikes that are anchored in the envelope membrane. The viral RNA genome forms ribonucleoprotein (RNP) complexes with the L protein and NP. The RNA genome is divided into three genome segments. The small segment encodes NP, the medium segment encodes GPC, which is co-translationally cleaved into Gn and Gc, and the large segment encodes the L protein. The genes are flanked by untranslated regions (UTRs). Created with BioRender.com.

An exception are the bi-segmented arenaviruses, which consist of a small and a large genome segment. The small segment encodes the GPC and the NP, and the large segment encodes the L protein and the zinc-binding matrix protein (Z) (59). The genes are arranged in ambisense orientation and are separated by a non-coding intergenic region (IGR), which forms a hairpin secondary structure and is important for transcription termination (60).

The genes of both bi-segmented and tri-segmented bunyaviruses are flanked by untranslated regions (UTRs), containing the promoter regions required for genome replication. The 3' and 5' termini of the genome sequences are conserved within the different bunyavirus families. The 3' and 5' termini share complementary sequences, allowing each genome segment to potentially form a panhandle structure, leading to the observed quasi-circularization of the genome segments (61,62). However, recent structural data show that the 3' and 5' termini are associated with the L protein via distinct binding sites and only form a distal duplex when the L protein is not engaged in RNA synthesis (63–65).

The UTRs and, if applicable, IGRs are the minimal *cis*-acting factors for viral transcription and genome replication. The minimal *trans*-acting factors are the viral proteins NP and L. Together with the viral RNA genome (vRNA), they form transcriptionally active ribonucleoprotein (RNP) complexes (66–69).

NP is the most abundant viral protein in infected cells and within the virions (70). It encapsidates the single-stranded RNA genome, protecting it from degradation and recognition by the innate immune system. The NPs of the different bunyavirus families share few similarities with highly family-specific characteristics (71). The ~49 kDa NP of the *Hantaviridae* consists of a core with an RNA binding cleft and N- and C-terminal arms, which are responsible for oligomerization (72). In contrast, the ~27 kDa NP of the *Phenuiviridae* consists of a tightly packed core with an RNA binding cleft and an N-terminal arm that can bind to the surface of the core of the neighboring NP for oligomerization (73). The ~65 kDa NP of the *Arenaviridae* consists of two domains, with the RNA binding cleft located in the N-terminal domain. The C-terminal domain contains a 3' to 5' exoribonuclease that cleaves double-stranded RNA for immune evasion (74,75).

The glycoproteins form spikes that are required for adhesion and entry into the host cell. Glycoprotein heterodimers of different bunyavirus families show different arrangements on the virion surface. For *Hantaviridae*, Gn and Gc heterodimers form tetrameric spikes, which are arranged in a grid-like pattern, whereas for *Phenuiviridae*, Gc and Gn heterodimers have been shown to form pentamers and hexamers (76,77). For *Arenaviridae*, GPC is cleaved into the glycoproteins GP-1, GP-2, and the stable signal peptide (SSP), which form a heterotrimer that in turn forms homotrimers on the virion surface (78,79).

The matrix protein Z is the smallest protein of the *Arenaviridae,* with only 11 kDa, and coats the inside of the virion. It is essential for virion release from the infected cell and is thought to regulate viral transcription and genome replication by inhibiting the L protein RNA synthesis (80–82).

In addition to the structural proteins, some bunyaviruses encode non-structural (NS) proteins within the small or medium genome segment, which are termed NSs or NSm, respectively. Phenuiviruses encode an NSs protein on the small segment using an ambisense coding strategy (83). In addition, most phenuiviruses encode an NSm on the medium segment (84). Some members of the *Hantaviridae* encode an NSs protein via a second open reading frame from an alternative start codon with a +1 frameshift on the small segment (85,86). While these proteins are generally not essential for the viral replication cycle, NSs proteins have been identified as important virulence factors by interfering with the innate immune response, e.g., as interferon (IFN) antagonists (58,83). The NSm proteins are less well characterized but appear to play a role in antagonizing the immune response, promoting viral assembly and infection, and dissemination in the mosquito host (87,88).

1.2.1 The bunyavirus L protein

The bunyavirus L protein is a large, multifunctional, multidomain protein that plays the key role in viral transcription and genome replication. It is the largest of the bunyavirus proteins, ranging in size from ~250 kDa in most families to ~450 kDa in the *Nairoviridae*. It comprises an endonuclease (EN) domain at the N-terminus, an RdRp in the central core region, a putative cap-binding domain (CBD) at the C-terminus, as well as distinct RNA binding sites (63–65,89). While the L protein core is rather compact and rigid, the N- and C-terminal regions undergo conformational changes that are essential for the different functions of the L protein.

Bunyavirus L proteins show functional and architectural similarities to the polymerase complex of influenza viruses (*Orthomyxoviridae*), which has been extensively studied and is comparatively well understood. As shown in Figure 3 the polymerase complex consists of three subunits: the acidic polymerase protein (PA), the basic polymerase protein 1 (PB1), and the basic polymerase protein 2 (PB2) (89,90). Consequently, bunyavirus L proteins are frequently divided into PA-like, PB1-like, and PB2-like domains.

The structures of the EN domains and CBDs of several bunyaviruses have been studied by crystallography (91–96), and more recently, the structures of full-length L proteins have been solved by cryogenic electron microscopy (cryo-EM), expanding the understanding of L protein structure and function (63–65,97–102).

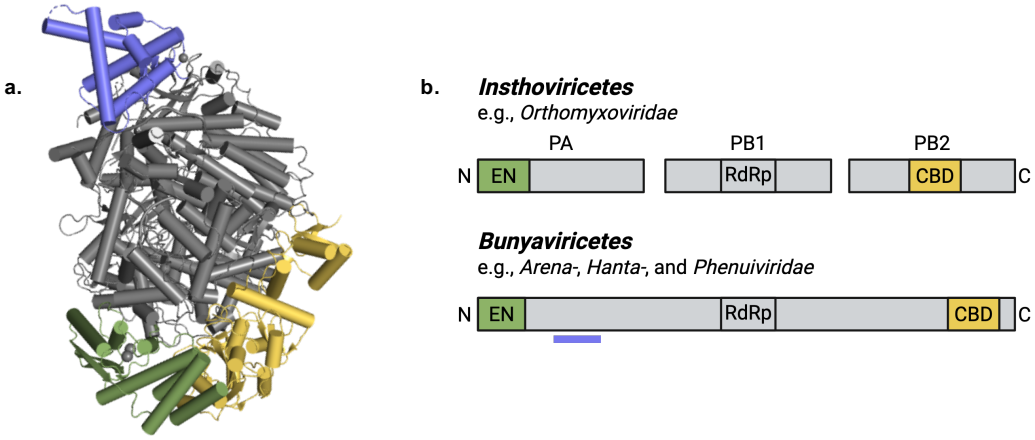

Figure 3: Domain organization of the bunyavirus L protein. a. Structure of full-length LASV L in elongation state (PDB: 7ojn) with the EN domain colored in green, the C-terminus, including the CBD-like domain, in yellow, and the rest, including the RdRp, in grey. The pyramid domain is highlighted in blue to facilitate orientation within the molecule. **b.** Schematic and linear representation of the *Orthomyxoviridae* (Class *Insthoviricetes*) polymerase complex and the *Arena-*, *Hanta-*, and *Phenuiviridae* (Class *Bunyaviricetes*) L protein. The *Orthomyxoviridae* polymerase complex consists of three subunits: PA, PB1, and PB2, whereas the bunyavirus L protein consists of one single polypeptide. EN, RdRp, and CBD are roughly indicated and colored according to a. Location of the pyramid domain of LASV is indicated by the blue line.

The central PB1-like domain contains the RdRp domain with palm, thumb, and finger, which is typical for RdRps of negative-strand RNA viruses. It is the domain with the highest degree of conservation across the different bunyavirus L proteins and contains the enzymatic activity for RNA synthesis (103).

The N-terminal PA-like domain contains the EN domain, which is required for cap snatching, a process in which the 5' cap structure of the host messenger RNA (mRNA) is bound and cleaved to initiate viral transcription (89). The active site of the EN contains two coordinated divalent metal ions that are required for its catalytic activity. Bunyavirus ENs can be classified as His+ or His- depending on the presence of a specific histidine residue. His+ ENs, as in the *Hantaviridae*, are highly active *in vitro*, whereas His- ENs, as in the *Arenaviridae*, show little or no activity *in vitro* (92–94,96).

The C-terminal PB2-like domain contains the putative CBD, which is also required for cap snatching. A CBD has so far only been functionally and/or structurally identified for the L proteins of some bunyaviruses, like RVFV, SFTSV, and La Crosse virus (family *Peribunyaviridae*), but it is likely that others also contain a CBD, and structural predictions support this hypothesis (89,91,94,97,104–106).

Bunyavirus L proteins share many similarities regarding their modes of function and overall protein architecture, but they differ significantly outside of the structurally conserved domains. For example, the L protein of LASV contains the pyramid domain, shown in Figure 3, which is specific to Old World arenaviruses (65). Especially the C-terminal domain is highly variable and, in analogy to influenza viruses, is thought to act as a platform for host protein interactions.

1.3 The bunyavirus replication cycle

The bunyavirus replication cycle can be divided into the following steps: (a) attachment and receptor-mediated endocytosis, (b) release of the RNPs into the cytoplasm, (c) transcription and (d) genome replication, (e) assembly and budding into the Golgi apparatus, and (f) exocytosis. A schematic representation is shown in Figure 4.

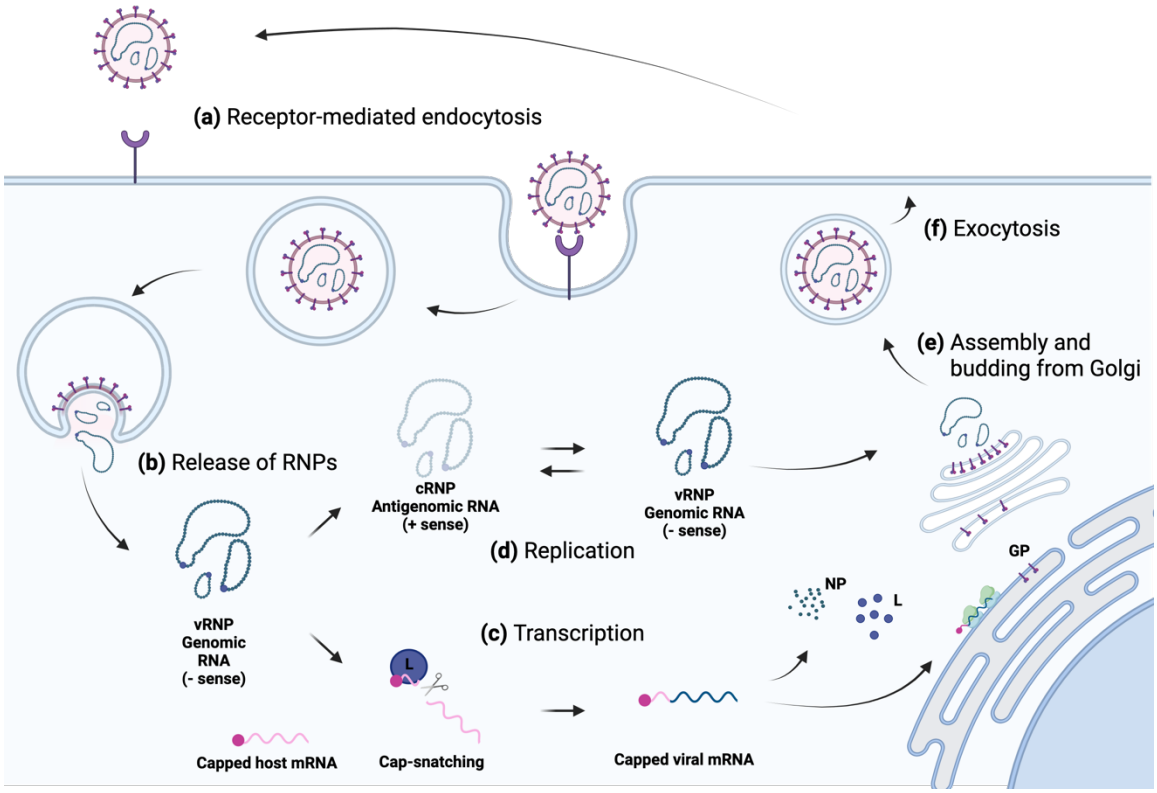

Figure 4: Bunyavirus replication cycle. (a) The bunyavirus particle enters the host cell via receptor-mediated endocytosis. **(b)** pH-dependent fusion with the endosomal membrane leads to the release of viral RNPs (vRNPs) into the cytoplasm. **(c)** Transcription is primed by a capped RNA fragment, acquired via a cap-snatching mechanism. **(d)** *De novo* genome replication proceeds via a complementary, antigenomic RNA intermediate (cRNP). **(e)** Newly synthesized RNA associates with NP and L to form new vRNPs. GPC is processed in the endoplasmic reticulum to glycoproteins (GP) Gn and Gc that form heterodimers. The bunyavirus particle is assembled at and buds into the Golgi apparatus. **(f)** The bunyavirus particle is transported to the plasma membrane and released by exocytosis. Created with BioRender.com.

Bunyavirus virions attach to the host cell with the glycoprotein spikes and enter the host cell via receptor-mediated endocytosis. Consistent with the diversity of host species that bunyaviruses infect, they rely on a wide variety of host cell receptors and co-receptors for this process, most of which are still unknown (79). Bunyaviruses exploit several endocytosis pathways, with many details remaining uncharacterized. Among others, LASV, JUNV, HTNV, and ANDV have been shown to use clathrin-mediated endocytosis (107–110). RVFV and ANDV have been reported to use caveolin-1-mediated endocytosis, and micropinocytosis-like endocytosis has also been described for ANDV and LASV (111,112). Acidification of the endosome triggers conformational changes of the glycoproteins,

leading to fusion of the viral and endosomal membranes and thereby release of the viral RNPs into the cytoplasm (113).

In the cytoplasm, two major processes take place that are catalyzed by the L protein: transcription and genome replication. Exactly where in the cytoplasm these processes take place or how the L protein switches from transcription to genome replication remains unclear.

Transcription is primed by a capped RNA fragment that is acquired by a cap-snatching mechanism and results in 5'-capped viral mRNA. Exactly how this works in bunyaviruses is unclear, but the cap-snatching mechanism has been extensively studied for influenza viruses (89,114). The 5' cap of host mRNAs is bound by a CBD within the L protein. A 5'-capped mRNA fragment is cleaved off by the EN and subsequently used to prime viral transcription (101). Capping of viral mRNA transcripts protects them from degradation and allows for translation through the host cell translation machinery. How the L protein gains access to the capped host mRNAs in the cytoplasm remains unclear, because, in contrast to the L protein, they are bound with high affinity to cellular cap-binding proteins (91,115,116).

Genome replication is initiated *de novo* by a prime and realign mechanism and takes place in two steps. First, a positive-sense antigenomic complementary RNA (cRNA) intermediate is generated, which then serves as a template for the synthesis of vRNA (80,117).

Some bunyaviruses, such as arenaviruses and phenuiviruses, use ambisense coding strategies. In this case, the transcription can be divided into early transcription from the vRNA and late transcription from the cRNA.

The newly synthesized vRNAs associate with newly expressed NP and L proteins to form RNPs. Accumulation of glycoproteins at the Golgi membrane initiates budding of viral particles into the Golgi. The cytoplasmic tail of the glycoprotein interacts with the NP, which is important for the packaging of RNPs (118–120). Golgi vesicles filled with virions reach the plasma membrane via the exocytic pathway, where they are released by membrane fusion (121). For some bunyaviruses, such as arenaviruses and New World hantaviruses, assembly takes place at the plasma membrane (122). In the case of arenaviruses, the matrix protein Z mediates the assembly and budding of viral particles by accumulating at the plasma membrane and recruiting RNPs through interaction with NP and the intracellular domain of SSP (123,124). Interactions between Z and the cellular endosomal sorting complex required for transport (ESCRT) ultimately lead to the release of the viral particles (125).

1.4 The family of DEAD-box RNA helicases

DEAD-box (DDX) proteins are a family of highly conserved and abundant ATP-dependent RNA helicases, which are named after the characteristic DEAD amino acid sequence in motif II (126). DDX proteins are found in all domains of life and are involved in nearly all aspects of RNA metabolism (127,128). Based on a series of conserved motifs within the helicase core, they are assigned to superfamily 2 of helicases (126,129). As shown in Figure 5 the helicase core comprises two domains that resemble the *Escherichia coli* (*E. coli*) recombinase A (RecA) and are therefore referred to as RecA-like domain 1 and RecA-like domain 2 (130).

DDX proteins use ATP to remodel RNA structures and RNA-protein complexes (131). They act as molecular switches, changing from an open to a closed conformation upon binding to ATP and RNA (132). Conserved motifs are distributed along the clamp that is formed by the helicase core in the closed conformation. These conserved motifs are assigned functions in ATP binding and hydrolysis, RNA binding, or coordination between these two functions (128). Since the helicase core binds to the sugar-phosphate backbone of RNA and shows almost no interaction with the RNA nucleotide bases, it is believed that the binding to RNA is sequence-independent but rather structure-dependent (133). The conserved helicase core is flanked by highly variable N- and C-terminal domains, which are responsible for the diversity in function and target specificity (134,135).

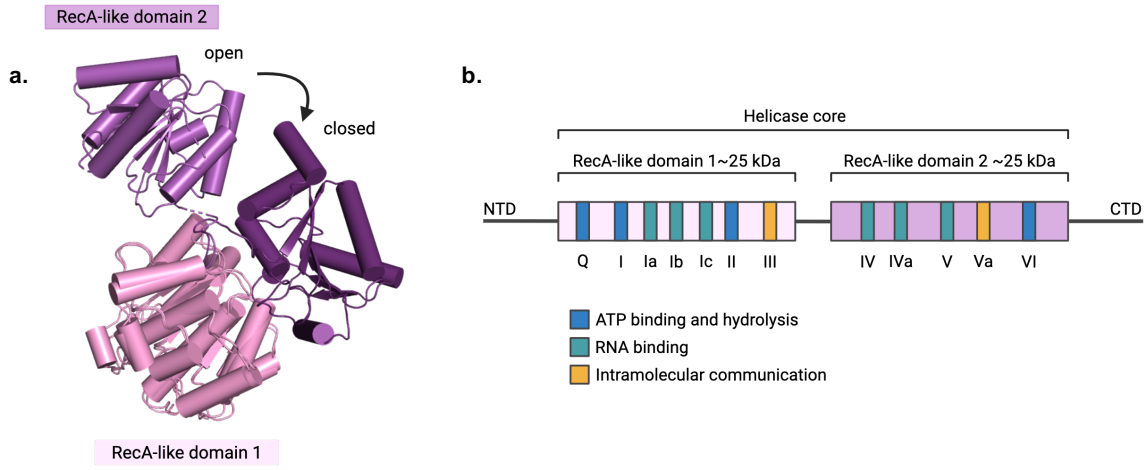

Figure 5: Domain organization of DDX proteins. a. Superimposed structures of the DDX17 core in open and closed conformations (PDB: 6UV0, 6UV1) with the RecA-like domain 1 colored in pink and the RecA-like domain 2 colored in violet. **b.** Schematic and linear representation of the DDX helicase core composed of two RecA-like domains. Conserved motifs are roughly indicated with their assigned functions: ATP binding and hydrolysis (blue), RNA binding (green), and intramolecular communication (yellow). The conserved helicase core is flanked by N- and C-terminal domains (NTD, CTD) of highly variable sequence, length, and structure. Created with BioRender.com.

DDX proteins play central and often essential roles in RNA metabolism (128). They usually function as components of larger complexes, such as the spliceosome and the eukaryotic translation initiation complex (136). Despite the high degree of conservation within their helicase core, DDX proteins

display remarkable functional diversity, ranging from disassembling RNPs to chaperoning during RNA folding and even stabilizing protein-RNA interactions (136,137). Many DDX proteins are associated with one or more biological processes, but the molecular mechanisms underlying these functions have not yet been elucidated. They have been implicated in a wide range of processes, including ribosome biogenesis, RNA storage and decay, translation, mRNA export, microRNA (miRNA) processing, precursor mRNA (pre-mRNA) splicing, and transcription (128,138). In addition, DDX proteins are often highly enriched in membraneless organelles (MLOs), such as nucleoli, nuclear speckles, stress granules (SGs), and processing bodies (P-bodies) (139–141). Their presence in MLOs appears not only to facilitate the interaction with their targets, but they also seem to contribute to the regulation of MLO formation through their condensation and ATPase activities (142).

In addition to their physiological functions in RNA metabolism, DDX proteins play various roles in innate immunity and viral infections, particularly of RNA viruses. Some DDX proteins act as cytoplasmic sensors of viral RNA and are essential for the innate immune response via type I IFNs. Well-known examples are the retinoic acid-inducible gene I (RIG-I)-like receptors (RLRs) DDX58, more commonly known as RIG-I, and melanoma differentiation-associated protein 5 (MDA-5) (143). In addition, many DDX proteins have been described to feed into RLR-dependent immune activation. For example, DDX3 has been shown to intervene at multiple steps of RLR signaling to enhance IFN production (144). In addition to their antiviral functions, some DDX proteins are hijacked by viruses to promote the viral replication cycle or modulate the immune response. For example, direct interaction with viral RNA has been shown to support the viral replication cycle for some DDX proteins and viruses, such as DDX6 and Dengue virus (DENV) (145). Taken together, both antiviral and proviral functions have been described for many DDX proteins. The role of the individual DDX proteins in modulating viral infection is often contradictory and highly context-dependent.

1.4.1 DDX17

DDX17 is mainly localized in the nucleus but can shuttle to the cytoplasm (146,147). It has also been observed in MLOs such as the nucleolus, nuclear speckles, SGs, and P-bodies (142,148). The N- and C-terminal domains of DDX17 are intrinsically disordered, resulting in a predicted high propensity for liquid-liquid phase separation (LLPS) (149,150). Functionally, DDX17 is involved in miRNA biogenesis by acting as a cofactor for the Drosha/DGCR8 complex (151). Furthermore, DDX17 interacts with zinc finger antiviral protein (ZAP) and appears to be required for ZAP-mediated degradation of viral mRNAs. DDX17 also serves as a transcriptional co-activator for several

transcription factors, thereby regulating gene expression (152–154). In addition, DDX17 is involved in alternative pre-mRNA splicing and ribosome biogenesis (154,155).

DDX17 has a closely related paralog, DDX5, which shares many of its cellular functions, including pre-mRNA splicing, transcriptional co-activation, miRNA biogenesis, and ribosome biogenesis (154–156). DDX17 and DDX5 share approximately 90 % sequence homology in their helicase core, 60 % in their N-terminal domain, and 30 % in their C-terminal domain (157).

Both pro- and antiviral roles have been described for DDX17 and its paralog DDX5. For example, during influenza A virus (IAV) infection, both proteins are essential for efficient viral RNA replication and transcription and translocate to the cytoplasm where they co-localize with the viral NP (158). Conversely, DDX17, but not DDX5, restricts RVFV infection, presumably by recognizing structured elements in the viral RNA in the cytoplasm and by its role in miRNA biogenesis in the nucleus. Again, redistribution to the cytoplasm and co-localization with NP have been described (159). In hepatitis B virus (HBV) infection, antiviral activity of DDX17 has been described by competing with the viral polymerase for binding of pregenomic RNA (160). In addition, DDX17 and DDX5 enhance viral transcriptional read-through, thereby promoting the destabilization of viral RNA (161). At the same time, a proviral role in HBV infection has been described for DDX17, which is upregulated by the viral protein HBx, thereby enhancing HBV infection (162).

1.4.2 DDX24

DDX24 is localized to both the nucleus and the cytoplasm (163). It has also been identified as part of MLOs, including nucleoli and P-bodies (142,148). The N- and C-terminal domains of DDX24 contain intrinsically disordered regions, resulting in a predicted high propensity for LLPS (149).

DDX24 is one of the less-studied DDX proteins, but has been implicated in ribosome biogenesis and pre-mRNA splicing (142,164). In addition, DDX24 is an IFN-stimulated gene (ISG) that negatively regulates RLR signaling, possibly by competing with RIG-I for viral RNA binding (165).

Although little is known about the role of DDX24 in viral infections, both proviral and antiviral functions have already been described. For example, DDX24 is required for human immunodeficiency virus 1 (HIV-1) infection for the packaging of viral RNA (166). In contrast, DDX24 functions as a pattern recognition receptor in Kaposi's sarcoma-associated herpesvirus (KSHV) infection, where its association with viral mRNA leads to increased IFN expression (167). Since the increased IFN expression is not caused by an increase in IFN mRNA, the effect appears to occur at the post-translational level.

1.4.3 DDX19

DDX19A (DDX19) shuttles between the cytoplasm and the nucleus, but is mainly localized to the nuclear pore complex (168). It is best known for its function as part of the nuclear pore complex, where it removes nuclear RNA export factor 1 (Nxf1) from mRNAs in the final step of mRNA export (169). Other functions include the export of transfer RNAs, ribosomal precursors, and telomerase RNA, as well as transcription initiation, translation initiation, and SG dissolving (142). DDX19 adopts an autoinhibitory conformation that is resolved upon binding to nucleoporins (169–171).

Mainly, proviral roles have been described for DDX19 (172). For example, DDX19 associates with IAV mRNAs to promote their nuclear export (173).

1.5 Objective

The class of *Bunyaviricetes* includes several important human pathogens such as the LASV, RVFV, HTNV, and ANDV. To date, there are no FDA- or EMA-approved vaccines or antiviral treatments available for human use, highlighting the urgent need for effective therapeutic strategies. Antiviral approaches can be broadly categorized into virus-directed and host-directed strategies. Targeting essential interactions between host proteins and viral proteins reduces the risk of developing resistance, as mutations at the interface could result in the loss of these essential interactions. In addition, interactions with host factors may be conserved among related viruses, offering the potential for broad-spectrum antivirals.

Although viruses of the *Bunyaviricetes* class are highly diverse in terms of host tropism, viral transmission, and their replication cycle, common strategies include the viral transcription and genome replication in the cytoplasm. The central protein for these processes is the L protein, making it a promising target for antiviral strategies. To date, little is known about the interactions between bunyavirus L proteins and host cell proteins. This work aims to characterize the interactions between bunyavirus L proteins and host proteins, particularly of the DDX family. These interactions will be studied both in the cellular context and with isolated components, offering well-controlled conditions. In addition, the functional relevance of selected host factors for the bunyavirus replication cycle will be investigated.

The study of interactions between bunyavirus L protein and host proteins aims to improve our understanding of the viral replication cycle and to identify new targets for antiviral strategies with broad-spectrum potential.

2 MATERIAL

2.1 Bacterial strains

2.1.1 *E. coli* for cloning

Table 1: List of *E. coli* strains used for cloning.

Name	Genotype	Supplier
DH5α	*fhuA2Δ(argF-lacZ)U169 phoA glnV44 Φ80Δ(lacZ)M15 gyrA96 recA1 relA1 endA1 thi-1 hsdR17*	NEB
SURE 2	e14-(McrA-) Δ(*mcrCB-hsdSMR-mrr*)*171 endA1 supE44 thi-1 gyrA96 relA1 lac recB recJ sbcC umuC*::Tn5 (Kan^r) *uvrC* [F′ *proAB lacI*^{q}ZΔ*M15* Tn*10* (Tet^r) Amy Cam^r].	Agilent

2.1.2 *E. coli* for protein expression

Table 2: List of *E. coli* strains used for protein expression.

Name	Genotype	Supplier
BL21 Gold (DE3)	B F$^-$ *ompT hsdS* (r_{B^-} m_{B^-}) *dcm*$^+$ Tet^r *gal* λ(DE3) *endA* Hte	Agilent
DH10EMBacY	F$^-$ *mcrA* Δ(*mrr-hsdRMS-mcrBC*) Φ80 *lacZ*ΔM15 Δ(*lacX74*) *recA1 endA1 araD139* Δ(*ara-leu*)7697 *galU galK* λ- *rpsL*^{R} *nupG* / pMON14272 (Kana^R) / pMON7124 (Tet^R)	EMBL Grenoble
Rosetta™ 2 (DE3)	F$^-$ *ompT hsdS*$_B$(r_{B^-} m_{B^-}) *gal dcm* (DE3) pRARE2 (Cam^R)	Novagen
Rosetta™ 2 pLysS (DE3)	F$^-$ *ompT hsdS*$_B$(r_{B^-} m_{B^-}) *gal dcm* (DE3) pLysSRARE (Cam^R)	Novagen

2.2 Cell lines

Table 3: List of eukaryotic cell lines used with information regarding the medium, origin, and source. The media are further specified in 2.4.2.

Name	Medium	Origin	Source
A549	DMEM 5 %	Human, lung cells from an adenocarcinoma	ATCC
HEK293	DMEM 10 %	Human, embryonic kidney cells	Abcam
HEK293 DDX17 KO	DMEM 10 %	Human, embryonic kidney cells CRISPR/Cas9 knockout of DDX17	Abcam
HEK293T	DMEM 5 %	Human, embryonic kidney cells Derivative of HEK293 Expression of SV40 T antigen	ATCC
High Five™	Express Five™ SFM	*Trichoplusia ni*, ovarian cells	Thermo Fisher Scientific

Name	Medium	Origin	Source
Huh7	DMEM 5 %	Human, liver cells from malignant hepatocytes	BNITM
Sf21	Sf-900™ SFM	*Spodoptera frugiperda*, ovarian cells	Thermo Fisher Scientific
Vero 76	DMEM 3 %	Green monkey, kidney cells	ATCC
Vero E6	DMEM 5 %	Green monkey, kidney cells	ATCC

2.3 Virus strains

Table 4: List of virus strains used with information regarding the source and the isolation host.

Virus	Source	Isolation host
LASV Ba366	BNITM	*Mastomys natalensis*
ANDV 9717869	Dr. H. Feldmann, Hamilton	*Oligoryzomys longicaudatus*
HTNV 76-118	Charité, Berlin	*Apodemus agrarius*
RVFV AR 20368	RKI, Berlin	*Culex zombaensis*
TCRV 11573	FLI, Isle of Riems	*Artibeus lituratus*

2.4 Growth media

2.4.1 Media and selective antibiotics for *E. coli* cultivation

Table 5: Compositions of the media for *E. coli* cultivation.

Name	Composition
Lysogeny broth (LB) medium	Peptone (10 g/l), yeast extract (5 g/l), NaCl (10 g/l)
LB agar	by Thermo Fisher Scientific
Super optimal broth with catabolite repression (SOC)	Peptone (20 g/l), yeast extract (5 g/l), 10 mM NaCl, 10 mM KCl, 10 mM $MgCl_2$, 10 mM $MgSO_4$, 20 mM glucose
Terrific broth (TB)	Peptone (12 g/l), yeast extract (24 g/l), glycerol (4 ml/l), 17 mM KH_2PO_4, 72 mM K_2HPO_4

Table 6: Selective antibiotics and concentrations for *E. coli* cultivation.

Name	Concentration
Carbenicillin	100 µg/ml
Chloramphenicol	34 µg/ml
Kanamycin	50 µg/ml

Name	Concentration
Tetracycline	10 µg/ml
Gentamycin	7 µg/ml

2.4.2 Media for cell culture

Media and supplements purchased from Thermo Fisher Scientific: DMEM, DMEM GlutaMAX™, fetal bovine serum (FBS), Opti-MEM™, Express Five™ SFM, Sf-900™ II SFM

Supplements purchased from PAN Biotech: L-glutamine (200 mM; 100x), penicillin-streptomycin (10,000 U/ml penicillin, 10 mg/ml streptomycin; 100x), MEM NEAA non-essential amino acid solution (100x)

Supplemented cell culture media were prepared as described below.

DMEM 3 % to 10 %: 500 ml DMEM GlutaMAX™, 15 - 50 ml FBS, 5 ml penicillin-streptomycin (100x), 5 ml MEM NEAA (100x)

Express Five™ SFM: 1000 ml Express Five™, 50 ml L-glutamine, 10 ml penicillin-streptomycin (100x)

Overlay medium 400cP: 400 ml DMEM 3 %, 200 ml 400 cP methyl cellulose (16.8 g in 600 ml water)

Overlay medium 4000cP: 300 ml DMEM 3 %, 300 ml 4000 cP methyl cellulose (12 g in 600 ml water)

2.5 Chemicals

Chemicals from Biozym: Agarose LE

Chemicals from Fresenius Kabi: Ampuwa® water

Chemicals from Merck: Magnesium chloride ($MgCl_2$), manganese chloride ($MnCl_2$)

Chemicals from Roth: β-mercaptoethanol, 1,4-dithiothreitol (DTT), 2-Propanol, 4-(2-hydroxyethyl)-1-piperazine ethanesulfonic acid (HEPES), 5-bromo-4-chloro-3-indolyl-β-Dgalactopyranoside (BluoGal), acetic acid, ammonium persulfate (APS), Brilliant Blue G250, carbenicillin, D-biotin, chloramphenicol, di-potassium hydrogen phosphate (K_2HPO_4), ethanol, ethidium bromide, ethylenediaminetetraacetic acid (EDTA), gentamycin, glycerol, hydrochloric acid (HCl) (37 %), imidazole, isopropyl-β-D-thiogalacto-pyranoside (IPTG), kanamycin, L-arginine, L-glutathion, peptone, phenylmethylsulfonyl fluoride (PMSF), potassium dihydrogen phosphat (KH_2PO_4),

potassium chloride (KCl), RNAse Away, Roti®Block, Rotiphorese® Gel 40, sodium chloride (NaCl), sodium dodecyl sulphate (SDS) ultra-pure, sodium hydroxide (NaOH), tetracyclin hydrochlorid, tetramethylethylenediamine (TEMED), tris-(hydroxymethyl)-amino methane (TRIS), Triton® X 100, Tween®20, yeast extract

Chemicals from SAV Liquid Production GmbH: Formaldehyde solution (4.5 %)

Chemicals from Serva: Bromphenol blue, xylencyanol FF

Chemicals from Sigma Aldrich: Branched polyethylenimine (PEI), Chloroquine diphosphate, Crystal Violet, Fast Green, Methylcellulose 400 cP, protamine sulfate, puromycin

Chemicals from Roche: cOmplete™ EDTA-free Protease Inhibitor Cocktail

Chemicals from Thermo Fisher Scientific: Methylcellulose 4000 cP, SYBR® Green I, SYPRO® Orange, 0.05 % Trypsin-EDTA

Chemicals from ZEISS: Immersol™ 518 F

2.6 Transfection reagents

Table 7: List of transfection reagents used.

Product	Supplier
Branched PEI 1 mg/ml	Sigma Aldrich
FuGENE® HD	Promega
Lipofectamine™2000	Thermo Fisher Scientific
Lipofectamine™ RNAiMAX	Thermo Fisher Scientific

2.7 Buffers and solutions

2.7.1 Buffers for electrophoresis and western blots

Table 8: Compositions of buffers used in electrophoresis and western blot.

Name	Composition
Agarose gel 0.8 to 1.5 %	0.8 to 1.5 % agarose (w/v) in 1x TRIS-acetate-EDTA (TAE) buffer
DNA loading dye (6x)	10 mM TRIS, 50 mM EDTA, 60 % (w/v) glycerol, 0.03 % bromphenol blue, 0.03 % (w/v) Xylenxyanol FF, pH 7.6
Fast Green staining solution	0.25 % (w/v) Fast Green, 10 % (v/v) acetic acid
Phosphate buffered saline (PBS) (10x)	1.37 M NaCl, 27 mM KCl, 100 mM Na2HPO$_4$, 18 mM KH$_2$PO$_4$, pH 7.4
PBS Tween (PBST) washing buffer	0.1 % Tween®20 (v/v) in 1x PBS

Name	Composition
Resolving gel (8 to 15 %)	125 mM TRIS, 20 to 37 % (v/v) Rotiphorese® Gel 40, 0.1 % (w/v) SDS, 0.1 % (w/v) APS, 0.3 % (v/v) TEMED, pH 6.8
Blocking solution	ROTI® Block (10x) by Roth
Safe Stain solution	0.008 % (w/v) Brilliant Blue G250, 0.126 % (v/v) HCl
SDS running buffer (10x)	1 % (w/v) SDS, 250 mM TRIS, 2 M glycine
SDS sample buffer (3x)	150 mM TRIS pH 6.8, 30 % (w/v) glycerol, 6 % (w/v) SDS, 0.025 % (w/v) bromphenol blue, 100 mM DTT added directly before usage
SDS sample buffer (4x)	125 mM TRIS pH 6.8, 50 % (w/v) glycerol, 5 % (w/v) SDS, 0.025 % (w/v) bromphenol blue, 4 % (v/v) β-mercaptoethanol or 100 mM DTT
Stacking gel (4 %)	125 mM TRIS, 10 % (v/v) Rotiphorese® Gel 40, 0.1 % (w/v) SDS, 0.1 % (w/v) APS, 0.1 % (v/v) TEMED, pH 8.8
Transfer buffer (20x)	25 mM bicine, 25 mM bis-TRIS (free base), 1 mM EDTA, pH 7.2
Tris-acetate-EDTA (TAE) (10x)	2 M TRIS, 50 mM Na_2EDTA, adjusted to pH 8 with acetic acid

2.7.2 Lysis buffers for eukaryotic cells

Table 9: Compositions of buffers used for the lysis of eukaryotic cells.

Name	Composition
Lysis buffer	50 mM HEPES, 150 mM NaCl, 5 % (w/v) glycerol, 0.5 % (v/v) Triton® X 100, cOmplete™ EDTA-free Protease Inhibitor Cocktail (1x), pH 7.4
Passive lysis buffer	Passive lysis buffer (5x) by Promega

2.7.3 Buffers for protein purification, co-immunoprecipitation, and protein interaction experiments

Table 10: Compositions of buffers used in protein purification, co-immunoprecipitation (co-IP), and protein interaction experiments.

Name	Composition
Co-IP washing buffer	50 mM HEPES, 150 mM NaCl, 5 % (w/v) glycerol, pH 7.4
DDX biotin elution buffer	50 mM HEPES, 500 mM NaCl, 10 % (w/v) glycerol, 2 mM DTT, 50 mM biotin, pH 7
DDX lysis buffer	20 mM TRIS, 1 M NaCl, 10 % (w/v) glycerol, cOmplete™ EDTA-free Protease Inhibitor Cocktail (1x), 200 mM L-arginine, pH 8
DDX washing buffer	50 mM HEPES, 500 mM NaCl, pH 7
DDX17.2 GST elution buffer	20 mM TRIS, 1 M NaCl, 5 % (w/v) glycerol, 50 mM L-glutathione, pH 7

Name	Composition
DDX17.2 His elution buffer	20 mM TRIS, 1 M NaCl, 5 % (w/v) glycerol, 200 mM L-arginine, 500 mM imidazole, pH 7
DDX17.2 lysis buffer	20 mM TRIS, 1 M NaCl, 5 % (w/v) glycerol, cOmplete™ EDTA-free Protease Inhibitor Cocktail (1x), pH 8
DDX17.2 SEC buffer	20 mM TRIS, 1 M NaCl, 5 % (w/v) glycerol, 200 mM L-arginine, pH 7
DDX17.2 washing buffer	20 mM TRIS, 500 mM NaCl, 5 % (w/v) glycerol, pH 7
LASV L assay buffer	25mM HEPES, 150 mM NaCl, 2 mM DTT, 2 mM $MnCl_2$, pH 7

2.7.4 Buffers for virus titration assays

Table 11: Compositions of buffers used for virus titration assays.

Name	Composition
Crystal violet solution	0.5 % (w/v) crystal violet in 20 % (v/v) ethanol
IFA blocking buffer	5 % FBS (v/v) in 1x PBS
Permeabilization buffer	0.05 % Triton® X-100 (v/v) in 1x PBS

2.8 Consumables

All consumables not listed in Table 12 were purchased from Sarstedt.

Table 12: List of consumables used.

Consumable	Supplier
Amersham™ Protran™ nitrocellulose blotting membrane (0.2 µm and 0.45 µm)	GE Healthcare Life Sciences
Amicon® Ultra centrifugal filter units	Merck Millipore
Cellulose Acetate Filter 0.2 µm	Sartorius
Express™ Plus membrane filter 0.22 µm	Merck Millipore
High precision microscope cover glasses 24 x 50 mm	Thorlabs
Microplate 96 well, U-bottom, natural	Greiner bio one
Mini-PROTEAN® TGX™ Precast Protein Gels (4 – 15 % or any kD)	Bio-Rad
Nunc™ MicroWell™ 96-Well Microplate, flat bottom, white and clear	Thermo Fisher Scientific
Reagent reservoirs, clear, 25 ml	Integra

2.9 Columns and affinity purification gels

Table 13: List of columns and affinity purification gels used.

Name	Supplier
Glutathione Sepharose™ 4 Fast Flow	Cytiva
HiTrap™ Heparin FF (1 ml)	Cytiva
HiLoad™ 16/60 Superdex™ 200 prep grade	GE Healthcare
Ni-NTA Agarose resin	Qiagen
Protein A Sepharose™ 4 Fast Flow	Cytiva
Strep-Tactin-XT 4Flow®	IBA
Superdex™200 Increase 10/300 GL	Cytiva

2.10 Laboratory equipment

Table 14: List of laboratory equipment used.

Device	Supplier
ÄKTA pure	GE Healthcare
ÄKTA prime plus	GE Healthcare
Scale	Kern & Sohn GmbH
Bio Photometer 6131	Eppendorf
Centrifuge 5415 R	Eppendorf
Centrifuge Rotin 420 R	Hettich
Centrifuge Sorvall Lynx 4000	Thermo Fisher Scientific
Precision scale	Sartorius
Fusion SL4 imaging system	Vilber Lourmant
Gel Imager	Intas Science Imaging
Fluorescence microscope LEICA DMIL	Leica
Fluorescence microscope	Euroimmune
Portable luminometer Junior LB 9509	Berthold
Microscope CKX31	Olymp

Device	Supplier
Mini-PROTEAN® electrophoresis chamber	Bio-RAD
Mini-Sub Cell GT Horizontal Electrophoresis System	Bio-Rad
Nanodrop Colibri+	Berthold
PCR cycler Primus	PeqLab
pH meter FiveEasy	Mettler Toledo
Pipets	Gilson
Pipetus®	Hirschmann
Plate Reader Tecan Sparks	Tecan
Power suppls EV231	PeqLab
Innova® 42 Shaker	Eppendorf
Shaking incubator Unimax 1010	Heidolph
Mass photometer	Refeyn
Thermomixer 5436	Eppendorf
HERAcell 150 incubator	Thermo Fisher Scientific
Power Supply EV231	Peqlab
Sonifier 250	Branson
Tunair® shake flask	Sigma Aldrich
XCell SureLock™ Mini-Cell	Thermo Fisher Scientific

2.11 Kits, enzymes and markers

Table 15: List of kits, enzymes and markers used.

Name	Supplier
Benzonase®	Merck Millipore
CellTiter-Glo® 2.0 Cell Viability Assay	Promega
Clarity Max™ Western ECL Substrate	Bio-Rad
Clarity™ Western ECL Substrate	Bio-Rad
dNTP Set, 100 mM	Thermo Fisher Scientific

Name	Supplier
Dual Luciferase® Reporter Assay System	Promega
HRV 3C protease	From own production
NativeMark™ Unstained Protein Standard	Thermo Fisher Scientific
NEBuilder® HiFi DNA Assembly	NEB
NucleoBond® Xtra Midi Plus Kit	Macherey Nagel
NucleoSpin® Gel and PCR Clean-up Mini Kit	Macherey Nagel
NucleoSpin® Plasmid Mini Kit	Macherey Nagel
Page Ruler Plus Prestained Protein Ladder	Thermo Fisher Scientific
Page Ruler Prestained Protein Ladder	Thermo Fisher Scientific
Q5® High-Fidelity DNA Polymerase	NEB
Quick Load 1kb Ladder	NEB
TMB substrate	Mikrogen
Restriction enzymes	NEB
Z-Competent™ *E. coli* Transformation Buffer Set	Thermo Fisher Scientific

2.12 Oligonucleotides

The DNA oligonucleotides used for DNA amplification and sequencing were purchased from IDT and are listed in Table A. 1.

Ambion® Silencer® Select small interfering RNAs (siRNAs) and Mission® small hairpin RNAs (shRNAs) were used for knockdown experiments and were purchased from Life Technologies™ and Merck, respectively.

Table 16: List of Ambion® Silencer® Select siRNAs sequences.

Name	siRNA ID	Sequence Sense (5’ to 3’)	Sequence Antisense (3’ to 5’)
Scrambled	4390843		
DDX17 #1	S20624	CUACCAAUAUGAUAGGUUAtt	UAACCUAUCAUAUUGGUAGct
DDX17 #2	S20623	GGAUCGUAGUGAAACCGAUtt	AUCGGUUUCACUACGAUCCcg
DDX19A #1	S30693	CAAUCGACCCUCCAAGAUAtt	UAUCUUGGAGGGUCGAUUGaa

Name	siRNA ID	Sequence Sense (5' to 3')	Sequence Antisense (3' to 5')
DDX19A #2	s30694	GAAGCUUGCCUAUGCCGUUtt	AACGGCAUAGGCAAGCUUCag
DDX24 #1	S32631	GAGUCCCAAUACAACCCAAtt	UAGGGUUGUAUUGGGAGUCat
DDX24 #2	S32632	GAGCAGACUGGAAAUCUAAtt	UUAGAUUUCCAGUCUGCUCtt

Table 17: List of Mission® shRNA sequences.

Name	shRNA ID	Targeted sequence
Scr	SHC016	
DDX17 045	TRCN00000287045	GACCACAAGTTGATCCAACTA
DDX24 314	TRCN0000050314	CGCTCAAGAAAGATGAGGATA

2.13 Plasmids

The plasmids used and created in this work are listed in Table A. 2.

2.14 Antibodies

Table 18: List of antibodies including the dilutions used in western blot (WB), immunofluorescence (IF), and immune focus assay (IFA).

Antibody	Dilution	Source
Anti-FLAG® (M2) Horseradish peroxidase (HRP), mouse, monoclonal	1:10,000 (WB)	Sigma Aldrich
Anti-Junín Virus (NA05-AG12), monoclonal, mouse	1:500 (IFA)	BEI resources
Beta tubulin (BT7R), mouse, monoclonal	1:2,000 (WB)	Thermo Fisher Scientific
c-myc (9E10), mouse, monoclonal	1:1,000 (WB)	Thermo Fisher Scientific
DDX17 (H-7), mouse, monoclonal	1:500 (WB)	Santa Cruz Biotechnology
DDX19 (A300-546A), rabbit, polyclonal	1:1,000 (WB)	Bethyl Laboratories
DDX24 (15769-1-AP), rabbit, polyclonal	1:1,000 (WB)	Proteintech
Evan's Blue	0.01 % (IF)	Sigma Aldrich
Fluorescein (FITC) anti-mouse IgG (H+L), goat, polyclonal	1:200 (IF)	Jackson Immuno Research
GAPDH (6C5), mouse, monoclonal	1:1,000 (WB)	Santa Cruz Biotechnology
Hantavirus Hantaan N (B5D9), mouse, monoclonal	1:1,000 (IFA) 1:50 (IF)	Thermo Fisher Scientific

Antibody	Dilution	Source
Hantavirus Puumala N (A1C5), mouse, monoclonal	1:1000 (IFA) 1:50 (IF)	Thermo Fisher Scientific
HRP-conjugated anti-mouse IgG (H+L), sheep, polyclonal	1:5,000 (WB) 1:1,000 (IFA)	Jackson Immuno Research
HRP-conjugated α-rabbit IgG (H+L), goat, polyclonal	1:10,000 (WB)	Jackson Immuno Research
α-LASV-NP (2B5), mouse	1:1,000 (IFA)	BNITM, Petra Emmerich

2.15 Software

Table 19: List of software used.

Program	Supplier
AcquireMP	Refeyn
AlphaFold 3	DeepMind
BioRender.com	BioRender
DiscoverMP	Refeyn
deePhase	Knowles Lab, University of Cambridge
Excel, Powerpoint, Word	Microsoft Office
GraphPad Prism 10	Graphpad Software, Inc.
MacVector	Symanec Corporation
Mendeley	Mendeley Ltd.
PAE Viewer	University of Göttingen
PDBsum	European Bioinformatics Institute
ProtParam	Expasy, Swiss Institute of Bioinformatics
Mac PyMol	DeLano Scientific
Unicorn 7.0	GE Healthcare

3 METHODS

3.1 Microbiology

3.1.1 Generation of chemically competent *E. coli*

To generate chemically competent *E. coli*, the Z-Competent™ *E. coli* Transformation Buffer Set was used according to the manufacturer's instructions. Aliquots of 50 µl were flash frozen in liquid nitrogen and subsequently stored at -80°C.

3.1.2 Transformation of *E. coli*

Aliquots (50 µl) of chemically competent *E. coli* were thawed on ice. 100 to 300 ng of plasmid DNA or 2 µl of assembly reaction mix (3.2.5) was added and incubated on ice for 10 min. A heat shock at 42°C was performed for 45 s and the cells were then cooled on ice for 2 min. 45 to 100 µl prewarmed SOC medium was added and the *E. coli* were cultivated at 37°C with shaking at 300 rpm for 45 min. The transformed cells were either plated on LB agar or cultivated in LB medium as described in 3.1.3.

3.1.3 Cultivation of transformed *E. coli*

To obtain single colonies, transformed *E. coli* were plated on LB agar supplemented with selective antibiotics (2.4.1) and grown overnight at 37°C.

For the cultivation of transformed *E. coli* in liquid culture, LB medium supplemented with selective antibiotics (2.4.1) was inoculated and incubated overnight at 37°C with shaking at 180 rpm.

3.2 Molecular biology

3.2.1 Polymerase chain reaction

Polymerase chain reaction (PCR) was used to amplify DNA fragments. If not stated otherwise, the reaction mix was prepared as shown in Table 20 and the reaction was performed according to the general program described in Table 21. The annealing temperature depends on the melting temperatures of the specific primers and was selected accordingly. DNA was either purified from the PCR reaction as described in Section 3.2.3 or stored at -20°C until further use.

Table 20: List of components and concentrations used in a 50 µl PCR.

Component	Concentration	Volume [µl]
DNA template	10 ng/µl	1.0
dNTP mix	10 mM	1.0
Forward primer	10 µM	1.0
Reverse primer	10 µM	1.0
Q5 polymerase	2,000 U/ml	0.5
5x Q5- reaction buffer	5x	10.0
Ampuwa water		35.5

Table 21: General program used for PCR.

Phase	Temperature [°C]	Duration	
Initial denaturation	98	1 min	
Denaturation	95	20 s	30 cycles
Annealing	56-64	30 s	
Elongation	72	30 s per kb	
Final elongation	72	5 min	

3.2.2 Agarose gel electrophoresis and visualization of nucleic acids

In agarose gel electrophoresis, negatively charged DNA is separated according to size by migrating through an agarose matrix in an electric field. It can be used to analyze or purify DNA samples.

Depending on the expected size of the DNA, agarose gels with 0.8 to 1.5 % agarose in 1x TAE buffer were used. DNA samples were mixed with 6x DNA loading dye and loaded onto the agarose gel with a DNA marker. The agarose gel was placed in a horizontal electrophoresis chamber, covered with 1x TAE buffer, and run at 90 to 150 V for 20 to 45 min.

For visualization of the DNA, analytical agarose gels were stained for 20 min with 0.01 % ethidium bromide in 1x TAE buffer and detection was performed with ultraviolet (UV) light at 254 nm. Due to the mutagenic risk of ethidium bromide, preparative agarose gels were stained with 0.05 % SYBR-Green in 1x TAE buffer. Detection could be either performed with UV light at 254 nm or with blue light at 470 nm, avoiding DNA damage through exposure to UV light.

3.2.3 Purification of DNA from PCR reactions and agarose gels

To purify DNA from PCR reactions (3.2.1) or preparative agarose gels (3.2.2), the NucleoSpin Gel and PCR Clean-up Mini Kit was used according to the manufacturer's instructions. The DNA was bound to a silica membrane in the presence of chaotropic salt and washed with an ethanol-containing buffer. The DNA was eluted with Ampuwa water, deviating from the manufacturer's instructions.

3.2.4 Restriction of DNA

Restriction endonucleases cleave double-stranded DNA at specific sequences. They were used to linearize vectors for assembly cloning (3.2.5) or to analyze plasmid DNA. The reaction conditions were set according to the manufacturer's instructions. The cleaved DNA was then separated and analyzed by gel electrophoresis (3.2.2).

3.2.5 Assembly cloning

In assembly cloning, DNA fragments are assembled based on overlapping sequences. The reaction mix includes an exonuclease that catalyzes the formation of single-stranded 3' overhangs, allowing the annealing of insert and vector. It also includes a polymerase for filling in gaps and a ligase for sealing nicks in the assembled DNA.

Assembly cloning was performed using the NEBuilder HiFi DNA Assembly Kit, according to the manufacturer's instructions. 15 to 30 base pairs were added to both ends of the insert DNA fragment with PCR, matching the ends of the linearized vector. Linearized vector and insert were mixed with a molar ratio of 1:2 and 2x NEBuilder HiFi DNA Assembly Master Mix was added. The assembly reaction mix was incubated at 50°C for 1 h and then either stored at -20°C or transformed directly into competent *E. coli* according to Section 3.1.2.

3.2.6 Purification of plasmid DNA from *E. coli*

Plasmid DNA was either purified from 4 ml (mini preparation) or 150 ml (midi preparation) transformed *E. coli* cultures, depending on the required amount and purity of plasmid DNA.

For a mini preparation, the NucleoSpin Plasmid Mini Kit was used according to the manufacturer's instructions. Plasmid DNA was released from the *E. coli* cells by alkaline lysis and bound to a silica membrane. The silica membrane was washed with an ethanol-containing buffer and DNA was eluted in Ampuwa water, deviating from the manufacturer's instructions.

For a midi preparation, the NucleoBond Xtra Midi Plus Kit was used according to the manufacturer's instructions. Plasmid DNA was released from the *E. coli* cells by alkaline lysis and purified by anion

exchange chromatography followed by isopropanol precipitation. DNA was eluted in Ampuwa water, deviating from the manufacturer's instructions.

3.2.7 Concentration determination of DNA

DNA concentration was measured with a NanoDrop Colibri+ spectrophotometer. The sample's absorbance was measured at a wavelength of 260 nm, which corresponds to the maximum absorbance of double-stranded DNA. The concentration was calculated based on the assumption that 50 ng/µl double-stranded DNA has an absorbance of 1 at 260 nm. To obtain information about contamination with proteins or organic substances, the absorbance was also measured at 230 and 280 nm.

3.2.8 Sequencing of plasmid DNA

Sequencing of plasmid DNA was performed by the company LGC Genomics GmbH. Samples were prepared according to the company's instructions with 1 µg plasmid DNA and 20 pmol sequencing primer filled to 14 µl with Ampuwa water.

3.2.9 Generation of recombinant bacmids

For the production of recombinant bacmids, the donor plasmid pFASTBac HTB encoding the gene of interest and a gentamycin resistance was transformed into DH10EMBacY *E. coli*. This strain contains a bacmid with a kanamycin resistance and a helper plasmid encoding a transposase and a tetracycline resistance. The transposase integrates the gene of interest into the bacmid. The bacmid contains the baculovirus genome required to produce baculovirus particles, the yellow fluorescent protein (YFP) gene to track the infection in cells, and a lacZ gene, which includes the transposition site. Successful integration of the gene of interest disrupts the lacZ gene, enabling blue-white screening. DH10EMBacY *E. coli* were transformed according to Section 3.1.2 and cultivated in 150 µl SOC medium without selective antibiotics for 4 h at 37°C with shaking at 180 rpm. *E. coli* cells were plated on LB agar with selective antibiotics (7 µg/ml gentamycin, 10 µg/ml tetracycline, 50 µg/ml kanamycin), 100µg/ml BluoGal, and 40 µg/ml IPTG for blue-white screening. Plates were incubated at 37°C for 48 h, and white colonies were restreaked on fresh LB agar containing the supplements mentioned above and incubated again at 37°C for 48 h. White colonies were picked and cultivated in 4 ml LB medium with selective antibiotics overnight as described in 3.1.3. 1 ml of the culture was used for a mini preparation as described in 3.2.6. to validate the integration of the gene of interest via PCR. Bacmid DNA was isolated from the remaining 3 ml of culture by alkaline lysis using the Qiagen buffers P1 to P3, followed by isopropanol precipitation. The bacmid DNA was then washed with 70 % ethanol and resuspended in Ampuwa water.

3.3 Cell biology

3.3.1 Cultivation of adherent cell lines

Adherent mammalian cells were cultivated at 37°C and 5 % CO_2 in supplemented medium (2.4.2) in sterile cell culture flasks. Cells were passaged twice a week according to the size of the cell culture flask (Table 22). Cells were washed with 1x PBS and detached with Trypsin/EDTA. They were then resuspended in supplemented medium and either diluted 1:5 to 1:20 depending on cell density and cell line or seeded for further experiments.

Table 22: Volumes used for the cultivation of adherent mammalian cell lines depending on flask format.

Format	PBS	Trypsin/EDTA	Medium
T-25	5 ml	0.5 ml	5 ml
T-75	10 ml	1 ml	12 ml
T-175	20 ml	2 ml	20 ml

3.3.2 Transfection of adherent cell lines

3.3.2.1 Transfection of DNA

Adherent cells were transfected with DNA by lipid-based transfection with Lipofectamine 2000 or by polymer-based transfection with PEI.

Cells were seeded 24 h before transfection. Transfection reagent Lipofectamine 2000 or PEI was used at a ratio of 2 µl for 1 µg DNA. A DNA mix and a transfection reagent mix were prepared in the same volumes (Table 23). The DNA mix contained the DNA diluted in OptiMEM. The transfection reagent mix contained the transfection reagent diluted in either OptiMEM (Lipofectamine 2000) or DMEM (PEI). The DNA mix and the transfection reagent mix were mixed gently, and the transfection mix was incubated for up to 15 min at room temperature. Medium was removed from the cells and fresh medium (OptiMEM or DMEM) was added. The transfection mix was added dropwise onto the cells. After 4 to 5 h incubation at 37°C and 5 % CO_2, the transfection mix was removed and supplemented medium was added.

Table 23: Volumes used for the transfection of mammalian cell lines depending on the format.

Format	Transfection mix	Medium
96-well plate	20 µl	40 µl
24-well plate	100 µl	200 µl
6-well plate	500 µl	1 ml
100 mm dish	1 ml	5 ml

3.3.2.2 Transfection of siRNA

Adherent cells were transfected with siRNA by lipid-based transfection with Lipofectamine RNAiMAX. If not stated otherwise, cells were seeded in 24-well plates with 0.8 x 10^5 cells/well in 500 µl medium only supplemented with FBS and transfected after 4 h. The transfection mix was prepared according to the manufacturer's instructions with 1.5 µl Lipofectamine RNAiMAX and 10 pmol siRNA per well. After 10 min incubation at room temperature, the transfection mix was added dropwise to the cells.

3.3.3 Lysis of adherent cells

Adherent cells were lysed using detergent-based lysis methods. Cells were washed with 1x PBS and lysed for 10 to 20 min at 4°C with 100 µl lysis buffer in a 24-well format or 500 µl lysis buffer in a 6-well format. If the cell lysate was later used in a luciferase reporter assay (3.4.11), passive lysis buffer was used. Otherwise, self-made lysis buffer containing non-ionic detergent Triton X-100 was used.

3.3.4 Cultivation of insect cells

Insect cells were cultivated at 27°C and 150 rpm as suspension cultures in supplemented medium (2.4.2). Cells were passaged twice a week and diluted to 0.5 x 10^6 cells/ml.

3.3.5 Cell viability assay

To determine cell viability, the CellTiter-Glo 2.0 assay was used. This assay is based on the quantification of ATP, which indicates the presence of metabolically active cells. The Ultra-Glo™ Luciferase catalyzes the mono-oxygenation of luciferin in the presence of ATP, Mg^{2+}, and O_2. The luminescent signal is proportional to the number of viable cells and can be detected with a luminometer.

CellTiter-Glo 2.0 reagent was added to the cells equal to the volume of medium present in each well. The plates were incubated for 12 min at room temperature, gently shaking to induce cell lysis and stabilization of the luminescent signal. Luminescence was recorded using a Tecan Spark reader with an integration time of 150 ms/well.

3.4 Protein biochemistry

3.4.1 Recombinant protein expression in *E. coli*

The *E. coli* strains BL21-Gold (DE3), Rosetta 2 (DE3), and Rosetta 2 pLysS (DE3) were used for recombinant protein expression. These strains carry the T7 RNA polymerase gene controlled by the lacUV5 promoter, enabling IPTG-inducible expression of T7 RNA polymerase and thus expression of T7-controlled genes.

Competent *E. coli* cells were transformed and cultivated overnight in selective LB medium as described in Sections 3.1.1 and 3.1.3. The overnight culture was diluted 1:100 into TB medium with selective antibiotics and incubated at 37°C with shaking at 180 rpm. Growth was monitored by measuring the optical density at 600 nm. Once the optical density reached a value between 0.8 and 1, protein expression was induced with 0.05 mM IPTG. The temperature was lowered to 17°C and the cultures were incubated for 16 to 18 h. Cells were harvested by centrifugation for 15 min at 6,000 x g and 4°C. The supernatant was discarded and the cell pellet was stored at -20°C until further use.

3.4.2 Recombinant protein expression in insect cells

High Five cells were used for recombinant protein expression in insect cells. To identify optimal expression conditions, small-scale test expressions were performed in 50 ml cultures with 0.5 x 10^6 cells/ml. Cells were infected with 0.25 % and 0.5 % (v/v) baculovirus particle-containing supernatant P_1 (see Section 3.5.9) and YFP fluorescence was monitored. Each day, 1 x 10^6 cells were harvested and analyzed by SDS polyacrylamide gel electrophoresis (SDS-PAGE) (3.4.7) to find the optimal virus amount and incubation time for large-scale expression. Large-scale expressions were performed in 600 ml with 0.5 cells/ml. Cells were infected with P_1 and incubated for the number of days given by the test expressions, which was 2 days for the DDX proteins. Cells were harvested by centrifugation for 15 min at 1,000 x g and 4°C and the pellet was stored at -20°C.

3.4.3 Cell lysis of *E. coli* and insect cells and protein extraction

Frozen *E. coli* or insect cell pellets (3.4.1 and 3.4.2) were thawed and resuspended in 5 ml protein-specific lysis buffer per 1 g pellet. *E. coli* cells were lysed by three cycles of sonication, lasting 30 seconds to 5 min, depending on the sample volume, while being continuously cooled in ice water. To separate unbroken cells, lipids, and insoluble components from the protein solution, the lysate was centrifuged for 25 min at 28,000 x g and 4°C. Insect cells were lysed by four cycles of sonication, lasting 30 seconds to 5 min. The lysate was centrifuged twice for 25 min at 28,000 x g and 4°C.

3.4.4 Chromatography methods for protein purification

In protein purification, specific properties of the target protein are used to separate it from other proteins. Proteins were purified from cell lysate supernatants (3.4.3) using different chromatography methods, including affinity chromatography and size exclusion chromatography (SEC).

3.4.4.1 Affinity chromatography

Affinity chromatography exploits specific interactions between a protein marked with an affinity tag and an immobilized ligand. Although different affinity tags exist, the purification protocols follow the same principle. Affinity tags used in this project are described in Table 24.

The cell lysate supernatant that contained the tagged target protein was incubated with an appropriate column volume (CV) of matrix for 1 h at 4°C, allowing the binding of the target protein. The appropriate CV was chosen according to the binding capacity of the matrix and the expected target protein yield. If not stated otherwise, the matrix was washed with 5x 10 CV washing buffer and the target protein was eluted with 4x 5 CV elution buffer containing a specific eluent. Samples from each step were analyzed by SDS-PAGE (3.4.7). The elution fractions were then either subjected to further purification steps or the protein was concentrated (3.4.9), flash frozen in liquid nitrogen, and stored at -80°C.

Table 24: Properties of different affinity tags.

Tag	Size	Binding matrix	Eluent
His	0.8 kDa	Ni^{2+}-NTA agarose	Imidazole
Glutathione S-transferase (GST)	26 kDa	Glutathione sepharose	Reduced L-glutathione
StrepII	8 kDa	Strep-Tactin sepharose	Biotin

3.4.4.2 Size exclusion chromatography

In SEC, proteins are separated according to their hydrodynamic radius using a porous matrix. Large proteins pass the column faster than smaller ones, as they do not get retained by the small pores and therefore follow a shorter path through the column.

For preparative SEC, either the HiLoad 16/60 200 prep grade column on the ÄKTA prime plus or the Superdex 200 Increase 10/300 GL column was used on the ÄKTA pure. The columns were equilibrated with degassed SEC buffer and 2 ml or 0.5 ml of concentrated protein solution was loaded onto the column. The run was performed at a maximum flow rate of 0.5 ml/min and the elution fractions that contained the target protein were concentrated (3.4.9), flash frozen in liquid nitrogen, and stored at -80°C.

3.4.5 Purification of the LASV L protein

Purified LASV L (Ba289) was kindly provided by Carola Busch. It was expressed in insect cells with a baculovirus expression system and purified by Strep-Tactin-XT Superflow affinity chromatography via an internal StrepII tag after amino acid residue 407 (StrepII 407) followed by heparin affinity chromatography and SEC (80).

3.4.6 Determination of protein concentration

The concentrations of protein solutions were determined photometrically using a NanoDrop Colibri+. The absorbance was measured at a wavelength of 280 nm, which is the absorption maximum of aromatic amino acids. The protein concentration was calculated from the absorbance using Lambert-Beer's law. The protein-specific extinction coefficient was determined using the program ProtParam and was included in the calculation.

3.4.7 SDS polyacrylamide gel electrophoresis and Coomassie staining

In SDS-PAGE, proteins are separated according to their molecular weight (MW). The anionic surfactant SDS denatures proteins into their primary structure and gives them a net negative charge proportional to their MW. Addition of DTT or β-mercaptoethanol to the protein samples disrupts disulfide bonds. The negatively charged denatured proteins migrate in an electric field through a polyacrylamide matrix and can be visualized by Coomassie staining.

Samples were mixed with 4x SDS sample buffer and boiled for 5 min at 95°C to accelerate denaturation. The stacking gel contained 4 % acrylamide, while the acrylamide concentration of the resolving gel was chosen between 8 and 15 %, depending on the MW of the target protein. The SDS gel was placed in an electrophoresis chamber filled with 1x SDS running buffer. The SDS gel was loaded with the samples together with an MW marker and run at 100 to 200 V for 60 to 90 min. After the run, Coomassie staining was performed to visualize the proteins. Therefore, the SDS gel was washed 3x 10 min in water to remove the SDS and stained for at least 10 min in Safe Stain solution. The SDS gel was then destained in water.

3.4.8 Western Blot

In western blot (WB), proteins are transferred from an SDS gel to a nitrocellulose membrane by applying an electric field, where they are specifically detected by immunostaining. All materials (paper, sponges, nitrocellulose membrane) were soaked in transfer buffer. Together with the SDS gel, they were stacked in the Xcell II Blot Module or Mini Gel Tank Blot Module, according to the manufacturer's instructions. The transfer was performed at 30 V for 45 min. The proteins transferred

to the membrane were stained with Fast Green staining solution for 5 min and the membrane was destained in water. Unspecific antibody sites were blocked by incubating the membrane in Roti Block blocking solution at 4°C overnight or at room temperature for 1 h. The membrane was incubated with a specific primary antibody for the target protein at 4°C overnight or at room temperature for 1 h and washed in PBST for 3x 10 min. The membrane was then incubated with an HRP-coupled secondary antibody at 4°C overnight or at room temperature for 1 h and washed in PBST for 3x 10 min. The membrane was then incubated with HRP-substrate Clarity or Clarity Max for 1 to 3 min at room temperature, and the light emitted by the HRP-reaction was detected with the chemiluminescence documentation system.

3.4.9 Concentration of protein solutions

To increase the concentration of protein solutions, Amicon Ultra filter units were used according to the manufacturer's instructions with an MW cutoff suitable for the target protein. The volume of the protein solution was reduced by repeated short centrifugation cycles at 2,000 to 4,000 x g and 12°C. This method was also used to exchange the buffer of a protein, by repeated dilution of the concentrated protein solution in a new buffer.

3.4.10 Assays to study protein-protein interaction

3.4.10.1 Co-immunoprecipitation assay

Co-immunoprecipitation (Co-IP) is a technique that can be used to study protein-protein interactions by capturing target proteins with specific antibodies. Interacting proteins in complex with the target protein are also captured and can be detected. It is particularly suitable for the detection of high-affinity and stable interactions.

Co-IP assays were performed with HEK293T cells, which were seeded in 6-well plates with 3.5 x 10^5 cells/well in 2 ml DMEM 5 %. If not stated otherwise, cells were transfected 24 h after seeding with 1 µg DNA per plasmid encoding the proteins of interest under the control of RNA polymerase II promoters with polymer-based transfection according to 3.3.2.1. Bunyavirus L proteins were expressed with a C-terminal FLAG tag (C-FLAG), except LASV L, which was expressed with an internal FLAG tag after amino acid residue 407 (FLAG 407). Host proteins and controls were expressed with an N-terminal myc tag (N-myc). In conditions where only one protein should be expressed, an empty plasmid (pCAGGS) was added so that the total amount of transfected DNA was always 2 µg. 48 h after transfection, the cells were detached, resuspended in medium, and centrifuged for 5 min at 500 x g and room temperature. The supernatant was discarded and the cell pellet was washed in 1 ml PBS. The suspension was centrifuged again for 5 min at 500 x g and room

temperature and the supernatant was discarded. For cell lysis, the cell pellet was resuspended in 500 µl lysis buffer (2.7.2) and incubated for 20 min at 4°C, gently shaking. To separate unbroken cells, lipids, and insoluble components from the protein solution, the lysate was centrifuged for 10 min at 12,000 x g and 4°C. The supernatant was mixed with 1.5 µg α-myc antibody and incubated for 1 h at 4°C, gently shaking, allowing the antibody to bind the target protein. Subsequently, 12.5 µl equilibrated protein A sepharose was added and the mixture was incubated for 2 h at 4°C, gently shaking, allowing the protein A sepharose to bind the Fc region of the antibody. The sepharose was washed with 5x 500 µl washing buffer (2.7.2) by centrifuging for 1 min at 5,000 x g at 4°C, discarding the supernatant after every round. Proteins and antibodies bound to sepharose were eluted by adding 50 µl 4x SDS sample buffer (2.7.1) and incubating at 95°C for 3 min. The elution was separated from the sepharose by centrifuging for 1 min at 5,000 x g at 4°C. Samples of the input (supernatant after centrifugation of the lysate) and the elution were analyzed via SDS-PAGE (3.4.7) and WB (3.4.8).

3.4.10.2 Mass photometry

Mass photometry enables the analysis of biomolecules at a single-particle level. It measures the light scattered by particles and uses the signal to quantify the particles and determine their mass. Measurements are performed in solution and are compatible with a wide range of buffers. (174)

Mass photometry was used to study complex formations of purified proteins. Therefore, immersion oil was applied to the objective and a coverslip with a 6-well silicon gasket was placed on the microscope stage. 18 µl buffer was added to the well and the objective was focused and locked. For calibration, 1 µl of NativeMark Unstained Protein Standard was diluted in 49 µl buffer. 2.5 µl of the dilution was added to the buffer, mixed, and data were acquired for 1 min. Contrast values were converted to molecular masses using the calibration function. To measure a sample, 2 µl of a 500 nM protein solution was added to the 18 µl of buffer and mixed to obtain a final protein concentration of 50 nM, and data was acquired for 1 min.

3.4.11 Minireplicon assay and luciferase reporter assay

Minireplicon systems are reverse genetic systems that can be used to study viral transcription and genome replication without the production of infectious viral particles and therefore under biosafety level (BSL)-2 conditions. In this work, minireplicon systems for LASV (Ba366) (67) and RVFV (68) were employed. The LASV minireplicon system consists of the LASV NP and L as well as the LASV minigenome (MG). The LASV MG is based on the LASV small genome segment, but instead of the viral genes, it contains reporter genes, including the Renilla Luciferase (RLuc). The RVFV

minigenome system contains the RVFV NP and L and the RVFV MG, which is based on the RVFV small genome segment, with the viral genes being exchanged to reporter genes, including the RLuc. The LASV and RVFV MGs contain the genome ends and the IGR of the respective small genome segment. The corresponding L, NP, and MG form the RNP complexes, which lead to viral transcription and genome replication of the MG and thereby to the expression of the reporter gene RLuc. An inactive L mutant serves as a negative control. The LASV and RVFV minireplicon assays were performed in Huh7 cells. As the constructs are under the control of a T7 promoter and Huh7 cells do not express the T7 RNA polymerase, a plasmid with T7 RNA polymerase under the control of the CAG promoter was transfected. Firefly Luciferase (FLuc) was transfected as a control for the transfection efficiency.

Cells were seeded 24 h before transfection in 24-well plates with 0.7 x 10^5 cells/well. They were transfected with lipid-based transfection as described in Section 3.3.2.1 with the components of the respective minireplicon system as shown in Table 25 and Table 26. 48 h after transfection, FLuc and RLuc activity were detected sequentially with the Dual-Luciferase Reporter Assay System according to the manufacturer's instructions. The cells were washed once with 0.5 ml PBS and lysed for 10 min in 100 µl passive lysis buffer at room temperature, gently shaking. 10 µl lysate was mixed with 50 µl luciferase assay reagent II containing the substrate of FLuc, beetle luciferin. FLuc activity was measured with a luminometer in relative light units (RLU). The reaction was quenched by adding 50 µl of Stop and Glo®, mixing thoroughly. Stop and Glo® also contains coelenterate luciferin, the substrate of RLuc, which allows subsequent measurement of RLuc activity with a luminometer in RLU. The RLuc activity in RLU was corrected by dividing by the square root of the FLuc activity in RLU, resulting in standardized RLU (sRLU).

Table 25: Components of the LASV minireplicon system in Huh7 cells.

Component	Amount of DNA per well
pLAS MG	250 ng
pCITE LASV L	250 ng
pCITE LASV NP	250 ng
pCITE FLuc	10 ng
pCAGGS T7	500 ng

Table 26: Components of the RVFV minireplicon system in Huh7 cells.

Component	Amount of DNA per well
pRVFV MG	750 ng
pCITE RVFV L	250 ng
pCITE RVFV NP	500 ng
pCITE FLuc	10 ng
pCAGGS T7	500 ng

3.5 Virology

3.5.1 Virus cultivation

For the cultivation of LASV and RVFV, cells were seeded 24 h before infection with 1x 10^6 cells per T75 flask. The medium was discarded and cells were infected with an MOI of 0.01 in 5 ml medium per T75 flask if the titer was unknown. After 1 h incubation at 37°C and 5 % CO_2, the inoculum was removed and 15 ml of supplemented medium was added.

For the cultivation of ANDV and HTNV, cells were seeded with 2 x 10^6 cells in a T75 flask and infected directly with an MOI of 0.01 or 100 µl per T75 flask if the titer was unknown.

Cells were incubated at 37°C and 5 % CO2 for several days (Table 27). The medium was removed and centrifuged for 5 min at 4,000 x g and 4°C. The virus-containing supernatant was aliquoted and stored at -80°C. The generation of viral particles was confirmed by immunofluorescence (IF) of the infected cells and quantified by immune focus assay (IFA), plaque assay, or 50 % tissue culture infectious dose (TCID50) assay (3.5.4 and 3.5.5).

Table 27: Conditions used for the cultivation of different viruses.

Virus	Cell line	Incubation time
ANDV	Vero E6	10 days
HTNV	Vero E6	6 days
LASV	Vero 76	5 days
RVFV	Vero 76	7 days
TCRV	Vero 76	3 days

3.5.2 Infection of adherent cells

Adherent eukaryotic cells were infected with bunyaviruses for various experiments, such as growth kinetics. If not stated otherwise, cells were infected 24 h after seeding. Medium was removed and 200 µl/well or 50 µl/well of virus inoculum was added in a 24-well or 96-well format, respectively. Cells were incubated for 1 h at 37°C and 5 % CO_2. The inoculum was removed and 1 ml/well or 200 µl/well of supplemented medium was added to the cells. Cells were cultivated for several days, depending on the experimental setup and the cell supernatants and cell lysates were harvested for further analysis.

3.5.3 Immunofluorescence of infected cells

IF was employed to detect the generation of viral particles within cells. Cells were detached and resuspended in medium during passaging (3.3.1) or with a cell scraper. Cell suspension was centrifuged at 500 x g for 5 min, the medium was removed, and the cells were resuspended in 1x PBS. The cell suspension was added to the wells of 12-well microscope slides, and medium was aspirated immediately to obtain a monolayer of cells on the slide. Cells were dried for 20 min and were then inactivated and fixed in acetone for 30 min. Slides were dried for 30 min and either stored at -20°C or stained immediately. A virus-specific primary antibody was diluted in PBS (2.14) and 15 µl were added to each well of the slide. Slides were incubated in a wet chamber at 37°C for 1 h and then washed with 1x PBS for 5 min. A suitable fluorophore-coupled secondary antibody was diluted in PBS together with Evans Blue (2.14) for whole cell staining, and 15 µl was added to each well. Slides were incubated in a wet chamber at 37°C for 1 h and then washed with 1x PBS for 5 min. The fluorescent signal was assessed with a fluorescence microscope.

3.5.4 Virus titer determination by immune focus assay and plaque assay

Cells were seeded 24 h before infection in 24-well plates with 1 x 10^6 cells/ plate. Cells were infected with 200 µl/well with serial dilutions of a virus-containing sample. The inoculum was removed after 1 h of incubation at 37°C and 5 % CO_2. Cells were coated with 1 ml/well overlay medium and incubated for several days at 37°C and 5 % CO_2 (Table 28). Overlay medium was discarded and cells were fixed and inactivated for 30 min in formalin (1x PBS with 4.5 % (v/v) formaldehyde). Plates were transferred to the BSL-2 lab, removed from the formalin, and washed 3x in water.

Table 28: Conditions for the titration of different viruses.

Virus	Cell line	Incubation time	Overlay medium
LASV	Vero 76	5 days	400 cP
RVFV	Vero E6	7 days	4000 cP
ANDV	Vero E6	12 days	4000 cP
HTNV	Vero E6	12 days	4000 cP
TCRV	Vero 76	5 days	400 cP

The number of infectious viral particles was determined using IFA for non-cytopathic viruses (LASV, ANDV, HTNV) and TCRV or plaque assay for RVFV.

For IFA, cells were permeabilized with 200 µl/well permeabilization buffer for 30 min at room temperature. Cells were washed 3x with water and 200 µl/well IFA blocking buffer was added for 1 h at room temperature or overnight at 4°C. Cells were washed 3x with water and 200 µl/ well virus-specific primary antibody diluted in IFA blocking solution was added and incubated for 1 h at room temperature or overnight at 4°C. Cells were washed 3x with water and 200 µl/well HRP-coupled secondary antibody diluted in IFA blocking solution was added for 1 h at room temperature. Cells were washed 3x with water and 200 µl/well TMB-substrate was added and incubated for up to 30 min until blue foci were visible.

For plaque assay, cells were stained with 200 µl/well crystal violet solution for 10 to 20 min. Crystal violet solution was removed and cells were washed in water and dried. Plaques are visible as holes in the violet cell layer.

Foci or plaques were counted and the viral titer in focus forming units (FFU) or plaque forming units (PFU) per ml was calculated.

3.5.5 Virus titer determination by TCID50 assay

TCID50 is an endpoint dilution assay used to quantify infectious viral particles of cytopathic viruses.

24 h before infection, cells were seeded in 96-well plates with 1 x 10^6 cells/plate. 50 µl/well of serial dilutions of a virus-containing sample were added to the cells and medium. Cells were incubated for several days at 37°C and 5 % CO_2 (Table 28). Medium was discarded and cells were fixed and inactivated for 30 min in formalin (1x PBS with 4.5 % (v/v) formaldehyde). Plates were transferred to the BSL-2 lab, removed from the formalin, and washed 3x in water. Cells were stained with 50 µl/well crystal violet solution for 10 to 20 min. Crystal violet solution was removed and cells were washed in water and dried. Wells that show a cytopathic effect were counted and the viral titer in TCID50/ml was calculated using the Spearman and Kärber algorithm (175,176).

3.5.6 Production of lentiviral vectors

Replication-defective lentiviral vectors were used to integrate genes or shRNAs into the chromosomes of cells for the stable overexpression or knockdown of specific host proteins.

The production of lentiviral vectors is based on the transfection of four plasmids into a producer cell line. The transfer plasmid contains all cis-active elements that are necessary for packaging, reverse transcription, and integration of a gene or shRNA. The first packaging plasmid (pMDLg/pRRE) encodes Gag, which provides the structural proteins of the virion, and Pol, which fulfills the function of the reverse transcriptase, integrase, and protease. The second packaging plasmid (pRSV-Rev) encodes Rev, a regulatory protein that facilitates the export of viral RNA transcripts from the nucleus. The third packaging plasmid (phCMV-VSV-G) encodes the vesicular stomatitis virus (VSV) glycoprotein, which allows a broad spectrum of cells to be infected. After transfection, the cells produce, assemble, and release the lentiviral vectors that can be used to transduce a target cell line (177).

For the production of lentiviral vectors, HEK293T cells were seeded in 100 mm dishes with 5 x 10^6 cells/dish. 16 h after seeding, the packaging plasmids were co-transfected with a specific transfer plasmid with the amounts shown in Table 29. For overexpression of specific host proteins LeGO-iG2 plasmids were used, which also express green fluorescent protein (GFP) and a puromycin resistance as marker genes (178). For the knockdown of specific host proteins, Mission shRNA plasmids were used, which also express a puromycin resistance as a marker gene.

Table 29: Amount of plasmid DNA transfected per 100 mm dish.

Plasmid	Amount
Transfer plasmid	10 µg
pMDLg/pRRE	5 µg
pRSV-Rev	2 µg
phCMV-VSV-G	10 µg

Cells were transfected by polymer-based transfection as described in Section 3.3.2.1 with additional 25 µM chloroquine in the medium. The medium was changed after 6 h to 8 ml supplemented medium. The supernatant containing the lentiviral vectors was harvested 24, 32, and 48 h after transfection. When LeGO-iG2 plasmids were used as transfer plasmids, cells were checked for GFP fluorescence. The supernatant was then removed, filtered through 0.45 µm syringe filters, aliquoted, and stored at -80°C. 8 ml supplemented medium was added to the cells for the harvest of the next time point.

3.5.7 Transduction of adherent cells with lentiviral vectors and puromycin selection

Cells were seeded in 24-well plates with 0.5 x 10^5 cells/well. 24 h after seeding, the medium was removed from the cells and 50 to 500 µl of lentiviral vector containing supernatant was added to the wells and filled to 500 µl with supplemented medium. Protamine sulfate was added to the wells with a final concentration of 8 µg/ml. Plates were sealed with parafilm and centrifuged for 30 min at 200 x g. Parafilm was removed and plates were incubated for 6 h at 37°C and 5 % CO_2. Plates were sealed with parafilm and centrifuged again for 30 min at 200 x g. Parafilm was removed and plates were incubated overnight at 37°C and 5 % CO_2. 24 h after transduction, the medium was removed and 1 ml/well supplemented medium was added. 48 h after transduction, puromycin selection was started by changing the medium to supplemented medium containing additional 3 µg/ml puromycin. Successful integration of the transgene or shRNA was verified by checking GFP fluorescence and by WB (3.4.8).

3.5.8 Generation of baculovirus particles

For the generation of baculovirus particles, SF21 cells were seeded in 6-well plates with 1 x 10^6 cells/well in 3 ml medium. A DNA mix and a transfection reagent mix were prepared. The DNA mix contained freshly isolated bacmid DNA (3.2.9), dissolved in 50 µl Ampuwa water and mixed with 200 µl medium. The transfection reagent mix contained 10 µl FuGene reagent diluted in 100 µl medium. The transfection reagent mix was added to the DNA mix and incubated for 5 min at room

temperature. The transfection mix was split between two wells and added dropwise to the cells. Cells were cultivated at 27°C for 72 h until fluorescence could be detected. The baculovirus particle-containing supernatant (first virus passage P_0) was centrifuged for 5 min at 500 x g and the supernatant was stored at 4°C.

3.5.9 Amplification of baculovirus particles

For the amplification of baculovirus particles, a 50 ml culture of SF21 cells with 0.5 x 10^6 cells/ml was infected with 3 ml of P_0. Infected cells were cultivated at 27°C and 150 rpm and monitored daily by counting and assessing the fluorescence. A proliferation arrest was usually reached after 72 h and the baculovirus particle-containing supernatant (second virus passage P_1) was harvested and stored at 4°C or -80°C for long-term storage.

3.6 Bioinformatics

3.6.1 Structural modeling

The structural modeling of the RVFV L protein fragment in complex with DDX17 was performed with AlphaFold 3 (179). All modeling parameters were set to default.

The structural modeling of the LASV L protein fragments in complex with host proteins was performed by Dingquan Yu of the Kosinski group at EMBL Heidelberg. Multiple sequence alignments and template alignments were computed with full-length sequences using the sequence database corresponding to AlphaFold version 2.2.0. Full-length LASV L protein was divided into 8 fragments to predict the interaction with host proteins using AlphaPulldown version 1.0.0 and AlphaFold Multimer version 2.3.0 (180). All modeling parameters were set to default.

4 RESULTS

4.1 Strategy

This work investigated the interactions between host proteins and bunyavirus L proteins. The basis for this was the previous work of Silke Olschewski-Pavlita, in which potential interaction partners of LASV L were identified.

Potential interaction partners of the LASV L were selected from extensive data sets for further investigation. The procedure and the selected proteins are described in Section 4.2.

First, the physical interactions of the selected proteins with the LASV L were validated. This was done in the cellular context using co-IP (Section 4.3). It was then tested whether these interactions could also be detected for further bunyavirus L proteins (Section 4.4).

The effect of the selected interaction partners on the bunyavirus replication cycle was investigated in cell-based assays. Viral minireplicon systems were used to study viral transcription and genome replication activity (Section 4.5), and viral infection experiments were employed to examine the entire viral replication cycle (Section 4.6). The influence of the selected interaction partners was investigated by studying the effects of their overexpression, knockdown, and knockout.

Finally, the physical interactions between the host proteins and LASV L were studied with recombinantly expressed and purified proteins outside the cellular context using mass photometry (Section 4.8).

4.2 Selection of host factors

In previous work by Silke Olschewski-Pavlita, affinity purification coupled with mass spectrometry (AP-MS) and a genetic knockout screen were performed to identify cellular interaction partners of LASV L and cellular genes that are essential for LASV replication (181). The AP-MS experiments were performed with StrepII-tagged arenavirus L proteins (LASV and LCMV) in human cell lysates and with a recombinant LASV (rLASV) with StrepII-tagged L during infection. In the AP-MS experiments with purified arenavirus L proteins, 991 potential interaction partners were identified, with 88 % overlap between the LASV and LCMV data sets. 92 of the identified interaction partners were also found in the AP-MS experiment with rLASV. The genetic knockout screen identified 106 genes that were essential for LASV replication. 19 of these genes were also found in the AP-MS data sets. The data from the AP-MS screens and the genetic knockout screen were combined with the interactome of LCMV L by Khamina et al. (182), which was generated with a recombinant LCMV (rLCMV) during infection.

This combined data set contained 1279 potential interaction partners. For further bioinformatic analysis and prioritization of the potential interaction partners, previously published interactomes of the arenavirus RNP were considered: LASV NP (Loureiro et al.) (183) and LCMV NP (Iwasaki et al.) (184). A Gene Ontology (GO) analysis of the biological processes of the combined data set showed that mRNA processing, RNP complex formation, and RNA catabolic processes were particularly enriched.

During this project, another interactome of the LASV L in the minireplicon system was published by Fang et al. (185), which was obtained by proximity-based labelling of the interaction partners followed by AP-MS. Moreover, an *in silico* pulldown using AlphaPulldown based on Artificial Intelligence (AI)-powered protein-protein interaction prediction was performed by our cooperation partners at EMBL Heidelberg (180). These two new data sets were used later in the course of this project for the prioritization and selection of potential interaction partners for further investigation.

An overview of the data sets that form the combined data set, as well as the data sets that contributed to the prioritization of the hits, is shown in Figure 6.

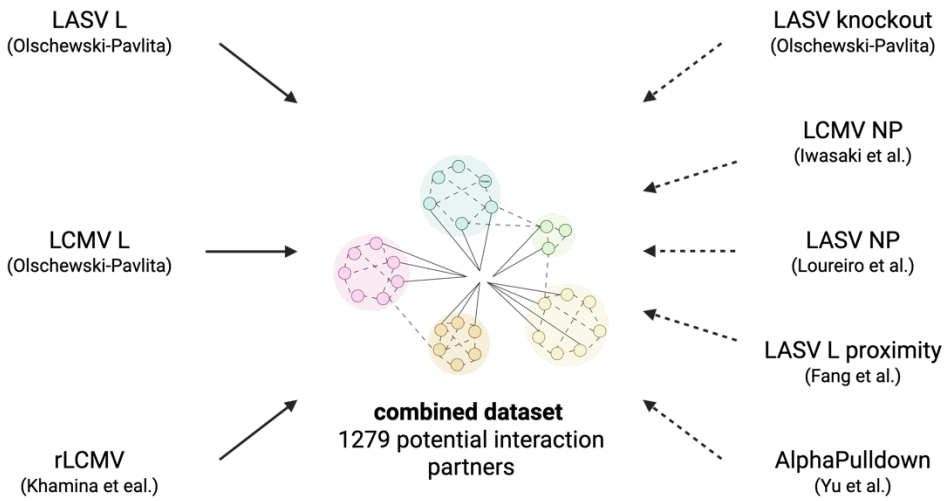

Figure 6: Composition of the combined dataset. The solid arrows indicate that the data sets have been included in the combined data set. The dashed arrows indicate that the data sets have contributed to the prioritization and selection of the hits from the combined data set.

The selection of candidates for further investigation was based on several criteria. The appearance and prioritization in the combined data set were the primary criteria. In particular, candidates that came up in the AP-MS screen with LASV L and in the genetic knockout screen were of interest, as they might not only interact with LASV L but also be essential for LASV replication. In addition, extensive literature research was carried out to obtain information on the functions, cellular localizations, and already published roles in viral infections. Practical aspects, such as the availability of plasmids, specific antibodies, and siRNAs, as well as previously published protein structures and purification protocols, were also considered.

One group of proteins that appeared abundantly and with increased prioritization in the combined data set were the proteins of the DDX family. These proteins are involved in almost all aspects of RNA metabolism, and their involvement in viral infections has been widely described. DDX17, DDX19, and DDX24 were selected for further investigation. Those proteins will be briefly described below. A more detailed description of these proteins can be found in Sections 1.4.1, 1.4.2, and 1.4.3.

DDX17 was identified as a potential interaction partner in the AP-MS screens with both LASV L and LCMV L. It was also found to be essential for LASV replication in the genetic knockout screen and appeared in the AP-MS screen with rLCMV (Khamina et al.). It was also identified in the proximity-based interactome of LASV L (Fang et al.), although it was classified as not significant ($p > 0.05$). In addition, a model of LASV L protein fragment (1398 – 1830) in complex with DDX17 was identified with AlphaPulldown as a high-confidence hit. Literature research connected DDX17 to viral infections in several studies.

DDX24 was identified in the AP-MS screens with both LASV L and LCMV L. It was also found in the genetic knockout screen with LASV and in the proximity-based interactome of LASV L (Fang et al.), although it was classified as not significant in either (p-value > 0.05). A few connections to viral infections have also been described for DDX24, but in general, it is one of the less-studied candidates.

DDX19 was identified only in the AP-MS screens with both LASV L and LCMV L. Nevertheless, it was connected to viral infections. Of particular note is a study with IAV in which DDX19 was identified as a major hit in an RNA interference (RNAi) screen and interacted with the viral polymerase (173). In addition, previous work suggested an influence of DDX19 on LASV transcription and genome replication (186).

After the publication of the proximity-based interactome of LASV L by Fang et al. (185) and the delivery of the results of the AlphaPulldown of LASV L by our cooperation partners from EMBL Heidelberg, further candidates were selected. This heterogeneous mix of possible interaction partners of the LASV L protein is briefly introduced below.

Cyclin T1 (CCNT1) was identified in the AP-MS screens with both LASV L and LCMV L. Additionally, a model of LASV L protein fragment (1-200) in complex with CCNT1 was identified with AlphaPulldown as a high-confidence hit. CCNT1 is part of the positive transcription elongation factor b, which regulates the elongation phase of transcription by RNA polymerase II (187). It is mainly localized in the nucleus.

Similar to DDX17, DDX5 was identified in the AP-MS screens with both LASV L and LCMV L and was also found in the genetic knockout screen with LASV, although it was classified as not significant (p > 0.05) and only showed one killing insertion. It was also identified in the AP-MS screen with rLCMV (Khamina et al.) and in the proximity-based interactome of LASV L (Fang et al.). In addition, a model of LASV L fragment (1398 – 1830) in complex with DDX17 was identified with AlphaPulldown as a high-confidence hit. DDX5 is the closely related paralog of DDX17 with many overlapping cellular functions. It was also connected to viral infections in several studies (158,161). It is localized both in the nucleus and in the cytoplasm.

Heterogeneous nuclear ribonucleoprotein D0 (HNRPD) was identified in the AP-MS screens with both LASV L and LCMV L, as well as in the AP-MS screens with rLASV and rLCMV (Khamina et al.). It was also identified in the proximity-based interactome of LASV L (Fang et al.), although it was classified as not significant (p-value > 0.05). HNRPD is an RNA-binding protein that controls the

stability and translation of target mRNAs by binding to AU-rich sequences within the 3' UTRs (188). It is localized both in the nucleus and in the cytoplasm.

Non-POU domain containing octamer-binding protein (NONO) was identified in the AP-MS screens with both LASV L and LCMV L, as well as in the AP-MS screens with rLASV and rLCMV (Khamina et al.). It was also found in the genetic knockout screen with LASV and in the proximity-based interactome of LASV L (Fang et al.), although it was classified as not significant (p-value > 0.05) in both and showed only one killing insertion in the genetic knockout screen. It is a multifunctional DNA and RNA binding protein involved in several nuclear processes, including participation in transcriptional and posttranscriptional regulation (189). It is mainly localized in the nucleus.

Proline- and glutamine-rich splicing factor (SFPQ) was identified in the AP-MS screens with both LASV L and LCMV L, as well as in the AP-MS screen with rLCMV (Khamina et al.). It was also identified in the proximity-based interactome of LASV L (Fang et al.), although it was classified as not significant (p-value > 0.05). It forms a heterodimer with NONO and is therefore involved in the same nuclear processes (189). It is localized both in the nucleus and in the cytoplasm.

RNA-binding protein 10 (RBM10) was identified in the AP-MS screens with both LASV L and LCMV L. Additionally, a model of LASV L protein fragment (1904 - 2077) in complex with RBM10 was identified with AlphaPulldown as a high-confidence hit. RBM10 is an RNA-binding protein that regulates the alternative splicing of transcripts (190). It is mainly localized to the nucleus.

E3 ubiquitin/ISG15 ligase TRIM25 was identified in the AP-MS screens with both LASV L and LCMV L. It was also found in the proximity-based interactome of LASV L (Fang et al.), although it was classified as not significant (p-value > 0.05). It is involved in the innate immune defense against viruses by mediating ubiquitination of RIGI (191) and also enhances the antiviral activity of ZAP (192). It is localized both in the nucleus and in the cytoplasm.

Tubulin gamma-1 chain (TUBG1) was identified in the AP-MS screens with both LASV L and LCMV L. It was also found in the proximity-based interactome of LASV L (Fang et al.), although it was classified as not significant (p-value > 0.05). Additionally, a model of LASV L fragment (700 – 1398) in complex with TUBG1 was identified with AlphaPulldown as a high-confidence hit. TUBG1 is a structural component of the cytoskeleton that is essential for microtubule nucleation and for organizing the microtubule network during cell division and intracellular transport (193).

An overview of the selected host proteins with details on their appearance in different datasets and their involvement in the top 20 biological processes of the combined dataset can be found in Table A. 3.

4.3 Validating the physical interactions of host proteins with LASV L protein in the cellular context

Physical interactions between LASV L and host proteins in the cellular context were investigated using co-IP. In co-IP, target proteins are captured and precipitated via specific antibodies. Proteins in complex with the target protein are also captured and can be detected. It is particularly suitable for the detection of stable, direct, as well as indirect interactions.

The co-IP workflow used in this work is shown in Figure 8a. FLAG-tagged LASV L and myc-tagged host proteins were overexpressed in HEK293T cells. The host protein was then immunoprecipitated using an α-myc antibody. Possible interacting proteins, such as the LASV L, were co-immunoprecipitated. The immunoprecipitated proteins were subsequently detected by WB analysis.

4.3.1 Establishment of experimental conditions for co-IP

First, the experimental conditions had to be established. In preliminary tests, four different cell lines (A549, BSR-T7, HEK293T, and Huh7) were tested for their suitability as a mammalian expression system. HEK293T cells were chosen as they were easy to transfect and yielded high levels of overexpressed protein. In addition, five different protein tags were tested (FLAG, HA, His, myc, and StrepII). The combination of a myc-tagged protein and a FLAG-tagged protein proved to be favorable. Myc- and FLAG tags are small epitope tags (10 and 8 amino acids), which minimize the risk of interfering with proper protein folding and function. Additionally, they could be reliably detected with high sensitivity and specificity in WB using the purchased antibodies and showed low background binding (186).

A FLAG-tagged LASV L gene was already available in a mammalian expression vector (Table A. 2). The genes of the host proteins first had to be cloned into a suitable mammalian expression vector. Therefore, the corresponding genes were amplified by PCR from the plasmids listed in Table A. 2. The amplified genes were inserted into the linearized pDEST-myc vector by assembly cloning as described in 3.2.5. This allowed the expression of host proteins in mammalian cells with the addition of an N-myc tag.

To optimize the precipitation conditions, different incubation times, buffer compositions, CVs, and antibody amounts were tested. For example, the optimal amount of α-myc antibody was evaluated to bind high amounts of myc-tagged host proteins and precipitate them in combination with the protein A Sepharose without overloading the samples and potentially leading to a high background. 1, 3, and 5 µg of α-myc antibody were tested as shown in Figure 7. As can be observed in the WB analysis of flowthrough and elution, more myc-tagged DDX17 could be precipitated by using higher amounts of

α-myc antibody. However, in the condition with the highest amount of α-myc antibody (5 µg), a higher background was observed in the elution. In addition, the faint band corresponding to the α-myc antibody in the flowthrough showed that not the entire amount of α-myc antibody was bound by the protein A sepharose. Based on these results and also taking into account the cost of the reagents, 3 µg of α-myc antibody was chosen as a suitable condition.

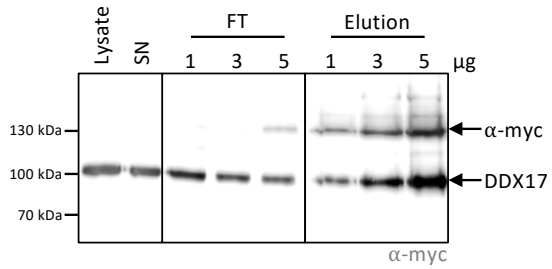

Figure 7: Optimization of antibody concentration for co-IP. WB analysis of IP performed as described in 3.4.10.1. Three wells of HEK293T cells were transfected with 2 µg DDX17 (N-myc). 48 h after transfection, cells were lysed, the lysates were combined, and the insoluble components were removed by centrifugation. The supernatant (SN) was divided again and incubated with 1, 3, or 5 µg of α-myc antibody and protein A sepharose. The flowthrough (FT) was separated from the sepharose. The sepharose was then washed and subsequently eluted with 4x SDS sample buffer without DTT or β-mercaptoethanol. Samples (15 µl) of the lysate, SN, FT, and elution were separated with an 8 % SDS polyacrylamide gel together with 3 µl of Page Ruler protein ladder as a MW marker and blotted according to Section 3.4.8. The membrane was stained with primary α-myc antibody, followed by secondary HRP-coupled α-mouse antibody. For detection, Clarity (Max) ECL chemiluminescent substrate was applied. Black arrows indicate the bands corresponding to DDX17 and α-myc antibody.

Next, suitable positive and negative controls were generated for the co-IP of LASV L. The same cloning strategy was used as previously described for the host proteins. As a positive control, LASV Z, a known interaction partner of LASV L, was cloned into the pDEST-myc vector. LASV L could be successfully co-immunoprecipitated with LASV Z. However, at 14 kDa, myc-tagged LASV Z was too small to be detected on a WB together with the significantly larger LASV L (see Figure 8). Therefore, a LASV Z with an N-terminal GST tag (LASV GST-Z) was cloned into the pDEST-myc vector to improve the technical feasibility of the positive control. LASV L could be successfully co-immunoprecipitated with LASV GST-Z, and at a size of 41 kDa, LASV GST-Z could be detected by WB together with LASV L. As a negative control, GFP was cloned into the pDEST-myc vector, which is not a known interaction partner of LASV L and has a molecular weight of 30 kDa with the N-myc tag. As expected, LASV L did not co-immunoprecipitate with GFP, making it a suitable negative control.

4.3.2 Validating the interactions of DDX proteins with LASV L protein

Physical interactions between LASV L and DDX proteins were tested in the cellular context using co-IP as described in 3.4.10.1. LASV L was expressed in HEK293T cells together with DDX17, DDX19, or DDX24. Expression of LASV L alone and with GFP served as negative controls, while expression of LASV L with LASV GST-Z served as a positive control.

As can be seen in the WB analysis of the supernatants in Figure 8b, LASV L, DDX17, DDX19, DDX24, and GFP were successfully expressed. LASV Z was not detectable in the WB analysis due to its small size (14 kDa). Nonetheless, the strong band corresponding to LASV L in the elution of the positive control condition with LASV Z indirectly confirmed its successful expression and immunoprecipitation. Together with the absence of a band corresponding to LASV L in the negative control conditions with GFP and LASV L alone, successful performance of the co-IP was confirmed.

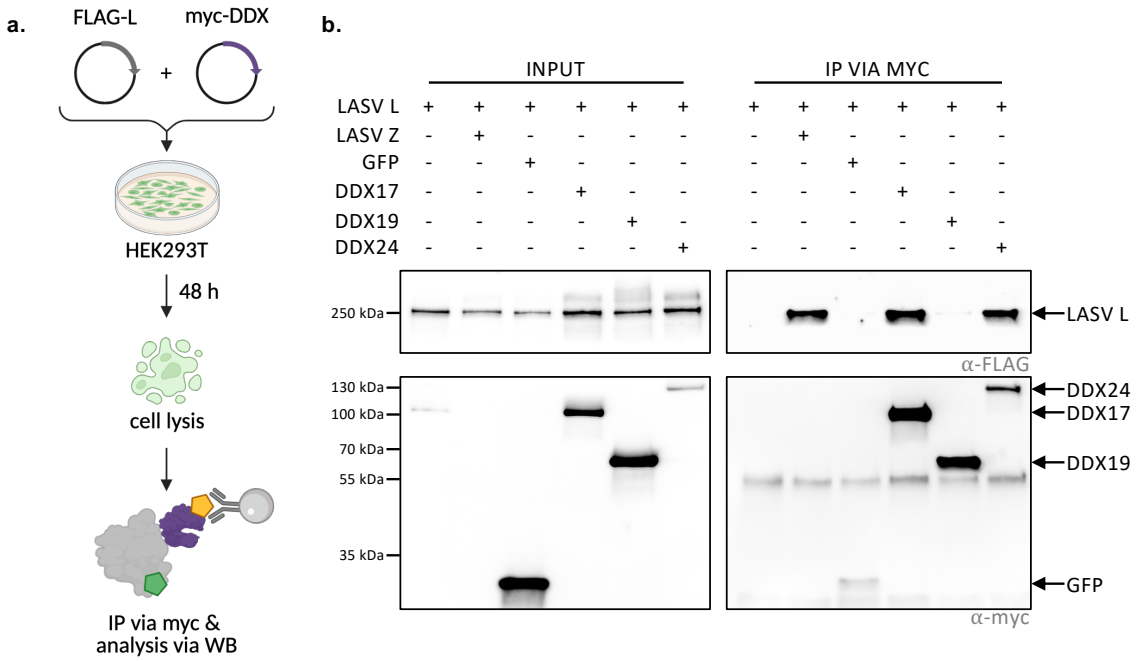

Figure 8: Co-IP of DDX17, DDX19, and DDX24 with LASV L. a. Schematic overview of the co-IP workflow. Created with BioRender.com. **b.** WB analysis of co-IP performed as described in 3.4.10.1. HEK293T cells were transfected with 1 µg LASV L (FLAG 407) and 1 µg DDX, LASV Z, or GFP (N-myc) as indicated. 48 h after transfection, cells were lysed, and the insoluble components were removed by centrifugation. The supernatant was incubated with α-myc antibody and protein A sepharose. The sepharose was washed and subsequently eluted with 4x SDS sample buffer. Samples (20 µl) of the supernatant (input) and elution (IP via myc) were separated with precast protein gels (BioRad; 10-well; any kD) together with 3 µl of Page Ruler Plus protein ladder as a MW marker and blotted according to Section 3.4.8. The membranes were split and stained with HRP-coupled α-FLAG antibody or primary α-myc antibody, followed by secondary HRP-coupled α-mouse antibody. For detection, Clarity (Max) ECL chemiluminescent substrate was applied. Black arrows indicate the bands corresponding to LASV L, DDX17, DDX19, DDX24, and GFP. LASV Z was not detectable in this experiment.

In the conditions with DDX17 and DDX24, a strong band corresponding to LASV L was detected in the elution, suggesting an interaction. In the condition with DDX19, only a very weak band corresponding to LASV L was visible. However, since a more distinct band was visible in other co-IP experiments (Figure 9, Figure A. 1), an interaction could also be assumed for DDX19.

As a side note, the distinct bands in the elution at 25 and 50 kDa correspond to the heavy and light chains of the reduced α-myc antibody used in the co-IP.

Taken together, a physical interaction between LASV L and DDX17, DDX19, and DDX24 could be validated in the cellular context with co-IP.

4.3.3 Testing the role of the enzymatic functionality of DDX proteins and nucleic acids on the interaction with LASV L protein

The interactions between the LASV L and the DDX proteins were examined in more detail. Since both the LASV L protein and the DDX proteins are RNA-binding proteins, it was investigated whether the observed interactions are nucleic acid-dependent. For this purpose, Benzonase, an endonuclease that degrades all forms of DNA and RNA (single-stranded, double-stranded, linear, and circular), was added to the co-IP lysis buffer.

In addition, it should be tested whether the enzymatic function of the DDX proteins is essential for the interaction with LASV L. DDX proteins bind and hydrolyze ATP to bind and unwind RNA and dissociate RNA-protein complexes (131). Binding of ATP and RNA also leads to a conformational change of the DDX helicase core from open to closed (132). To test the influence of the enzymatic function of the DDX proteins, a point mutation of lysine to glutamine in motif I was introduced by PCR, resulting in the ATPase mutants DDX17 K221Q, DDX24 K243Q, and DDX19 K143. This mutation is known to disrupt the binding and hydrolysis of ATP (194,195).

As can be seen in the WB analysis of the supernatants in Figure 9, LASV L, DDX17, DDX24, DDX19, as well as the respective ATPase mutants and GFP, were successfully expressed. The ATPase mutants of DDX17, DDX24, and DDX19 were expressed at comparable levels to the wildtype variants. LASV Z was not detectable in this WB analysis due to its small size (14 kDa), but the strong band corresponding to LASV L in the elution of the positive control condition with LASV Z indirectly confirmed its successful expression and immunoprecipitation. Together with the absence of a band corresponding to LASV L in the negative control conditions with GFP and LASV L alone, successful performance of the co-IP was confirmed.

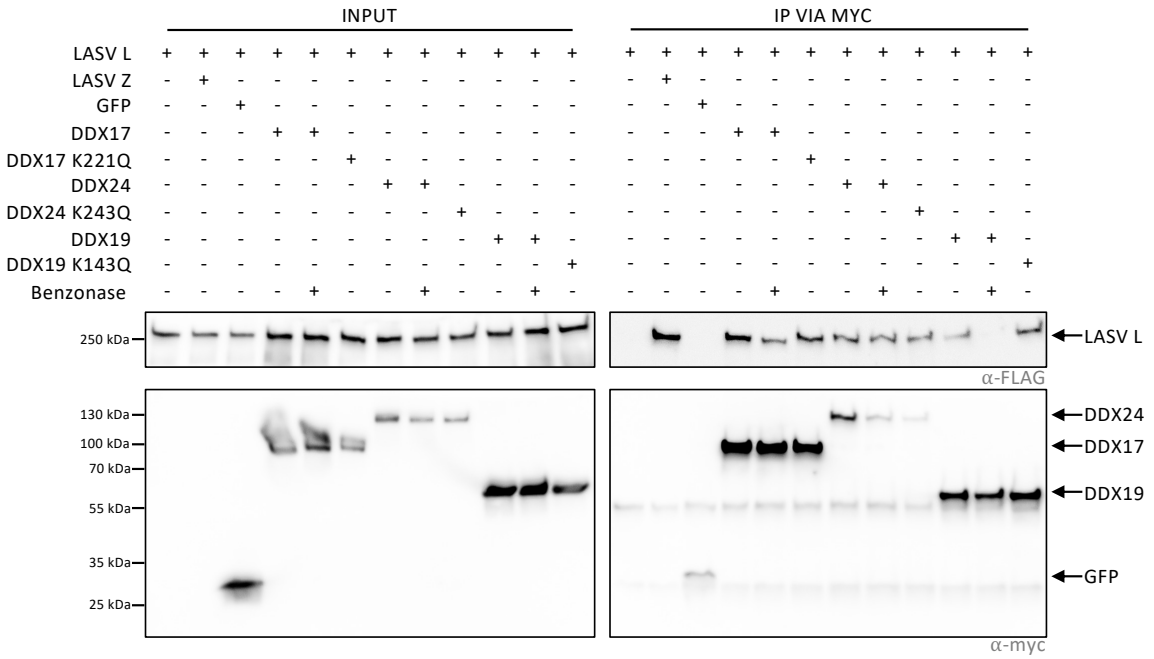

Figure 9: Co-IP of DDX17, DDX24, DDX19, and the corresponding ATPase mutants DDX17 K221Q, DDX24 K243Q, and DDX19 K143Q with LASV L with Benzonase treatment. WB analysis of co-IP performed as described in 3.4.10.1. HEK293T cells were transfected with 1 µg LASV L (FLAG 407) and 1 µg DDX, LASV Z, or GFP (N-myc) as indicated. 48 h after transfection, cells were lysed with lysis buffer (2.7.2) and partially supplemented with 200 U/ml Benzonase and 2 mM $MgCl_2$ as indicated. The insoluble components were removed by centrifugation. The supernatant was incubated with α-myc antibody and protein A sepharose. The sepharose was washed and subsequently eluted with 4x SDS sample buffer. Samples (15 µl) of the supernatant (input) and elution (IP via myc) were separated with precast protein gels (BioRad; 15-well; 4 – 15 %) together with 3 µl of Page Ruler Plus protein ladder as a MW marker and blotted according to Section 3.4.8. The membranes were split and stained with HRP-coupled α-FLAG antibody or primary α-myc antibody, followed by secondary HRP-coupled α-mouse antibody. For detection, Clarity (Max) ECL chemiluminescent substrate was applied. Black arrows indicate the bands corresponding to LASV L, DDX17, DDX19, DDX24, and GFP. LASV Z was not detectable in this experiment.

In the conditions with DDX17, DDX24, and DDX19, a distinct band corresponding to LASV L was detected in the elution, confirming the interaction that was also shown in Figure 8b. Addition of Benzonase did not change that result for DDX17 and DDX24, suggesting the interaction is not nucleic acid-dependent. However, in the condition with DDX19, no band corresponding to LASV L could be detected upon addition of Benzonase. This suggests that the interaction may occur indirectly via nucleic acids or that the nucleic acids have a structural role in the interaction by inducing conformational changes in the proteins, assuming that Benzonase also degrades already bound nucleic acids. In the conditions with the ATPase mutants, no difference could be detected compared to the wildtype proteins, suggesting that the interaction is not dependent on the enzymatic function of the DDX proteins. This co-IP experiment was performed twice with the same result (Figure 12 and Figure A. 1).

In summary, the interaction of LASV L with DDX19 was shown to be nucleic acid-dependent, while the interaction with DDX17 and DDX24 was nucleic acid-independent in co-IP. Moreover, the enzymatic function of the DDX proteins did not influence their capability to interact with LASV L.

4.3.4 Testing the interactions of DDX17 isoform 2 and core with LASV L protein

The interaction between LASV L and DDX17 was analyzed in more detail concerning the regions of DDX17 that are involved. The aim was to test whether LASV L also interacts with the shorter DDX17 (729 amino acids) isoform DDX17.2 (amino acid residues 80-729) and the core DDX17.c (amino acid residues 111-556). This experiment was particularly interesting for the further course of the project, in which the interaction between DDX17 and LASV L should also be tested with purified proteins. While the purification of full-length DDX17 from *E. coli* could not be accomplished in previous experiments (186), the purification of DDX17.2 and DDX17.c from *E. coli* had already been published (147).

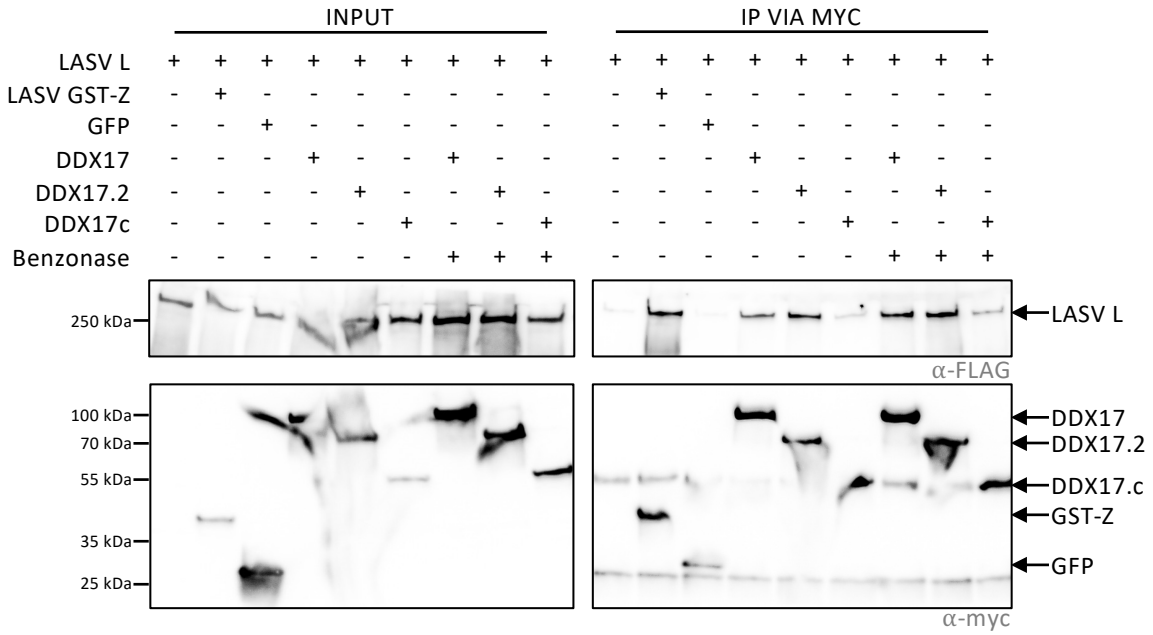

Figure 10: Co-IP of DDX17, DDX17.2, and DDX17.c with LASV L with Benzonase treatment. WB analysis of co-IP performed as described in 3.4.10.1. HEK293T cells were transfected with 1 µg LASV L (FLAG 407) and 1 µg DDX, LASV GST-Z, or GFP (N-myc) as indicated. 48 h after transfection, cells were lysed with lysis buffer (2.7.2) and partially supplemented with 200 U/ml Benzonase and 2 mM $MgCl_2$ as indicated. The insoluble components were removed by centrifugation. The supernatant was incubated with α-myc antibody and protein A sepharose. The sepharose was washed and subsequently eluted with 4x SDS sample buffer. Samples (20 µl) of the supernatant (input) and elution (IP via myc) were separated with precast protein gels (BioRad; 12-well; 4 – 15 %) together with 3 µl of Page Ruler Plus protein ladder as a MW marker and blotted according to Section 3.4.8. The membranes were split and stained with HRP-coupled α-FLAG antibody or primary α-myc antibody, followed by secondary HRP-coupled α-mouse antibody. For detection, Clarity (Max) ECL chemiluminescent substrate was applied. Black arrows indicate the bands corresponding to LASV L, DDX17, DDX17.2, DDX17.c, LASV GST-Z, and GFP.

As can be seen semi-optimally in the WB analysis of the supernatants in Figure 10, LASV L, DDX17, DDX17.2, DDX17.c, LASV GST-Z, and GFP were successfully expressed. The strong band

corresponding to LASV L in the elution of the positive control condition with LASV GST-Z, together with the absence of a band corresponding to LASV L in the negative controls with GFP and LASV L alone, confirmed the successful performance of the co-IP.

In the conditions with DDX17 and DDX17.2, distinct bands corresponding to LASV L were detected in the elution, confirming the interaction of DDX17 and LASV L (as shown before in Figure 8b, Figure 9, and Figure A. 1) and suggesting an interaction between LASV L and DDX17.2. In the elution of the condition with DDX17.c, the band corresponding to LASV L was noticeably weaker, suggesting a weaker interaction with LASV L than DDX17 and DDX17.2. Addition of Benzonase did not change these results, suggesting the interaction of LASV L with DDX17, DDX17.2, and DDX17.c was not dependent on nucleic acids.

In summary, the interaction of DDX17.2 with LASV L was comparable to DDX17, while the interaction of DDX17.c with LASV L appeared to be weaker. Concerning the question whether the expression and purification of the shorter DDX17 versions DDX17.2 and DDX17.c from *E. coli* was worthwhile to conduct interaction studies with purified proteins, the answer for DDX17.2 was positive. However, purification of DDX17.c was no longer considered, as the N- and/or C-terminal domains of DDX17 appeared to be important to stabilize the interaction with LASV L.

4.3.5 Validation of the interactions of further host proteins with LASV L protein

Of note, the experimental data in this section was generated by Malte Morische, who completed an internship under my supervision.

In addition to the DDX proteins already investigated, further host proteins were tested for interaction with LASV L. These host proteins were a heterogeneous group of proteins that were prioritized based on their occurrence in the different data sets, including CCNT1, DDX5, HNRPD, NONO, RBM10, SFPQ, TRIM25, and TUBG1 (see short description in Section 4.2).

As can be seen in the WB analysis of the supernatants in Figure 11, LASV L, CCNT1, DDX5, HNRPD, NONO, RBM10, SFPQ, TRIM25, TUBG1, and GFP were successfully expressed. In the condition with TRIM25, a double band was observed in the α-myc immunostaining in the supernatant and the elution. This can be explained by the autoubiquitination of TRIM25 (196). LASV Z was not detectable in this WB analysis due to its small size (14 kDa). However, the strong band corresponding to LASV L in the elution of the positive control condition with LASV Z indirectly confirmed its successful expression and immunoprecipitation. Together with the absence of a band corresponding to LASV L in the negative control conditions with GFP and LASV L alone, successful performance of the co-IP was confirmed.

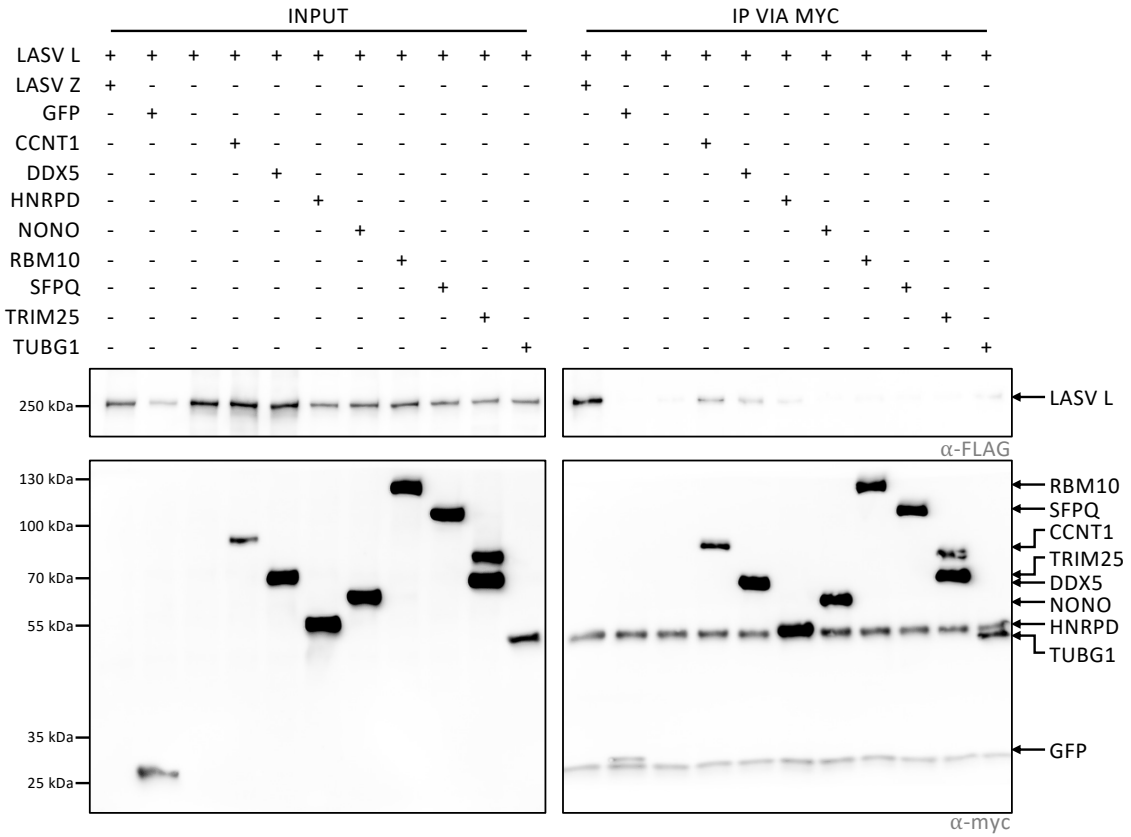

Figure 11: Co-IP of CCNT1, DDX5, HNRPD, NONO, RBM10, SFPQ, TRIM25, and TUBG1 with LASV L. WB analysis of co-IP performed as described in 3.4.10.1. HEK293T cells were transfected with 2 µg LASV L (FLAG 407) and 2 µg host protein, LASV Z or GFP (N-myc) as indicated. 48 h after transfection, cells were lysed, and the insoluble components were removed by centrifugation. The supernatant was incubated with α-myc antibody and protein A sepharose. The sepharose was washed and subsequently eluted with 4x SDS sample buffer. Samples (15 µl) of the supernatant (input) and elution (IP via myc) were separated with 8 % SDS polyacrylamide gels together with 3 µl of Page Ruler Plus protein ladder as a MW marker and blotted according to Section 3.4.8. The membranes were split and stained with HRP-coupled α-FLAG antibody or primary α-myc antibody, followed by secondary HRP-coupled α-mouse antibody. For detection, Clarity (Max) ECL chemiluminescent substrate was applied. Black arrows indicate the bands corresponding to LASV L, CCNT1, DDX5, HNRPD, NONO, RBM10, SFPQ, TRIM25, TUBG1, and GFP. LASV Z was not detectable in this experiment. The data from this figure was generated by Malte Morische.

In the conditions with CCNT1 and DDX5, a distinct band corresponding to LASV L was detected in the elution, suggesting an interaction. In the conditions with HNRPD and TUBG1, a faint band corresponding to LASV L was detected in the elution, also suggesting an interaction. This co-IP experiment was performed twice (Figure 11 and Figure A. 2). The result for CCNT1 and DDX5 could be reproduced. However, the interaction of HNRPD and TUBG1 with LASV L could not be reproduced. Although weak bands corresponding to LASV L could be detected in the elution, their intensity was comparable to the bands that also appeared in the negative control conditions (Figure A. 2). For NONO, RBM10, SFPQ, and TRIM25, no band corresponding to LASV L could be detected in either of the co-IP experiments, suggesting no interaction with LASV L under the tested conditions.

Taken together, a physical interaction between LASV L and CCNT1 and between LASV L and DDX5 could be validated in the cellular context with co-IP.

4.4 Testing the interactions of DDX17 with different bunyavirus L proteins in the cellular context

Following the validation of the interaction between LASV L and DDX17 in the cellular context using co-IP, further bunyavirus L proteins should be tested for their interaction with DDX17. In addition to LASV L as a representative of an Old World arenavirus L, representatives of the New World arenavirus (TCRV L), New World hantavirus (ANDV L), Old World hantavirus (HTNV L), and phenuivirus (RVFV L) L proteins were tested next.

4.4.1 Cloning of bunyavirus L proteins

To perform co-IP experiments with further bunyavirus L proteins, they first had to be cloned into mammalian expression vectors together with a FLAG tag.

Since there was no suitable mammalian expression vector with a FLAG tag that could be used, one was constructed. Therefore, an RVFV L gene with a C-FLAG tag should be cloned into the pCAGGS vector with suitable restriction sites so that the RVFV L gene could be easily exchanged for further bunyavirus L genes. A LASV L C-FLAG pCAGGS plasmid (Table A. 2) was used as a template for the C-FLAG tag. PCR was used to amplify the FLAG tag and 500 bp of the downstream pCAGGS backbone up to the HindIII restriction site. In this step, a short linker (GSSG) including an XhoI cleavage site was added upstream of the FLAG tag using a primer. The RVFV L gene was amplified by PCR using the RVFV L pCITE plasmid (Table A. 2) as a template, and primers were used to add overhangs. A NotI restriction site and a short fragment of the pCAGGS backbone were added upstream of the RVFV L gene. Downstream of the RVFV L gene, the short linker with an XhoI restriction site and part of the FLAG tag were added. pCAGGS vector was linearized with NotI and HindIII restriction enzymes and joined with the RVFV L gene segment and the FLAG tag segment using assembly cloning as described in 3.2.5. It was then possible to cleave the RVFV L C-FLAG pCAGGS plasmid using NotI and XhoI, thereby removing the RVFV L gene. Further bunyavirus L genes could now be amplified by PCR using the plasmids listed in Table A. 2 and inserted into the linearized C-FLAG pCAGGS vector by assembly cloning. ANDV, HTNV, and TCRV L genes were cloned into the C-FLAG pCAGGS vector by using this strategy. Since an active hantavirus endonuclease restricts its expression, endonuclease mutants were used for ANDV L (K44A) and HTNV L (D97E, K124E) (197).

As the sequences of the bunyavirus L genes are quite long at around 6.5 kb, the success rate in finding positive clones was considerably low. In addition, many sequencing reactions (3.2.8) were required to completely sequence the entire L genes and to ensure that they were complete and no

mutations had been introduced. Therefore, an alternative strategy was developed to speed up cloning and reduce costs. After transforming the assembly reaction (3.1.2) and culturing the transformed *E. coli* on LB agar (3.1.3), a larger number of single colonies was cultivated and purified (3.2.6). Instead of sending them directly for sequencing, 400 ng of plasmid DNA was transfected into HEK293T cells in a 24-well format with polymer-based transfection (3.3.2.1). After 48 h, the cells were lysed (2.7.2), centrifuged (10 min at 12,000 x g and 4°C), and the supernatant was analyzed with WB as described in 3.4.8. Consequently, the clones that generated a signal with α-FLAG immunostaining at the correct height in the WB could be identified straight away. These clones were highly unlikely to have major deletions or frameshifts, and it was possible to directly assess whether the cloned constructs were expressed and soluble. The positive clones were then sent for sequencing.

4.4.2 Interactions of DDX17 with bunyavirus L proteins

Physical interactions between DDX17 and bunyavirus L proteins were tested in the cellular context using co-IP as described in 3.4.10.1. LASV L, TCRV L, RVFV L, ANDV L, and HTNV L were expressed in HEK293T cells together with DDX17. Expression of L proteins alone served as negative controls. Additionally, LASV L was expressed together with LASV GST-Z and GFP as a positive and negative control, respectively.

As can be seen in the WB analysis of the supernatants in Figure 12, all bunyavirus L proteins, as well as DDX17, GST-Z, and GFP, were successfully expressed. Hantavirus L proteins, especially ANDV L, showed comparatively low expression, which is why double the amount of DNA was transfected in the experiment, and the WB membranes were exposed separately. The distinct band corresponding to LASV L in the elution of the positive control condition with LASV GST-Z, as well as the absence of a band corresponding to LASV L in the negative control condition with GFP, confirmed the successful performance of the co-IP.

For all tested bunyavirus L proteins, a band corresponding to the respective bunyavirus L protein was detected in the elution in the condition with DDX17. The bands were considerably stronger than in the respective negative control conditions without DDX17. This co-IP experiment was performed twice with the same result (Figure 12 and Figure A. 3).

Taken together, a physical interaction between DDX17 and different bunyavirus L proteins, including LASV L, TCRV L, RVFV L, ANDV L, and HTNV L, could be identified in the cellular context by co-IP.

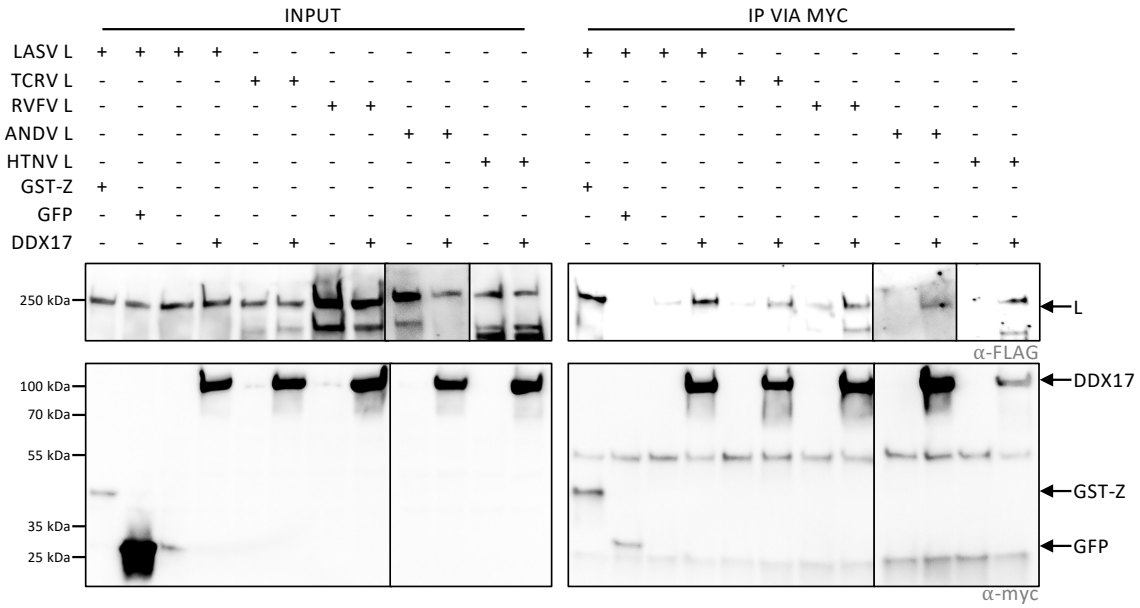

Figure 12: Co-IP of DDX17 with LASV L, TCRV L, RVFV L, ANDV L, and HTNV L. WB analysis of co-IP performed as described in 3.4.10.1. HEK293T cells were transfected with 1 µg LASV L (FLAG 407), TCRV L, RVFV L, or 2 µg ANDV L or HTNV L (C-FLAG) and 1 µg DDX17, LASV GST-Z or GFP (N-myc) as indicated. 48 h after transfection, cells were lysed, and the insoluble components were removed by centrifugation. The supernatant was incubated with α-myc antibody and protein A sepharose. The sepharose was washed and subsequently eluted with 4x SDS sample buffer. Samples (15 µl) of the supernatant (input) and elution (IP via myc) were separated with precast protein gels (BioRad; 12-well; 4 – 15 %) together with 3 µl of Page Ruler Plus protein ladder as a MW marker and blotted according to Section 3.4.8. The membranes were split and stained with HRP-coupled α-FLAG antibody or primary α-myc antibody, followed by secondary HRP-coupled α-mouse antibody. For detection, Clarity (Max) ECL chemiluminescent substrate was applied. Black arrows indicate the bands corresponding to L, DDX17, LASV GST-Z, and GFP.

4.5 Investigating the functional roles of DDX proteins in bunyavirus transcription and genome replication

Minireplicon systems were used to study the effects of DDX proteins on bunyavirus transcription and genome replication. A minireplicon system for LASV (67) and a minireplicon system for RVFV (68) were available. These minireplicon systems consist of the viral proteins NP and L as well as an MG, which contains the genome ends and IGR of the small segment with reporter genes instead of viral genes. The formation of RNPs leads to viral transcription and genome replication of the MG, resulting in the expression of the reporter gene RLuc. Those minigenome systems were originally designed to study the role of L protein residues in viral transcription and genome replication. Here, they were used to study the effects of DDX protein knockdown and overexpression on the viral transcription and genome replication processes.

4.5.1 Testing the effects of siRNA-mediated knockdown of DDX17, DDX19, and DDX24 in the minireplicon system

The effect of knockdown of DDX17, DDX19, and DDX24 on bunyavirus transcription and genome replication was investigated in the LASV and RVFV minigenome systems.

For the knockdown of DDX17, DDX19, and DDX24, siRNAs were used. These operate within the RNAi pathway, where they form the RNA-induced silencing complex (RISC) together with other factors. The binding of the siRNA to a complementary mRNA leads to its degradation and thereby silencing of the target gene (198).

Huh7 cells were transfected 4 h after seeding with two different siRNAs against DDX17, DDX19, and DDX24 as described in 3.3.2.2. Transfection of a non-targeted scrambled siRNA and mock transfection of no siRNA served as controls. 24 h after seeding, cells were transfected with the minireplicon components (3.4.11). 48 h after transfection of the minireplicon components, the reporter gene expression was measured, and the lysates were analyzed with WB to verify a successful knockdown. In addition, the influence of the siRNAs on cell viability was tested to ensure that possible effects were not caused by an unspecific cytotoxic effect.

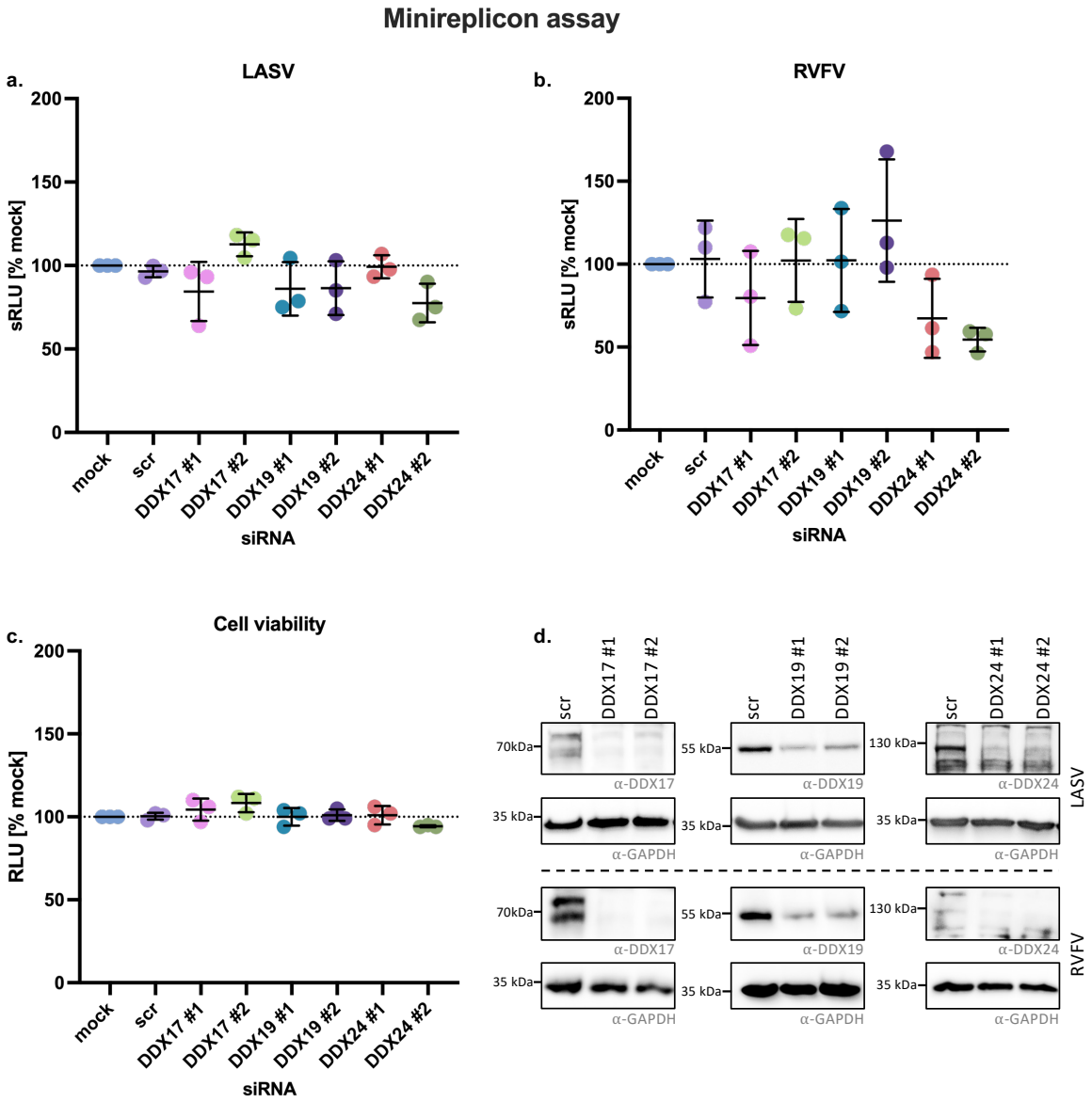

Figure 13: Effects of siRNA-mediated knockdown of DDX17, DDX19, and DDX24 on viral transcription and genome replication in the LASV and RVFV minireplicon systems. a. – b. 4 h after seeding, Huh7 cells were transfected with 10 pmol/well of two different siRNAs against DDX17, DDX19, and DDX24 as described in 3.3.2.2. Transfection of a non-targeted scrambled siRNA (scr) and no siRNA (mock) served as controls. 24 h after seeding, cells were transfected with the LASV minireplicon components (**a.**) or RVFV minireplicon components (**b.**) according to 3.3.2.1 and 3.4.11. 48 h after transfection of the minireplicon components, the FLuc and the RLuc activities were measured sequentially with the Dual-Luciferase Reporter Assay System as described in 3.4.11. RLuc activity [RLU] was corrected by dividing by the square root of the FLuc activity [RLU], resulting in standardized RLU [sRLU], and normalized to the mock siRNA-transfected control (set to 100 %). Shown are the individual values, the mean, and the standard deviation of three individual experiments. **c.** Influence of siRNA-mediated knockdown of DDX17, DDX19, and DDX24 on cell viability. Huh7 cells were seeded in a 96-well plate with 2 x 10^4 cells/well. Cells were transfected 4 h after seeding with 2 pmol/well of two different siRNAs against DDX17, DDX19, and DDX24 as described in 3.3.2.2. Transfection of a non-targeted scrambled siRNA (scr) and no siRNA (mock) served as controls. 72 h after seeding, cell viability was determined using the CellTiter-Glo 2.0 assay as described in 3.3.5. Luciferase activity [RLU] was normalized to the mock siRNA-transfected control (set to 100 %). Shown are the individual values, the mean, and the standard deviation of one individual experiment performed in technical triplicates. **d.** Representative WB analysis of cell lysates of **a.** and **b.** to verify the knockdown of DDX17, DDX19, and DDX24. 15 µl lysate was separated with 12 % SDS polyacrylamide gels together with 3 µl Page Ruler protein ladder as a MW marker and blotted according to Section 3.4.8. The membranes were split and stained with primary antibodies α-DDX17, α-DDX19, α-DDX24, and α-GAPDH as a loading control, followed by

secondary HRP-coupled α-mouse or α-rabbit antibody. For detection, Clarity (Max) ECL chemiluminescent substrate was applied.

As can be seen in Figure 13a and b, no clear effect of the knockdown of DDX17, DDX19, and DDX24 was observed compared to the scrambled control in both the LASV and RVFV minireplicon systems. Although the mean values of the individual conditions differed to some extent, those effects were mostly not consistent between the two different siRNAs targeting one DDX protein, and the variations of the individual values were quite high, especially in the RVFV minireplicon system. Only the knockdown of DDX24 with DDX24 #2 siRNA showed an effect in the LASV and RVFV minireplicon system, although it was not statistically significant (Mann-Whitney test; DDX24 #2 vs. scr; LASV $p = 0.1$; RVFV $p = 0.1$). Due to the high variation and the minor effects, it is questionable whether a possible effect could be recognized at all in this experimental setup.

The WB analysis showed that although the knockdown of DDX17, DDX19, and DDX24 worked, the target proteins were still present in the sample (Figure 13d). The investigation of the influence of siRNAs on cell viability did not reveal any pronounced cytotoxic effect (Figure 13c).

In summary, no apparent effects could be observed in the LASV and RVFV minireplicon systems upon knockdown of DDX17, DDX19, and DDX24.

4.5.2 Testing the effects of overexpression of DDX17, DDX19, and DDX24 in the minireplicon system

The effect of overexpression of DDX17, DDX19, and DDX24 and the respective ATPase mutants on bunyavirus transcription and genome replication was investigated in the LASV and RVFV minigenome system.

For the overexpression of the DDX proteins and the respective ATPase mutants, pDEST-myc plasmids were used. Overexpression of the unrelated maltose binding protein (MBP) in the pDEST-myc vector and an empty vector (pCAGGS) served as controls. 24 h after seeding, Huh7 cells were co-transfected with the minireplicon components (3.4.11) and the DDX or control plasmids. After 48 h, the reporter gene expression was measured, and the lysates were analyzed with WB to verify successful overexpression.

In addition, the influence of the overexpression of those proteins on cell viability was tested to ensure that possible effects were not caused by an unspecific cytotoxic effect.

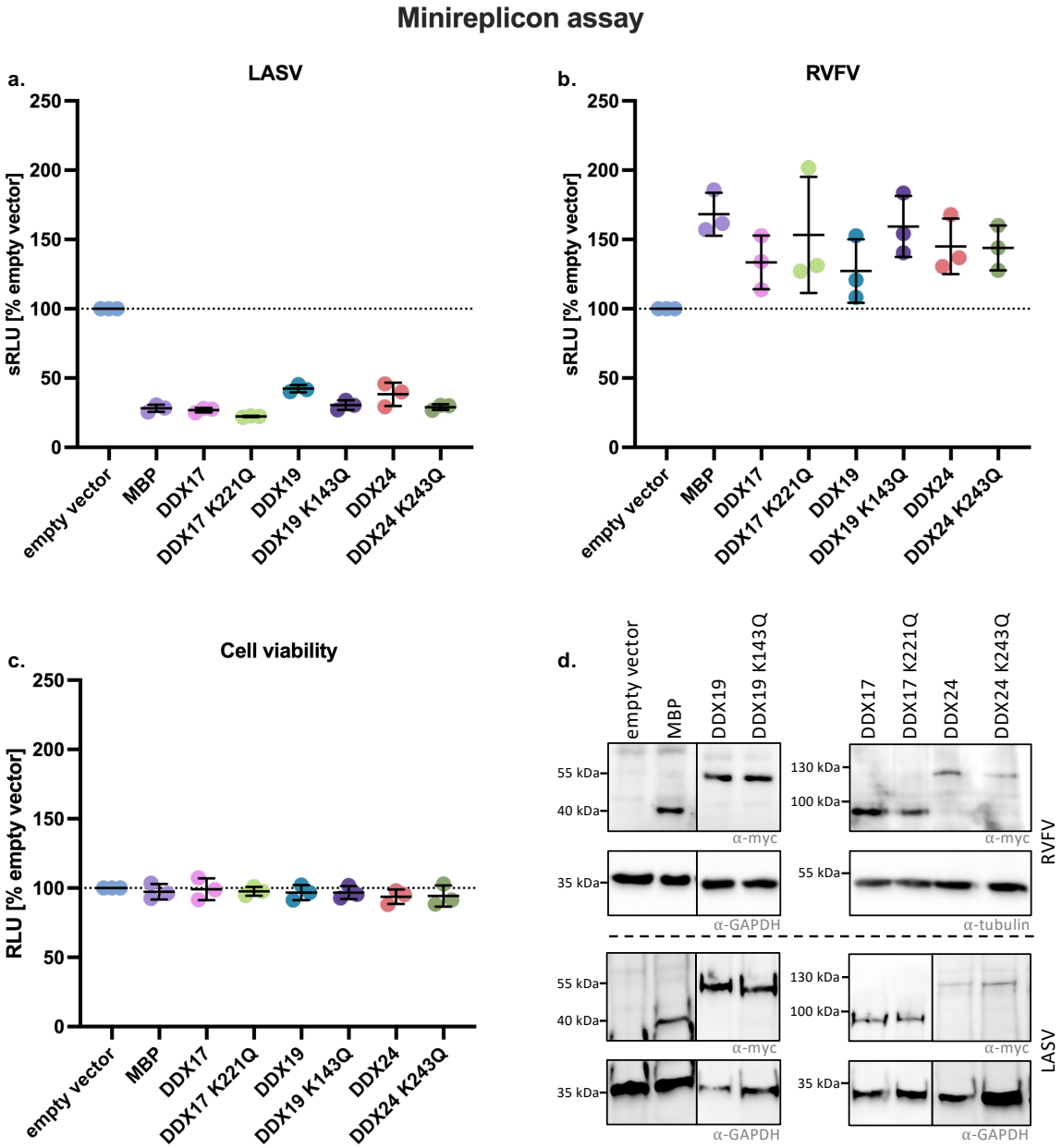

Figure 14: Effects of overexpression of DDX17, DDX19, and DDX24 and their respective ATPase mutants on viral transcription and genome replication in the LASV and RVFV minireplicon systems. a. – b. Huh7 cells were transfected 24 h after seeding with the **a.** LASV minireplicon components or **b.** RVFV minireplicon components together with 250 ng (**a.**) or 100 ng (**b.**) of DDX plasmid (N-myc) according to 3.3.2.1 and 3.4.11. Transfection of an empty vector and MBP (N-myc) served as controls. 48 h after transfection, the FLuc and the RLuc activities were measured sequentially with the Dual-Luciferase Reporter Assay System as described in 3.4.11. RLuc activity [RLU] was corrected by dividing by the square root of the FLuc activity [RLU], resulting in standardized RLU [sRLU], and normalized to the empty vector-transfected control (set to 100 %). Shown are the individual values, the mean, and the standard deviation of three individual experiments. **c.** Influence of DDX17, DDX19, and DDX24 overexpression on cell viability. Huh7 cells were seeded in a 96-well plate with 2 x 10^4 cells/well. 24 h after seeding, cells were transfected with 50 ng/well of DDX plasmid as described in 3.3.2.2. Transfection of an empty vector and MBP served as controls. 48 h after transfection, cell viability was determined using the CellTiter-Glo 2.0 assay as described in 3.3.5. Luciferase activity [RLU] was normalized to the empty vector-transfected control (set to 100 %). Shown are the individual values, the mean, and the standard deviation of one individual experiment performed in technical triplicates. **d.** Representative WB analysis of cell lysates of **a.** and **b.** to verify the overexpression of DDX17, DDX19, DDX24, and MBP (N-myc). 15 µl lysate was separated with 8 % and 12 % SDS polyacrylamide gels together with 3 µl Page Ruler protein ladder as a MW marker

and blotted according to Section 3.4.8. The membranes were split and stained with primary antibodies α-myc and α-GAPDH or α-tubulin as loading controls, followed by secondary HRP-coupled α-mouse antibody. For detection, Clarity (Max) ECL chemiluminescent substrate was applied.

As can be seen in Figure 14a, overexpression of DDX17, DDX19, and DDX24 leads to a pronounced reduction in RLuc activity in the LASV minireplicon system by more than 50 % compared to the empty vector control. However, the overexpression of MBP had a similar effect. Only the overexpression of DDX19 and DDX17 K221Q showed a more pronounced effect compared to the MBP control, with an increase of 51 % and a decrease of 21 %, respectively, when normalized to the MBP control (Figure A. 4). However, statistical testing of MBP vs. DDX19 and MBP vs. DDX17 K221Q normalized to the empty vector control showed no significant difference (Mann-Whitney test; MBP vs. DDX19 $p = 0.1$; MBP vs. DDX17 K221Q $p = 0.1$). Thus, overexpression of DDX17, DDX19, and DDX24 showed no effect compared to the MBP control.

As shown in Figure 14b, overexpression of DDX17, DDX19, and DDX24 in the RVFV minireplicon system showed the opposite effect, a pronounced increase in RLuc activity by up to 60 % compared to the empty vector control. Again, the overexpression of the MBP control had the same effect. The overexpression of DDX17, DDX19, and DDX24, therefore, showed no effect compared to the MBP control in the RVFV minireplicon system as well.

No distinct difference between the wildtype DDX protein and the corresponding ATPase mutant was observed in either the LASV or the RVFV minireplicon system, as shown in Figure A. 4. Generally, the variation of the individual values was again higher in the RVFV minireplicon system than in the LASV minireplicon system, as observed before in the knockdown experiments (4.5.1).

The WB analyses confirmed successful overexpression of DDX17, DDX19, and DDX24 and their respective ATPase mutants, as well as MBP (Figure 14d). The investigation of the influence of the overexpression on cell viability did not reveal any cytotoxic effects (Figure 14c).

In summary, no difference could be observed between the overexpression of DDX17, DDX19, and DDX24 compared to the MBP control in the LASV and RVFV minireplicon systems. However, compared to the empty vector control, overexpression in the LASV minireplicon system led to a reduction, and overexpression in the RVFV minireplicon system led to an increase in RLuc activity. No distinct difference between the DDX wildtype and ATPase mutants could be seen in any of the minireplicon systems. Since it is not known whether one of the controls is suitable for this kind of experiment and, if so, which one, no valid conclusions can be drawn from this data.

4.6 Investigating the functional roles of DDX proteins in the bunyavirus replication cycle

Infection experiments were performed to investigate the roles of DDX proteins in the bunyavirus replication cycle. In contrast to the experiments with the minireplicon systems from Section 4.5, the complete replication cycle was considered here, with the analysis being based on the quantification of infectious viral particles in the cell culture supernatants. Since the overexpression of the DDX proteins proved to be complicated in regards to the availability of suitable controls (4.5.2), the following experiments focused primarily on the effect of DDX knockdown or knockout on bunyavirus replication.

4.6.1 Testing the effects of siRNA-mediated knockdown of DDX proteins on RVFV replication

The effects of siRNA-mediated knockdown of DDX17 and DDX24 on RVFV replication were investigated. DDX19 was not investigated further based on the previous experiments, as the interaction in the co-IP assays was rather weak (4.3.2) and nucleic acid-dependent (4.3.3) compared to DDX17 and DDX24, and no apparent effects of its knockdown in the minireplicon system were observed (4.5.1).

4 h after seeding, Huh7 cells were transfected with two different siRNAs against DDX17 and DDX24 as described in 3.3.2.2. Transfection of a non-targeted scrambled siRNA and mock transfection of no siRNA served as controls. 24 h after seeding, cells were infected with RVFV with an MOI of 0.1 as described in 3.5.2. Based on published protocols of similar experiments (199), the cell supernatants were harvested after 24 h, and infectious viral particles were quantified with the TCID50 assay as described in 3.5.5. Cell lysates were analyzed with WB to verify a successful knockdown.

As can be seen in Figure 15a, the knockdown of DDX17 led to an increase in RVFV titers from 2.06 x 10^5 TCID50/ml for the non-targeted scrambled siRNA to 6.14 x 10^5 TCID50/ml for DDX17 #1 and 1.22 x 10^6 TCID50/ml for DDX17 #2. Knockdown of DDX24 led to a slight increase in RVFV titters to 5.13 x 10^5 TCID50/ml for DDX24 #1 and 3.08 x 10^5 TCID50/ml for DDX24 #2. As previously observed in the siRNA-mediated knockdown experiments in combination with the minireplicon systems (4.5.1), the variation between the individual values was quite high. Due to this variation, the individual values of the observed effects appeared to be within the normal variation of the assay. WB analyses showed that although the knockdown of DDX17 and DDX24 worked, the target proteins could still be detected in the lysates (Figure 15b).

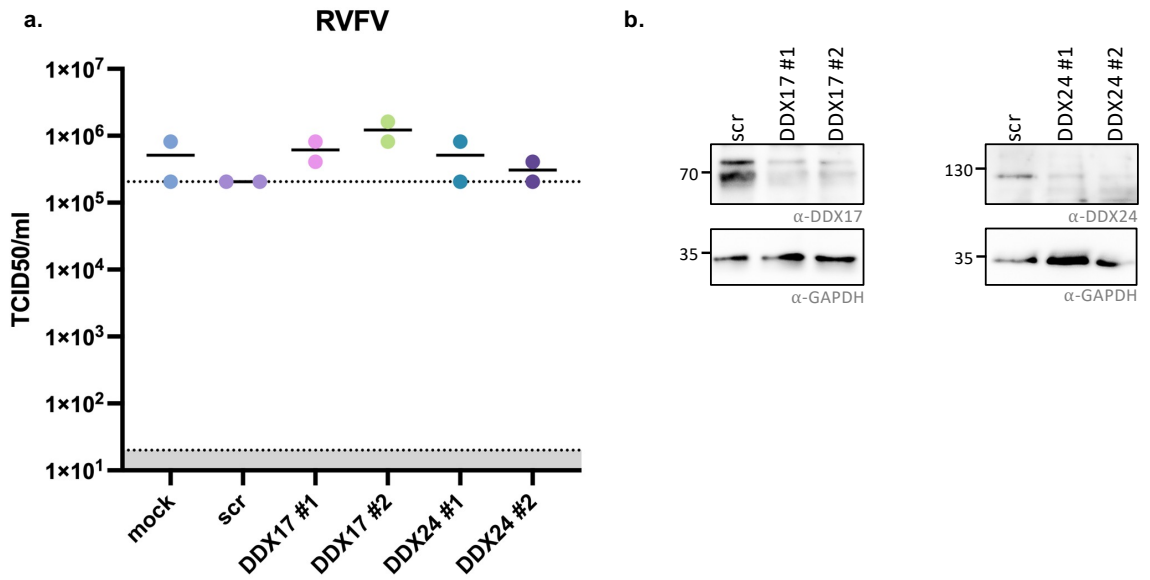

Figure 15: Effect of siRNA-mediated knockdown of DDX17 and DDX24 on RVFV replication. Huh7 cells were seeded in a 96-well plate with 0.6 x 10^6 cells/well and transfected after 4 h with 5 pmol/well of two different siRNAs for DDX17 and DDX24 as described in 3.3.2.2. Transfection of a non-targeted scrambled siRNA (scr) and no siRNA (mock) served as controls. 24 h after seeding, cells were infected with RVFV with an MOI of 0.1 according to 3.5.2. 24 h after infection, cell supernatants and lysates were harvested. The experiment was conducted once in technical duplicates. **a.** Infectious viral particles in the cell supernatant were quantified with the TCID50 assay as described in 3.5.5. Viral titers are shown as TCID50/ml with individual values and the median. The assay's limit of detection is marked by the grey area. **b.** WB analysis to verify the knockdown of DDX17 and DDX24. 15 µl lysate was separated with a 12 % SDS polyacrylamide gel together with 3 µl Page Ruler protein ladder as a MW marker and blotted according to Section 3.4.8. The membrane was split and stained with primary antibodies α-DDX17, α-DDX24, and α-GAPDH as a loading control, followed by secondary HRP-coupled α-mouse or α-rabbit antibody. For detection, Clarity (Max) ECL chemiluminescent substrate was applied.

In summary, only small effects on RVFV replication could be observed upon knockdown of DDX17 and DDX24, which seemed to be within the normal variation of the assay.

It was decided to leave this experiment at the one performed biological replicate and move on to a different knockdown strategy to achieve a higher knockdown efficiency and thereby possibly clearer results.

4.6.2 Testing the effects of stable shRNA-mediated knockdown of DDX proteins on bunyavirus replication

Bunyavirus replication was investigated in cells with DDX knockdown, achieved by the stable expression of shRNAs. For this purpose, shRNAs were integrated into the genome of the cells using lentiviral vectors. This has the advantage that the knockdown is not dependent on transfection efficiency, as it is the case with siRNAs, and should therefore be more consistent. shRNAs are processed by Dicer into siRNAs and operate within the RNA interference pathway in the same way as siRNAs, as described in Section 4.5.1.

In addition, the integration of DDX17 and DDX24 genes into the genome with lentiviral vectors was tested to evaluate the feasibility for possible overexpression experiments. The process by which the stable cell lines with DDX knockdown and overexpression were produced is described in the following section.

4.6.2.1 Generation of cell lines with stable knockdown or overexpression of DDX17 or DDX24

For the generation of cell lines with stable shRNA-mediated knockdown or overexpression of DDX17 or DDX24, replication-deficient lentiviral vectors were used to integrate shRNAs or genes into the genome of target cells. A schematic overview of the workflow is shown in Figure 16a.

First, lentiviral vectors were produced as described in Section 3.5.6. by co-transfecting HEK293T cells with four plasmids: a transfer plasmid and three packaging plasmids (pMDLg/pRRE, pRSV-Rev, and phCMV-VSV-G). For the knockdown of DDX proteins, Mission shRNA transfer plasmids were purchased, which express puromycin resistance as a marker gene. A non-targeted scrambled shRNA served as a control. For the overexpression of DDX proteins, LeGO-iG2 transfer plasmids were used, which express GFP and a puromycin resistance as marker genes.

After transfection, the cells produced, assembled, and released the lentiviral vectors into the supernatant, which was harvested at 24, 32, and 48 h post-transfection. Lentiviral vector production could be monitored via GFP fluorescence in the overexpression conditions, transfected with the LeGO-iG2 plasmids. The GFP fluorescence during production of lentiviral vectors in HEK293T cells transfected with LeGO-iG2 plasmids for the overexpression of DDX17 and DDX24, compared to a negative control in which no transfer plasmid was transfected, is shown in Figure 16b.

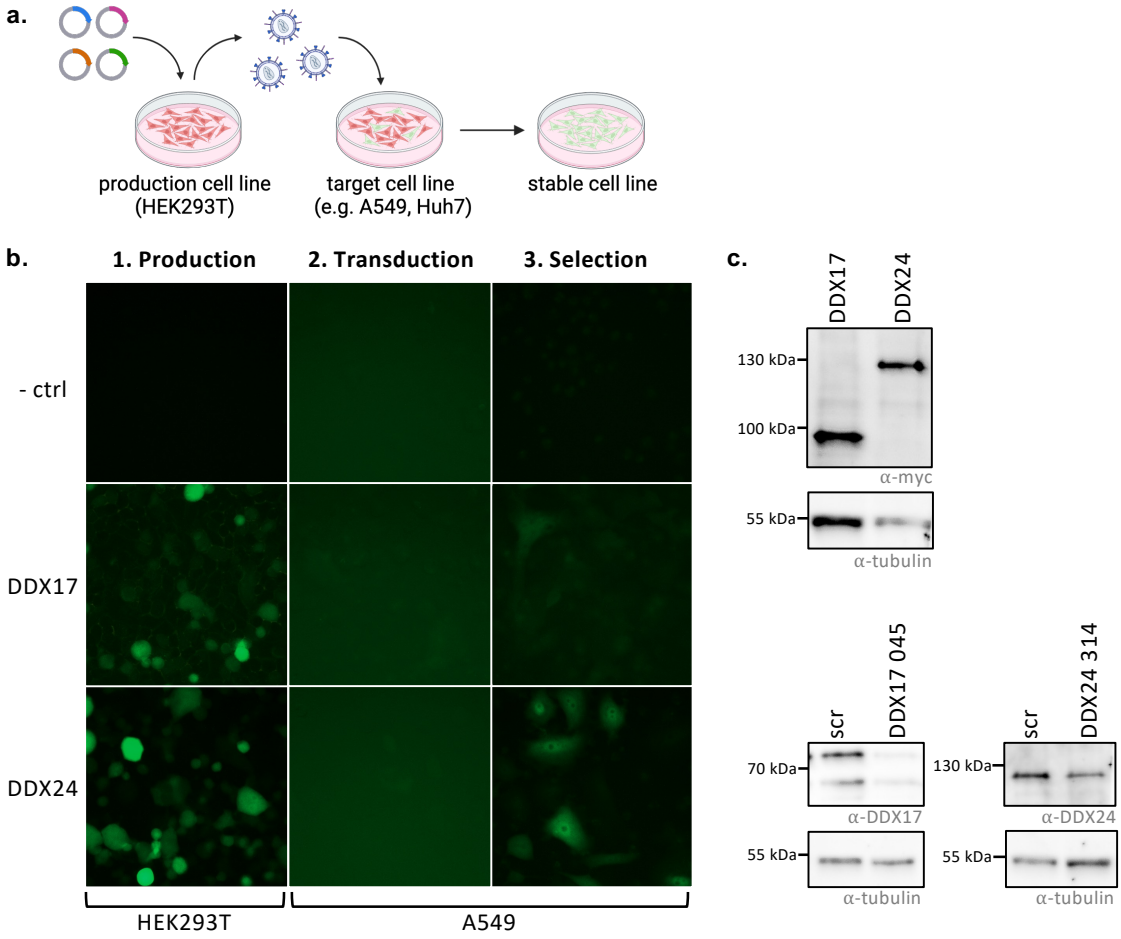

Figure 16: Lentiviral vector production and transduction for the generation of cell lines with stable overexpression or shRNA-mediated knockdown of DDX17 and DDX24. For the production of lentiviral vectors, HEK293T cells were co-transfected with packaging plasmids and specific transfer plasmids as described in 3.5.6. LeGO-iG2 plasmids were used for the overexpression of DDX17 and DDX24 (N-myc), which carry GFP and a puromycin resistance as marker genes. As a negative control (- ctrl), no transfer plasmid was co-transfected. For the knockdown of DDX17 and DDX24, shRNA plasmids (DDX17 045 and DDX24 314) were used, which carry a puromycin resistance gene. A non-targeted scrambled (scr) shRNA plasmid was used as a control. Lentiviral vector-containing supernatant was harvested at 24 – 48 h after transfection and was used for the transduction of A549 or Huh7 cells as described in 3.5.7. 48 h after transduction, puromycin selection was started. **a.** Schematic overview of the workflow for the generation of stable cell lines via lentivirus vector production and transduction. Created with BioRender.com. **b.** Detection of GFP fluorescence in HEK293T cells 40 h after transfection during lentiviral vector production for the overexpression of DDX17 and DDX24, and in A549 cells 48 h after transduction and after 5 days of selection. **c.** WB analysis to verify the integration of DDX17 and DDX24 (N-myc) genes or DDX17 045 and DDX 314 shRNAs. 15 µl lysate of A549 cells from 7 days after selection was separated with 8 % SDS polyacrylamide gels, together with 3 µl Page Ruler protein ladder as a MW marker and blotted according to Section 3.4.8. The membrane was split and stained with primary antibodies α-myc, α-DDX17, α-DDX24, and α-tubulin as a loading control, followed by secondary HRP-coupled α-mouse or α-rabbit antibody. For detection, Clarity (Max) ECL chemiluminescent substrate was applied.

Subsequently, the lentiviral vectors were used to transduce the target cell lines A549 and Huh7 to integrate the shRNA or gene into their genome for knockdown or overexpression of DDX17 or DDX24, respectively, as described in Section 3.5.7. 48 h after transduction, puromycin selection was started. Figure 16b shows the GFP fluorescence in A549 cells transduced with lentiviral vectors for the overexpression of DDX17 and DDX24 at 40 h after transfection and 5 days after the start of

puromycin selection. Especially for the overexpression of DDX24, it is visible how the GFP fluorescence increases under selection pressure. As shown in Figure 16c, WB analyses of the lysates confirmed the overexpression and the knockdown of DDX17 and DDX24, and thereby the successful integration of DDX17 and DDX24 genes as well as DDX17 045 and DDX24 314 shRNAs into the genome. Although the knockdown of DDX17 and DDX24 was visible, the target proteins could still be detected in the lysates, especially for the DDX24 knockdown.

Since overexpression proved complicated concerning the availability of suitable controls as described above (4.5.2), only the DDX17 and DDX24 knockdown cell lines were used in the following infection experiments.

4.6.2.2 Testing the effects of stable shRNA-mediated knockdown of DDX17 and DDX24 on LASV and RVFV replication

The effects of stable shRNA-mediated knockdown of DDX17 and DDX24 on LASV and RVFV replication were investigated. Huh7 cells that stably express DDX17 045, DDX24 314, or a non-targeted scrambled shRNA were infected with LASV or RVFV with an MOI of 0.01 as described in 3.5.2. Cell culture supernatants were harvested at 24, 48, and 72 h post infection, and infectious viral particles were quantified with IFA and TCID50 assay as described in 3.5.4 and 3.5.5. Cell lysates were analyzed with WB to verify a successful knockdown.

As can be seen in Figure 17a, LASV titers in the DDX17 045 shRNA knockdown cells were slightly higher after 48 h, with 7.7 x 10^5 FFU/ml, than in the scramble shRNA control cells with 3.0 x 10^5 FFU/ml. After 24 and 72 h, however, no difference was observed. LASV titers were slightly lower in the DDX24 314 knockdown cells at 48 and 72 h with 1.2 x 10^5 FFU/ml and 9.7 x 10^4 FFU/ml compared to the scrambled shRNA control cells with 3.0 x 10^5 FFU/ml and 5.5 x 10^5 FFU/ml, respectively. WB analysis of the lysates of the LASV infection confirmed a knockdown of DDX17 and DDX24, but the proteins could still be detected (Figure 17c).

For RVFV, titers in the DDX17 045 shRNA knockdown cells were increased by one log unit at 24 and 48 h with 6.3 x 10^6 TCID50/ml and 3.5 x 10^8 TCID50/ml compared to the scrambled shRNA control cells with 6.3 x 10^5 TCID50/ml and 3.5 x 10^7 TCID50/ml, respectively, as shown in Figure 17b. After 72 h, however, no difference was observed. RVFV titers were increased in the DDX24 314 knockdown cells at 24 h with 3.5 x 10^6 TCID50/ml compared to the scrambled shRNA control cells with 6.3 x 10^5 TCID50/ml, but no difference was visible at 48 and 72 h. WB analysis of the lysates of the RVFV infection did not confirm a knockdown of DDX17 and DDX24 as the proteins could be detected in comparable amounts to the scrambled shRNA control (Figure 17d). It is possible that the

knockdown of DDX17 and DDX24 was not stable over time despite the maintenance of selection pressure, as RVFV infection was carried out at a higher cell passage than LASV infection. Alternatively, RVFV infection itself could have led to an increased expression of these proteins.

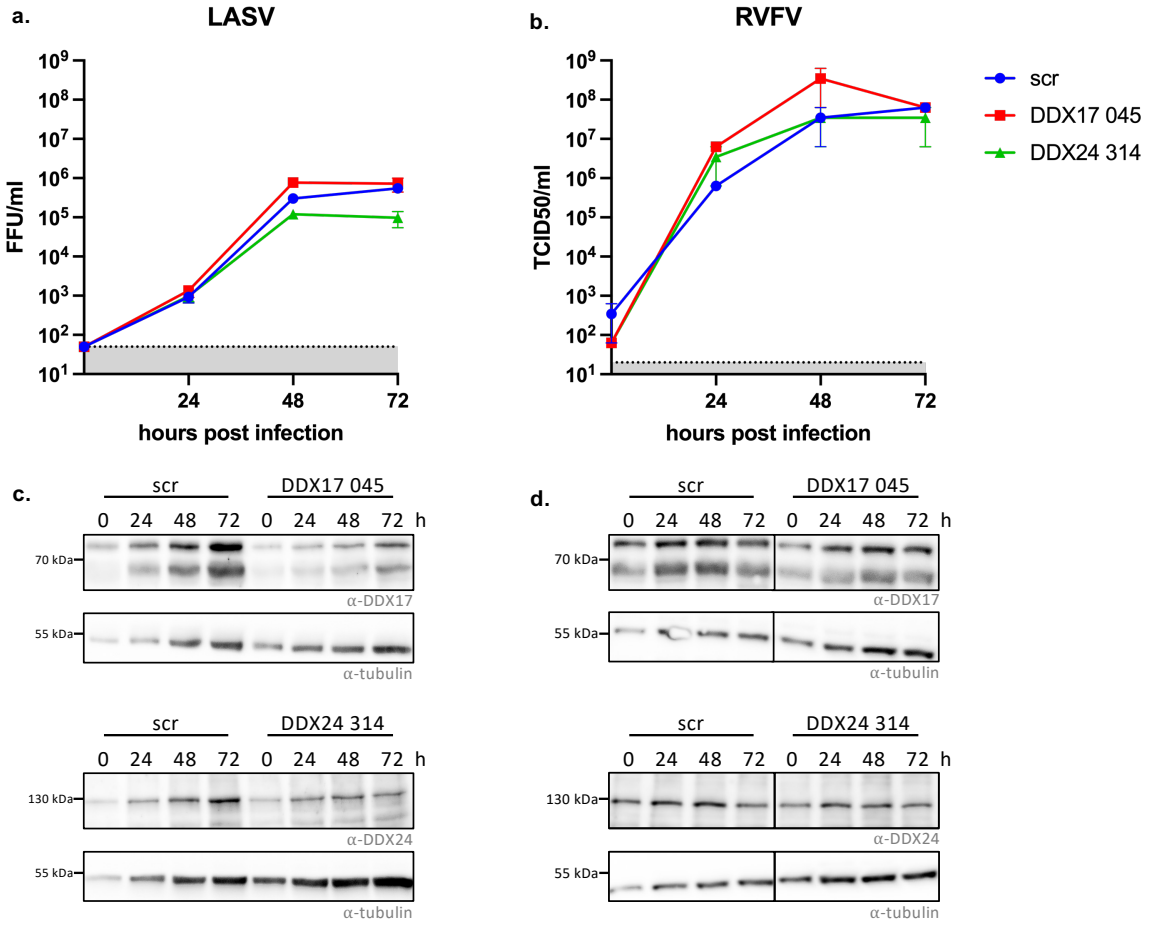

Figure 17: Effect of shRNA-mediated knockdown of DDX17 and DDX24 on LASV and RVFV replication. a. – b. Lentiviral vector transduced Huh7 cells with stable expression of DDX17 045, DDX24 314, or non-targeted scrambled (scr) shRNA in passage 4 (**a.**) or passage 6 (**b.**) were seeded in 24-well plates with 0.7 x 10^6 cells/well. 24 h after seeding, cells were infected with **a.** LASV or **b.** RVFV with an MOI of 0.01 according to 3.5.2. 24, 48, and 72 h after infection, cell supernatants and lysates were collected. The experiment was conducted once in technical duplicates. Virus particles in the cell supernatant were quantified with IFA (**a.**) as described in 3.5.4 or TCID50 assay (**b.**) as described in 3.5.5. Viral titers are shown as median with range. The assay's limit of detection is marked by the grey area. **c. – d.** WB analysis to verify the knockdown of DDX17 and DDX24 in the LASV (**c.**) and RVFV (**d.**) infection. 15 µl lysate was separated with 8 % SDS polyacrylamide gels together with 3 µl Page Ruler protein ladder as a MW marker and blotted according to Section 3.4.8. The membrane was split and stained with primary antibodies α-DDX17, α-DDX24, and α-tubulin as a loading control, followed by secondary HRP-coupled α-mouse or α-rabbit antibody. For detection, Clarity (Max) ECL chemiluminescent substrate was applied.

In summary, only a slight increase in LASV titer was observed in the DDX17 045 shRNA knockdown cells at 48 h, while increases were seen in RVFV replication at 24 and 48 h compared to the scrambled control cells. For the DDX24 314 shRNA knockdown, a small decrease in LASV titers was observed at 48 and 72 h, while RVFV titer was increased only after 24 h.

As the effects observed in cells with stable shRNA-mediated knockdown were also rather small, and the WB analyses could only detect a weak to no knockdown at all, the system was considered not suitable, and no further replicates were performed.

4.6.3 Testing the effect of DDX17 knockout on bunyavirus replication

The strategies previously used for the knockdown of DDX proteins with siRNA and shRNA showed only a partial knockdown. It was assumed that the observed effects on bunyavirus replication were mostly small, as the knockdown was not sufficient. Therefore, the effect of DDX17 knockout on bunyavirus replication was tested. HEK293 cells with a DDX17 knockout (DDX17 KO cells), achieved by CRISPR/Cas9, were purchased together with suitable HEK293 control cells. WB analysis of the cell lysates of DDX17 KO cells and control cells confirmed the knockout of DDX17 (Figure 18g).

DDX17 KO and control cells were infected with a collection of different bunyaviruses with an MOI of 0.1. According to the bunyavirus L proteins that showed an interaction with DDX17 in co-IP (Section 4.4.2), LASV, TCRV, ANDV, HTNV, and RVFV were used for infection. Cell supernatants were harvested at 24, 48, and 72 h post infection for LASV, TCRV, and RVFV, and additionally at 120 and 144 h post infection for ANDV and HTNV, as hantaviruses generally show a slower growth. Infectious viral particles were quantified with IFA and plaque assay as described in 3.5.4.

As can be seen in Figure 18, no difference in titer was observed for LASV (Figure 18a), TCRV (Figure 18b), and RVFV (Figure 18e) between the DDX17 KO cells and the control cells at any time point. No difference could be observed for ANDV either, but ANDV generally did not grow efficiently on this cell type, as the titers were only slightly above the detection limit of the assay, even after 144 h (Figure 18c). In contrast, a difference was observed for HTNV (Figure 18d). HTNV titers were increased at 72, 120, and 144 h in the DDX17 KO cells with 7.3×10^3 FFU/ml, 1.9×10^4 FFU/ml, and 2.0×10^4 FFU/ml compared to the control cells with 1.2×10^3 FFU/ml, 4.4×10^3 FFU/ml, and 8.5×10^3 FFU/ml, respectively.

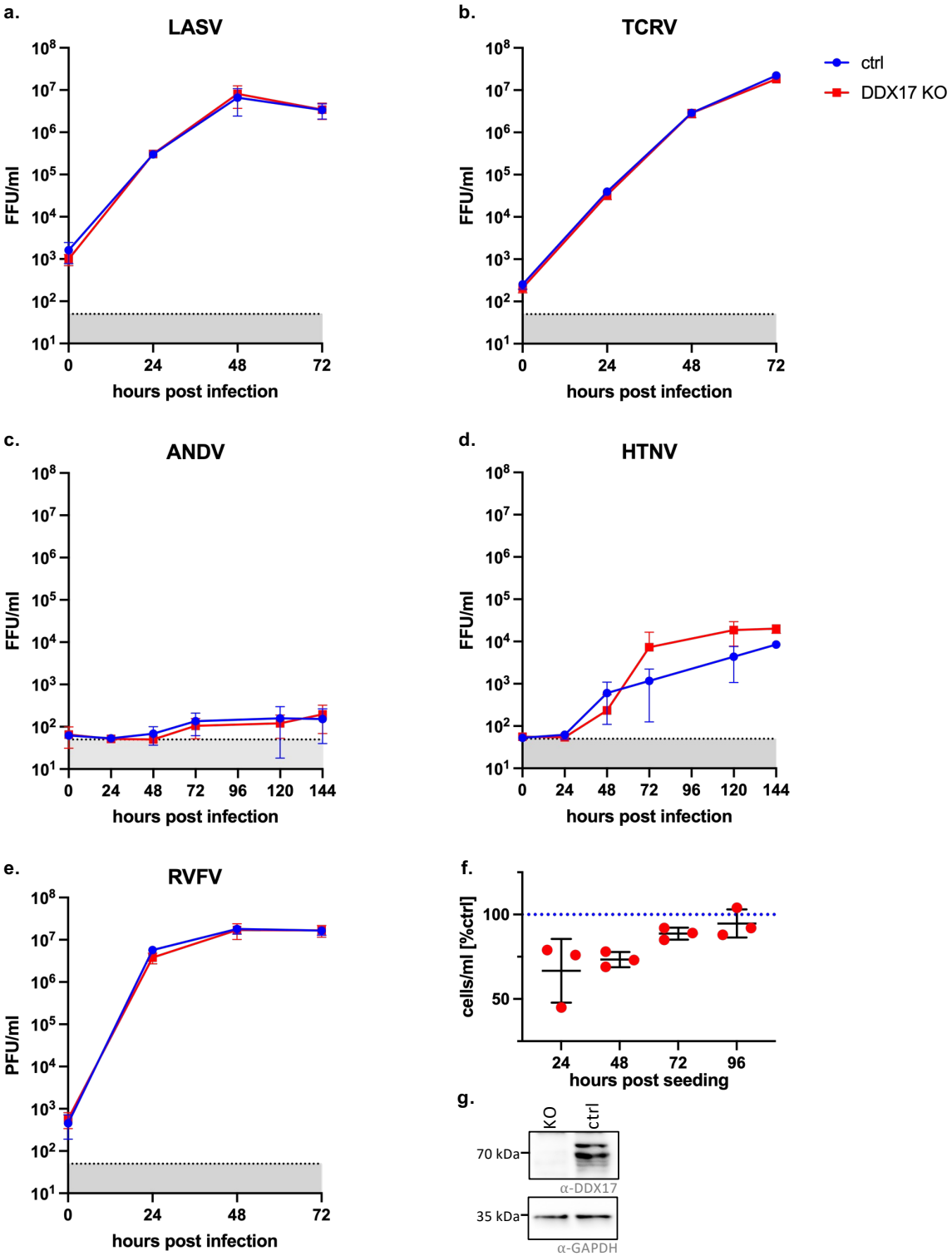

Figure 18: Effect of DDX17 knockout on bunyavirus replication. HEK293 DDX17 KO cells and control (ctrl) cells were seeded in 24-well plates with 0.8 x 10^5 cells/well. **a. – e.** 24 h after seeding, cells were infected with LASV (**a.**), TCRV (**b.**), ANDV (**c.**), HTNV (**d.**), or RVFV (**e.**) with an MOI of 0.1 according to 3.5.2. Cell supernatants were collected at 24, 48, and 72 h post infection and additionally at 120 and 144 h post infection (**c. – d.**). Infectious viral particles in the cell supernatant were quantified with IFA (**a. - d**) or plaque assay (**e.**) as described in 3.5.4. Viral titers are presented as the mean and standard deviation of three individual experiments, which were performed in technical duplicates. The assay's limit of detection is marked by the grey area. **f.** Cell growth of DDX17 KO cells compared to ctrl cells. 24, 48, 72, and 96 h after seeding, cells were detached with 200 µl trypsin and resuspended in 800 µl per well DMEM 5 % and counted. The cell count of the DDX17 KO cells was normalized to the cell count of the ctrl cells (set to 100 %). Shown

are the mean and standard deviation of one experiment performed in technical triplicates. **g.** WB analysis of cell lysates of DDX17 KO and ctrl cells before infection to verify the knockout of DDX17. 15 µl lysate was separated with 12 % SDS polyacrylamide gels together with 3 µl Page Ruler protein ladder as a MW marker and blotted according to Section 3.4.8. The membrane was split and stained with primary antibodies α-DDX17 and α-GAPDH as a loading control, followed by secondary HRP-coupled α-mouse antibody. For detection, Clarity (Max) ECL chemiluminescent substrate was applied.

During the infection experiments, it was observed that the DDX17 KO cells grew more slowly than the control cells. Therefore, the cells were seeded in 24-well plates and counted after 24, 48, 72, and 96 h. As can be seen in Figure 18f, there are considerably fewer DDX17 KO cells in the wells, especially after 24 and 48 h, with 67 and 73 % of the control cell count. This could have possibly led to lower titers in the DDX17 KO cells that are not specifically caused by the knockout of DDX17. The possible extent of the influence of this effect on the results is unclear.

In summary, no effect of DDX17 knockout on LASV, TCRV, ANDV, and RVFV replication was observed. For HTNV, however, viral titers were increased upon DDX17 knockout at 72 to 144 h post infection.

4.7 Structural modeling of the DDX-bunyavirus L complex

Structural modeling of the interactions between LASV L and DDX proteins was conducted by our collaboration partners of the Kosinski group at the EMBL Heidelberg. AlphaFold Multimer was used to predict models of DDX17 and DDX24 in complex with LASV L. Since structural modeling with full-length LASV L was computationally not possible at that time, it was divided into 8 fragments (180).

The quality of the models can be evaluated with different confidence scores. The predicted local distance difference test (pLDDT) provides a measure of the local confidence of the predicted model and is scaled from 0 to 100, with higher scores indicating higher confidence. The predicted aligned error (PAE) is a measure of the model's confidence in the relative position of two residues. It is particularly useful for evaluating the orientation of domains or interactions. The predicted template modeling (pTM) score measures the accuracy of the overall prediction, while the interface predicted template modeling (ipTM) score measures the accuracy of the interaction interface. AlphaFold Multimer also calculates the ipTM+pTM score, which is a weighted average of the ipTM and pTM scores. The suggested cutoff for the ipTM+pTM score is 0.6, with high confidence models resulting in higher scores.

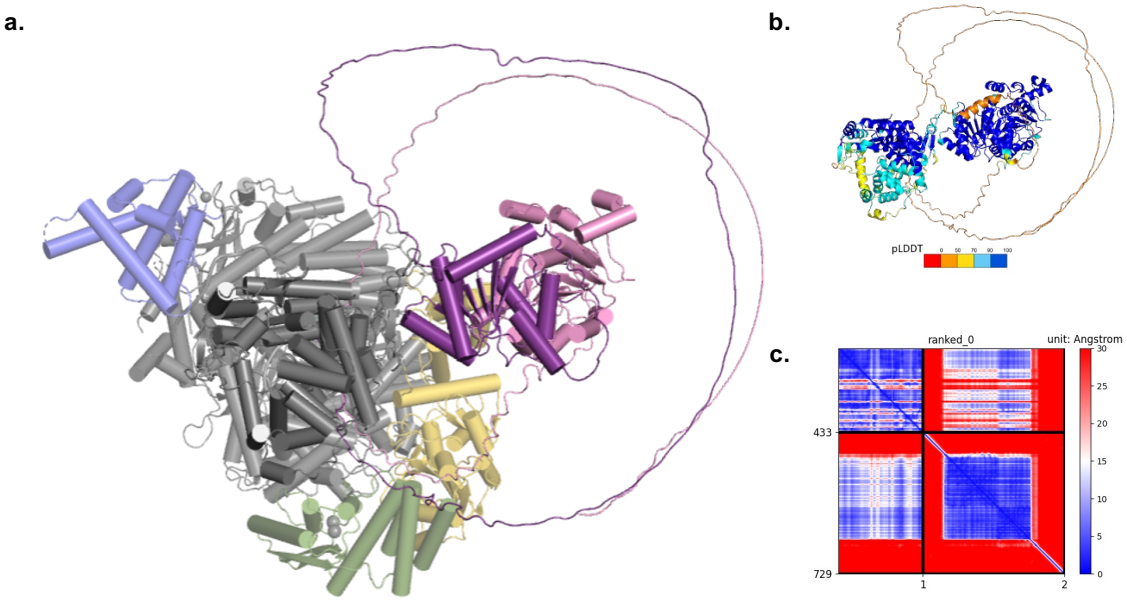

Figure 19: Model of DDX17 in complex with LASV L. a. The predicted complex of LASV L fragment (UniProt ID: O09705; 1398 – 1830) and full-length DDX17 (UniProt ID: Q92841) predicted by AlphaFold Multimer was superimposed onto the LASV L structure in elongation state (PDB: 7ojn). DDX17 RecA-like domain 1 and N-terminal domain are colored in pink, RecA-like domain 2 and C-terminal domain in violet, and LASV L fragment in grey. LASV L elongation structure (PDB: 7ojn) is faded in the background with the EN domain colored in green, the pyramid domain in blue, the C-terminus in yellow, and the rest, including the RdRp, in grey. **b.** Model of DDX17 in complex with LASV L fragment colored according to the pLDDT score. **c.** PAE plot of the model.

The scores of the individual models of DDX17 and DDX24 with the LASV L fragments are listed in Table A. 4 and Table A. 5. The model of LASV L fragment (1398 – 1830) and DDX17 was the only model to achieve an ipTM+pTM score of over 0.6, with 0.743. The models of DDX17 with the other LASV L fragments and all models with DDX24 resulted in ipTM+pTM scores below 0.6.

The model of the LASV L fragment (1398 – 1830) and DDX17 is shown in Figure 19a. The predicted interaction interface on LASV L was located on the thumb, thumb-ring, and lid domain of the RdRp (65). The interface on DDX17 was located on the RecA-like domain 2. A list of the interacting residues of the interface was generated with PDBsum and can be found in Table A. 6.

To test whether the interaction interface of LASV L and DDX17 could be similar for other bunyavirus L proteins, I performed structural modeling with RVFV L and DDX17 using AlphaFold 3 (179). An RVFV L fragment (1202 – 1586) corresponding to the LASV fragment (1398 – 1830), ranging from the thumb to lid domain of the RdRp (65), was used for the structural modeling. The predicted model of RVFV L and DDX17 is shown in Figure 20a. Unfortunately, the confidence scores of the model were very low with an ipTM+pTM score of 0.206, which is far below the suggested cutoff of 0.6. Therefore, no information on a possible interaction interface could be obtained based on the predicted model.

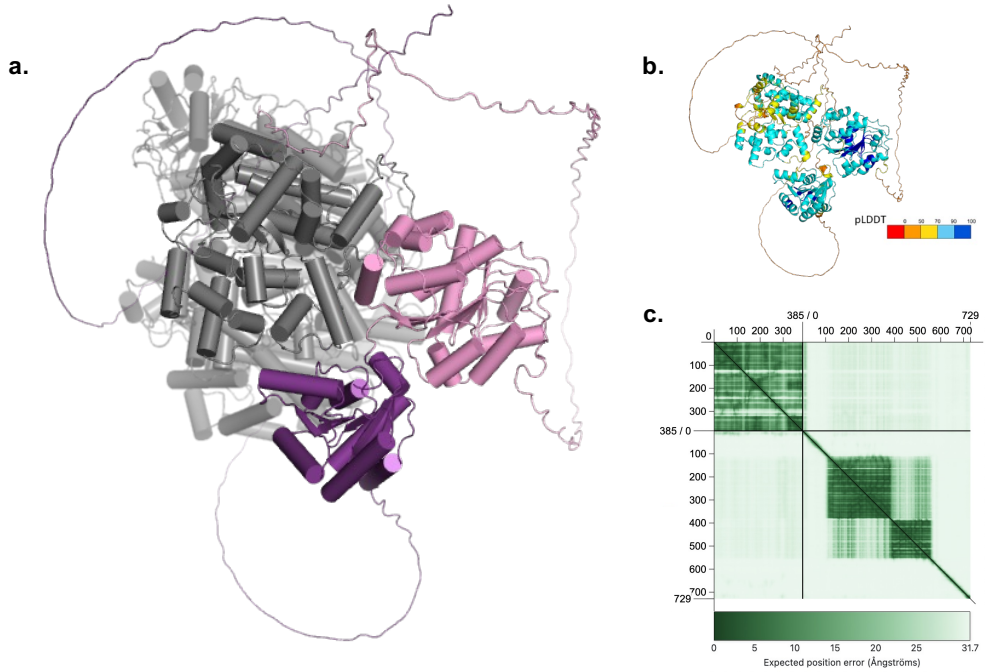

Figure 20: Model of DDX17 in complex with RVFV L. a. Complex of RVFV L fragment (UniProt ID: A2SZS3; 1202 – 1586) and full-length DDX17 (UniProt ID: Q92841) predicted by AlphaFold 3 was superimposed onto the RVFV L structure (PDB: 7EEI). DDX17 RecA-like domain 1 and N-terminal domain are colored in pink, RecA-like domain 2 and C-terminal domain in violet, and RVFV L fragment in grey. RVFV L structure is colored in grey and faded in the background. **b.** Model of the DDX17 in complex with RVFV L colored according to the pLDDT score. **c.** PAE plot of the predicted model.

In conclusion, structural modeling identified a potential high-confidence interaction between DDX17 and LASV L, while no reliable models were predicted for DDX24 in complex with LASV L or for DDX17 in complex with RVFV L. These results further support the hypothesis of a direct interaction between DDX17 and LASV L, but not between DDX17 and RVFV. This suggests that the interaction may not be conserved in related viruses. The complex prediction also does not support the hypothesis of an interaction between DDX24 and LASV L. However, it is also possible that structural modeling of virus-host interactions is still not good enough to predict these.

4.8 Testing the direct physical interactions of DDX proteins with LASV L protein

Interactions between proteins can be direct or indirect, e.g., via additional cofactors or scaffolding proteins. To test whether the interactions between DDX proteins and the LASV L are direct and to obtain information about the stoichiometry of the interaction, mass photometry was employed. In this method, the proteins are analyzed in a controlled environment outside the complex cellular environment, which requires stable and pure proteins.

In the following sections, the expression and purification strategies used to produce recombinant DDX17 and DDX24 for *in vitro* interaction studies are described. Full-length DDX17 and DDX24 could not be expressed and purified from *E. coli* in previous experiments (186). Therefore, the purification of the shorter isoform DDX17.2 from *E. coli* was tested first, followed by expression and purification of DDX17 and DDX24 from insect cells.

4.8.1 Protein expression and purification of DDX17 isoform 2 from *E. coli*

This section describes the different strategies explored to express and purify the shorter DDX17 isoform DDX17.2 from *E. coli*. An overview of the expression and purification strategies and the respective outcome is given in Table 30. The buffer composition for the purification of DDX17.2 was initially chosen according to a previously published protocol by Ngo et al.

DDX17.2 was first cloned into the pOPIN-F vector, which enabled expression in *E. coli* with an N-terminal His tag via the T7 RNA polymerase system. His-DDX17.2 could be successfully expressed in different *E. coli* strains with BL21 (DE3), resulting in the highest protein yield. His affinity purification was performed, followed by SEC. However, the purified His-DDX17.2 showed persistent impurities, which could not be separated from full-length His-DDX17.2 by SEC. These impurities appeared to consist of truncated expression or degradation products, as shown by WB analysis with immunostaining for the His tag. To improve the purity, combined ion exchange chromatography (IEC) and affinity purification with the heparin HiTrap™ Heparin FF column was performed, but also failed to eliminate the contaminants.

Next, DDX17.2 was cloned into the pOPIN-J vector, enabling expression with an N-terminal His-GST tag followed by a 3C protease cleavage site, and a C-terminal His tag. The idea was to bind His-GST-DDX17.2-His to glutathione sepharose and use 3C protease cleavage to release DDX17.2-His from the column and subsequently perform His affinity chromatography. Unfortunately, on-column cleavage caused strong precipitation of DDX17.2-His.

Table 30: List of expression and purification strategies tested for the purification of DDX17.2 from *E. coli*.

Construct	Expression and purification strategy	Outcome
Expression strategies		
His-DDX17.2	Testing different *E. coli* strains and expression conditions: BL21 (DE3), BL21 (DE3) + 10 mM glucose in the expression medium, Rosetta 2 (DE3), Rosetta 2 pLysS (DE3)	Highest yield in BL21 (DE3); Addition of glucose did not improve yield or purity
DDX17.2-His	Expression in BL21 (DE3)	Transformed *E. coli* did not grow in selective medium
Purification strategies		
His-DDX17.2	1. His affinity purification 2. SEC with HiLoad™ 16/60 Superdex 200	Contamination with truncated expression or degradation products
His-DDX17.2	1. His affinity purification 2. IEC and affinity chromatography with heparin HiTrap Heparin FF	Contamination with truncated expression or degradation products
His-GST-DDX17.2-His	1. GST affinity purification with 3C protease on-column cleavage to remove His-GST tag 2. His affinity purification	Protein precipitated during on-column cleavage
His-GST-DDX17.2-His	1. GST affinity purification with elution 2. 3C protease cleavage to remove His-GST tag 3. GST affinity purification to capture His-GST tag 4. His affinity purification 5. SEC with Superdex 200 Increase 10/300 GL	Cleaved His-GST tag could not be completely separated; Majority of DDX17.2-His was lost during purification
GST-DDX17.2-His	1. GST affinity purification with elution 2. 3C protease cleavage to remove GST tag 3. His affinity purification 4. SEC with Superdex 200 Increase 10/300 GL	Cleavage of GST tag was not complete; Contamination with truncated expression or degradation products; Protein was instable

As a solution, the protein was eluted from the glutathione sepharose using L-glutathione before the 3C protease cleavage. Cleaved His-GST tag was then removed via a second round of GST affinity purification. The flowthrough, containing DDX17.2-His, was subjected to His affinity purification to separate full-length DDX17.2-His from C-terminally truncated or degraded fragments. However, the cleaved His-GST tag was not completely removed by the GST affinity purification, making additional SEC necessary. After these extensive purification steps, only very little DDX17.2-His remained, while the cleaved His-GST tag was still very abundant and generated a distinct peak in the chromatogram.

To improve the separation of the cleaved GST tag from DDX17.2, another construct was generated. GST-DDX17.2 was amplified by PCR from His-GST-DDX17.2 pOPIN-J and cloned into pOPIN-E, which enabled expression of DDX17.2 with an N-terminal GST tag (without His tag) followed by a 3C protease cleavage site and a C-terminal His tag. A schematic overview of the construct is shown in Figure 21a. GST-DDX17.2-His was expressed in *E. coli* and initially purified via GST affinity chromatography with L-glutathione elution. SDS-PAGE analysis (Figure 21b) showed GST-DDX17.2-His in the elution, together with the truncated expression or degradation products that have been observed before. Elution fractions were pooled, diluted, and 3C protease cleavage was performed. His affinity purification was performed to separate DDX17.2-His from the cleaved GST tag and C-terminally truncated expression or degradation products. As shown in the SDS-PAGE analysis in Figure 21c, 3C protease cleavage was not complete, but the majority of the resulting protein after His affinity purification was DDX17.2-His. SEC was performed to separate DDX17.2-His from uncleaved GST-DDX17.2-His, the GST tag, and remaining degradation products that were visible in the SDS-PAGE analysis. The chromatogram (Figure 21d) revealed multiple peaks. SDS-PAGE analysis confirmed that DDX17.2-His was not fully separated from the impurities, likely due to the dimerization tendencies of both DDX17.2 and GST, which may have led to the formation of mixed oligomeric complexes. Figure 21e shows the SDS-PAGE analysis of different amounts of the final product. Although DDX17.2-His was the major species, it was not pure. Additionally, stability testing revealed that the protein degraded rapidly at 4°C, with significant degradation observed after just one day (Figure 21e). In general, buffer composition has a major impact on protein stability. Although the buffer composition had been successfully used in a published protocol for the purification of DDX17.2 (147), the authors did not provide all details, such as the type and position of the tag used, which could already change protein stability. Due to the instability of purified DDX17.2-His, it was not possible to optimize the buffer composition in, for example, thermal stability experiments (200).

Taken together, the purification of DDX17.2 from *E. coli* did not result in stable and pure protein despite multiple optimization attempts. One possible explanation was that DDX17.2 may require specific post-translational modifications for stability or chaperones for correct folding, which are not available in *E. coli*. Therefore, it was decided to change the expression system to insect cells.

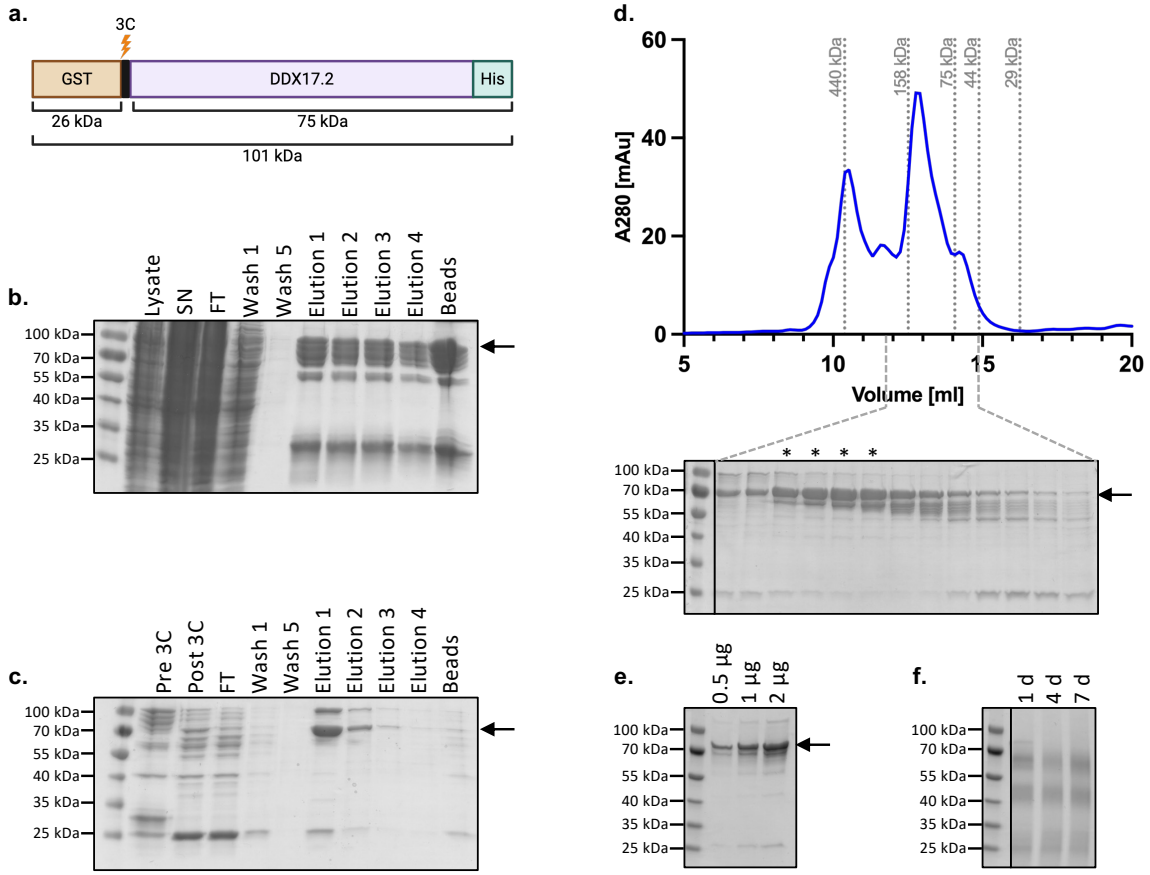

Figure 21: Protein purification of DDX17.2 from 1 l expression in *E. coli* BL21 (DE3). a. Schematic overview of the GST-DDX17.2-His construct with N-terminal GST tag, 3C protease cleavage site, and C-terminal His tag. Created with BioRender.com. **b.** SDS-PAGE analysis of GST affinity purification of GST-DDX17.2-His. Cells were lysed in DDX17.2 lysis buffer, and proteins were extracted as described in 3.4.3. Affinity chromatography was performed with 1.5 ml glutathione sepharose beads as described in 3.4.4.1 with DDX17.2 washing buffer and DDX17.2 GST elution buffer. Samples (6 µl for lysate, supernatant (SN), and flowthrough (FT) and 12 µl for wash and elution fractions and beads) of lysate, SN, FT, wash fractions 1 and 5, elution fractions 1, 2, 3, and 4, and beads were separated on a 12 % SDS polyacrylamide gel and visualized via Coomassie staining. The black arrow indicates the band that corresponds to GST-DDX17.2-His. **c.** SDS-PAGE analysis of 3C protease cleavage and His affinity purification of DDX17.2-His. The elution fractions were pooled, diluted in DDX17.2 washing buffer, and 1.5 mg of 3C protease was added (sample pre 3C) and incubated overnight at 4°C (sample post 3C). His affinity chromatography was performed with 1 ml Ni-NTA agarose beads as described in 3.4.4.1 with DDX17.2 washing buffer and DDX17.2 His elution buffer. Samples (12 µl) of pre 3C, post 3C, FT, wash fractions 1 and 5, elution fractions 1, 2, 3, and 4, and beads were separated on a 12 % SDS polyacrylamide gel and visualized via Coomassie staining. The black arrow indicates the band corresponding to DDX17.2-His. **d.** Chromatogram and SDS-PAGE analysis of SEC of DDX17.2-His. The elution fractions were concentrated as described in 3.4.9 and loaded onto the Superdex 200 Increase 10/300 GL column on the ÄKTA prime plus, and SEC was performed with DDX17.2 SEC buffer as described in 3.4.4.2. Absorbance at 280 nm was detected and plotted against the elution volume. The elution volumes of proteins with known size are shown in grey. Elution fractions containing predominantly DDX17.2-His (indicated by a star) were pooled and concentrated. The black arrow indicates the band that corresponds to DDX17.2-His. **e.** SDS-PAGE analysis of purified DDX17.2-His. Samples of 0.5, 1, and 2 µg DDX17.2-His were separated on a 12 % SDS polyacrylamide gel and visualized via Coomassie staining. The black arrow indicates the band that corresponds to DDX17.2-His. **f.** SDS-PAGE analysis of stability testing of purified DDX17.2-His. DDX17.2-His was stored at 4°C, and 1 µg samples were taken after 1, 4, and 7 days. Samples were separated on a 12 % SDS polyacrylamide gel and visualized via Coomassie staining **b. – f.** All samples were separated together with 2 µl of Page Ruler protein ladder as a MW marker.

4.8.2 Protein expression and purification of DDX17 and DDX24 from insect cells

DDX17 and DDX24 were expressed in insect cells using a baculovirus expression system.

For this, DDX17 and DDX24 were cloned into the donor plasmid pFASTBac HTB, providing them with a C-terminal StrepII-His tag (C-StrepII-His). Recombinant bacmid DNA was produced by transforming the donor plasmid into DH10EMBacY *E. coli*, as described in Section 3.2.9. For the production of baculovirus particles, the bacmid DNA was transfected into SF21 cells as described in Section 3.5.8. High Five cells were infected with the recombinant baculovirus particles to express the target proteins, as described in Section 3.4.2.

Figure 22 shows the SDS-PAGE analysis of the StrepII affinity chromatography of DDX17 and DDX24 from a 40 ml test expression in High Five cells. Although the expression volume was low and only one affinity chromatography step was performed, remarkable amounts of protein with acceptable purity could already be obtained, especially when compared to the results that were achieved in the purification of DDX17.2 from *E. coli* (4.8.1). The expression and purification were repeated on a larger scale with 600 ml expression volume. The elution fractions were combined and concentrated for use in further assays.

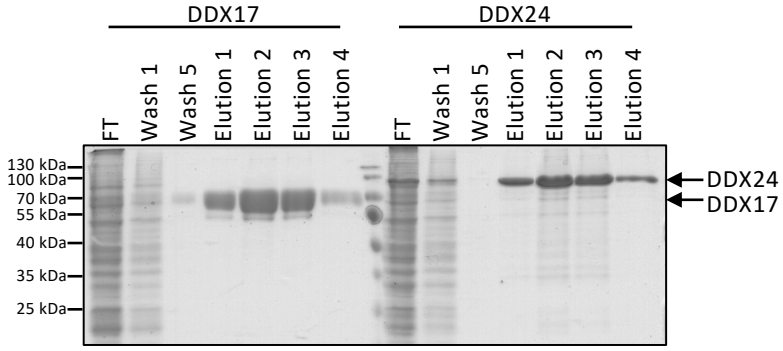

Figure 22: Protein purification of DDX17 and DDX24 from 40 ml expression in insect cells. SDS-PAGE analysis of StrepII affinity chromatography of DDX17 and DDX24 (C-StrepII-His). Cells were lysed in DDX lysis buffer, and proteins were extracted as described in 3.4.3. Affinity chromatography was performed with 100 µl strep-tactin beads as described in 3.4.4.1 with DDX biotin elution buffer. Samples (12 µl) of flowthrough (FT), wash fractions 1 and 5, and elution fractions 1, 2, 3, and 4 were separated on a 12 % SDS polyacrylamide gel and visualized via Coomassie staining. Black arrows indicate the bands that correspond to DDX17 and DDX24.

4.8.3 Analysis of the complex formation of DDX17 and DDX24 with LASV L protein with mass photometry

Mass photometry was used to investigate the complex formation of DDX17 and DDX24 with LASV L. Mass photometry is a light scattering-based, single-molecule technique that provides information on the relative abundance of individual molecules by molecular counting. It is a highly sensitive, label-free technique that requires very low concentrations of sample and is compatible with a wide range of buffers. Figure 23a shows the principle of mass photometry for the analysis of protein samples. The protein that binds to the measuring surface is exposed to a beam of light and causes light scattering, which interferes with the light reflected from this surface. The interference signal is proportional to the mass of the protein (201,202).

For the mass photometry measurement, 5 µM protein solutions were prepared with purified LASV L (StrepII 407) (80) and DDX17 or DDX24 (C-StrepII-His) alone and in combination with a molar ratio of 1 to 3 (L to DDX) in co-IP washing buffer (3.7.2). Protein solutions were incubated for 30 min at room temperature and diluted to 500 nM with co-IP washing buffer directly before the measurement. Mass photometry measurements were performed as described in Section 3.4.10.2.

The measurement of LASV L alone resulted in a mass distribution histogram with two peaks at 255 and 509 kDa corresponding to the LASV L monomer and dimer in approximately equal counts. Measurement of DDX24 alone resulted in a mass distribution histogram with two peaks at 99 kDa and 207 kDa corresponding to its monomeric and dimeric forms, with the dimer being much less abundant. When DDX24 was mixed with LASV L, mass photometry measurement revealed two additional peaks at 356 and 619 kDa corresponding to a complex between DDX24 and LASV L, as well as DDX24 and the LASV L dimer, respectively. Although these complexes were very rare, they were reproducible in at least two individual experiments and could also be observed using a different buffer composition (LASV L assay buffer 2.7.2). Measurement of DDX17 alone resulted in a mass distribution histogram with two peaks at 82 and 158 kDa, corresponding to its monomeric and dimeric forms. Similar to DDX24, the dimeric form occurred much less frequently, which contrasts with previous SEC results (4.8.1) where DDX17 consistently appeared in an oligomeric state. When DDX17 was mixed with LASV L, no distinct peaks corresponding to a complex between DDX17 and LASV L were detected. However, subtle increases in counts were observed in the mass distribution histogram at masses expected for a complex between DDX17 and LASV L, as well as DDX17 and the LASV L dimer. These subtle increases were not consistently reproducible and could not be observed using a different buffer composition (LASV L assay buffer 2.7.2), indicating that the alleged complex was likely of lower affinity or less stable under the tested conditions.

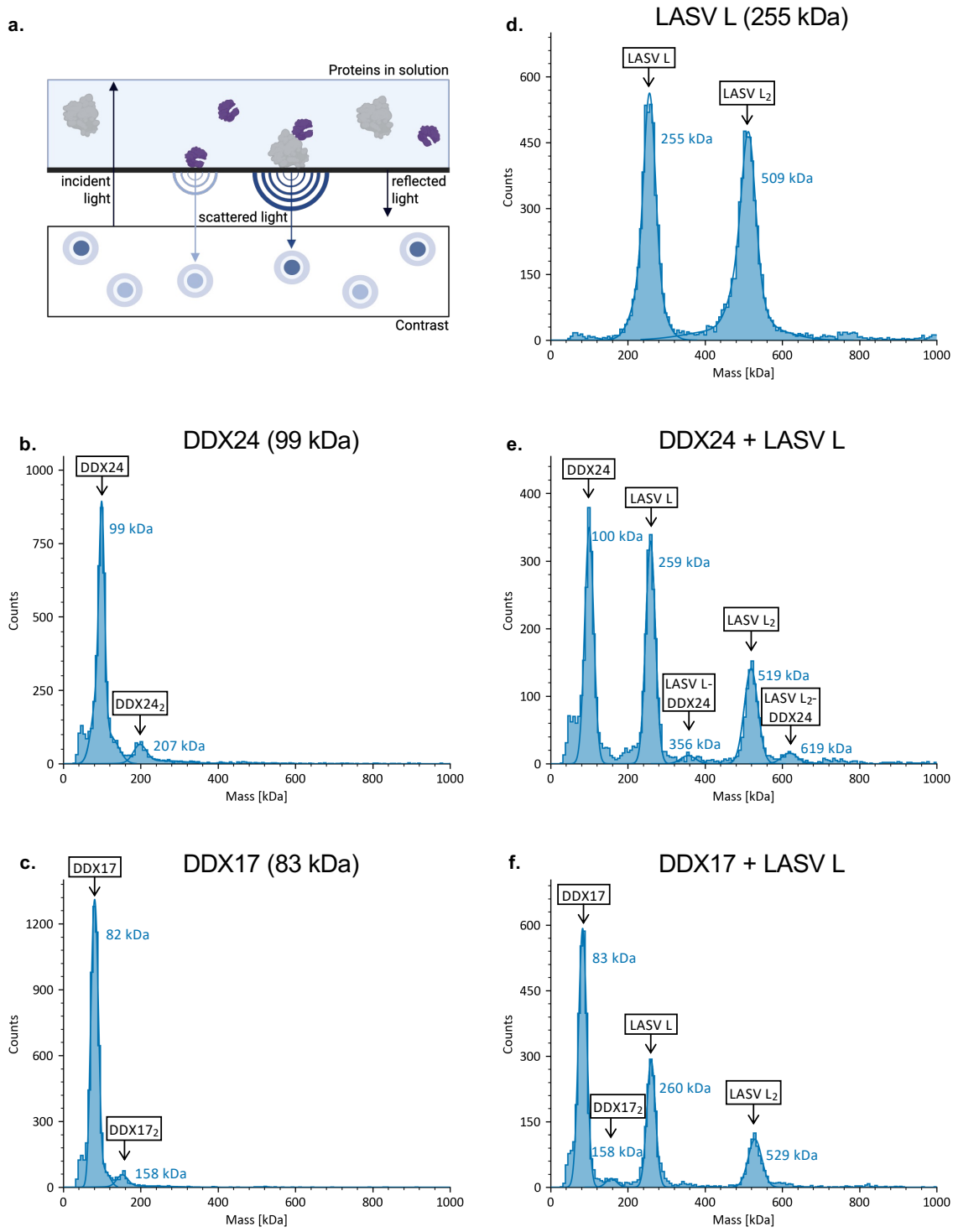

Figure 23: Analysis of complex formation of DDX17 and DDX24 with LASV L protein with mass photometry. a. Principle of mass photometry. The protein in contact with the measuring surface causes light scattering, which interferes with the light reflected from this surface. The interference signal is proportional to the mass of the protein. Adapted from Young et al. (202). Created with BioRender.com. **b. – f.** 5 µM protein solutions were prepared with purified LASV L (StrepII 407), DDX17 (C-StrepII-His), and DDX24 (C-StrepII-His) alone and in combination (molar ratio of L to DDX: 1 to 3) in co-IP washing buffer (2.7.2). Protein solutions were incubated for 30 min at room temperature and were diluted to 500 nM with co-IP washing buffer directly before the measurement. Mass photometry measurements were performed as described in 3.4.10.2. Shown are the molecular mass distribution histogram plots fitted with Gaussian functions. Experimental molecular masses of the peaks are shown in blue, and the theoretical molecular masses of the monomeric proteins are stated in the headings. Black arrows indicate the potential composition of the respective peaks.

Distribution of LASV L shifted slightly toward the monomeric form in the presence of DDX17 or DDX24. This is probably a result of the lower concentration of LASV L in the mixture, as there was only 1.25 µM LASV L in the 5 µM protein solution with DDX17 or DDX24 (molar ratio of L to DDX: 1 to 3) compared to 5 µM LASV L in the control.

Taken together, these results indicate that DDX24 is capable of forming complexes with LASV L *in vitro*, which is, however, a rare event. DDX17, in contrast, showed no evident complex formation with LASV L, but a slight increase in counts at the expected masses, which could suggest the rare formation of a very unstable complex.

5 DISCUSSION

The *Bunyaviricetes* class includes several important human pathogens with limited treatment options. Antiviral strategies targeting essential interactions between host and viral proteins are a promising approach. This work aimed to characterize the molecular interactions between bunyavirus L proteins and host proteins, thereby improving our understanding of the bunyavirus replication cycle and identifying potential new targets for antiviral strategies.

In previous work by Silke Olschewski-Pavlita, potential cellular interaction partners of LASV L and cellular genes that are essential for LASV replication were identified using AP-MS screens and a genetic knockout screen (181). Based on these results and additional published data sets, host proteins, in particular proteins of the DDX family, were chosen for further characterization.

Physical interactions with LASV L in the cellular context were studied with co-IP. Interactions of the LASV L with DDX17, DDX19, DDX24, DDX5, and CCNT1 could be demonstrated, which is discussed in Sections 5.2.1 and 5.2.2. Interactions of LASV L with HNRPD, NONO, RBM10, SFPQ, TRIM25, and TUBG1 could not be verified in this experimental setup. DDX17 was also tested for its interaction with further bunyavirus L proteins from three different families, which is discussed in Section 5.2.3. To further characterize those interactions, *in vitro* complex formation between purified LASV L and DDX17 or DDX24 was investigated with mass photometry. Evidence of complex formation between those proteins was observed in initial experiments and is discussed in Section 5.2.4. In addition, the complexes of DDX17 with LASV L, as well as DDX17 with RVFV L, and DDX24 with LASV L, were modeled using AlphaFold, which is discussed in Section 5.2.5.

Functional studies of the roles of selected host proteins DDX17, DDX19, and DDX24 remained inconclusive. The effect of overexpression and knockdown of DDX17, DDX19, and DDX24 on viral transcription and genome replication was tested in minireplicon systems for LASV and RVFV, which is discussed in Section 5.3.1. Additionally, the roles of DDX17 and DDX24 were studied in viral infection experiments using different gene silencing strategies, which is discussed in Section 5.3.2.

5.1 Virus-host interactions as targets for antiviral therapy

Conventional antiviral therapies are primarily designed to target viral enzymes. However, these approaches are often limited by rapid viral evolution and the emergence of resistance. Targeting essential host proteins or virus-host interactions is a promising alternative. Host proteins are not under selection pressure; therefore, antiviral resistance mutations are not expected. In addition, the dependency on specific host proteins may be conserved across a range of different viruses, offering the potential for broad-spectrum antivirals (203–205). A specific example is the eukaryotic initiation factor 4F (eIF4F) complex which is essential for the cap-dependent translation initiation. Many viruses, such as flaviviruses and coronaviruses regulate the phosphorylation of the eIF4F subunit eukaryotic initiation factor 4E (eIF4E) to control selective host mRNA translation and thereby IFN production (234). However, host-targeted antivirals carry an inherent risk of on-target cytotoxicity as they interfere with normal cell function and therefore tend to have a narrow therapeutic window (206). Antivirals that target virus-host interactions represent a more targeted strategy by preventing specific contacts between viral proteins and host proteins. By specifically blocking these interfaces, these antivirals can provide higher specificity and lower cytotoxicity compared to host-targeted antivirals, given that those interfaces are less likely to be essential for host protein-protein interactions. Since viruses cannot easily change their dependence on essential interactions with host proteins, the barrier to resistance is higher than with antivirals that only target viral proteins. However, the development of small molecule inhibitors targeting these specific interactions remains a technical challenge, as many protein-protein interfaces have large surface areas and lack obvious pockets for small molecule binding (207,208). Novel technologies such as molecular glues offer an alternative approach that can be used to inappropriately stabilize virus-host interactions (209).

More recent work highlights the potential of DDX proteins as prospective targets for antiviral strategies with broad-spectrum potential. For example, small molecule inhibitors targeting DDX3, such as RK-33 or NZ5, are effective against a broad range of viruses *in vitro*, including severe acute respiratory syndrome coronavirus 2 (SARS-CoV-2), hepatitis C virus (HCV), respiratory syncytial virus (RSV), West Nile virus (WNV), Zika virus (ZIKV), and human immunodeficiency virus (HIV) (210,211). Although these developments are still at an early stage, they demonstrate the therapeutic potential of targeting virus-host protein networks, including members of the DDX family.

5.2 Interactions of host proteins with bunyavirus L proteins

The combined data set of potentially important host factors mainly consists of cellular interaction partners of LASV L and LCMV L that were identified with AP-MS (181). In this method, the bait protein, the StrepII-tagged L protein, was enriched together with its interaction partners. One of the biggest challenges in AP-MS experiments is the distinction between true interaction partners and co-purifying contaminants, e.g., through nonspecific binding to the matrix and proteins (212). Due to the high sensitivity of MS, it is impossible to completely remove contaminants, especially since low stringency is preferred to preserve specific interactions. Therefore, a control experiment is performed to test for non-specific binding to the matrix. In this case, no StrepII-tagged L protein was present. Quantitative MS was then employed to compare the enrichment of proteins in both experiments. Nevertheless, experimental artifacts still occur. In this case, recombinantly expressed and purified StrepII-tagged LASV L and LCMV L were incubated with cell lysates. This means that the L proteins not only differ from the naturally occurring L proteins, particularly in terms of quantity, but could also come into contact with cellular proteins to which they would not have access during the natural replication cycle. Therefore, AP-MS data sets of the screens with rLCMV (Khamina et al.) and rLASV were also included in the bioinformatic analysis, as well as the contaminant repository for AP (CRAPome) database, which contains common contaminants in AP experiments (181,182,213). Even though AP-MS is a powerful method to identify protein-protein interactions, orthogonal methods are necessary to validate the results.

In this work, co-IP was used to validate the interactions of possible cellular interaction partners of LASV L. Since the potential interaction partners were identified by enrichment of LASV L, a reverse approach was used for validation by immunoprecipitation of the host protein.

In co-IP, protein-protein interactions are studied in the cellular context, which is a highly complex environment. Interactions that are observed with co-IP are not necessarily direct, as the investigated proteins may be part of a larger protein complex. Furthermore, it is not possible to obtain information on the stoichiometry and possible cofactors of the interaction. Nevertheless, co-IP is a good initial approach to study protein-protein interactions, as it is relatively straightforward, cost-efficient, and does not require purified proteins.

Although co-IP seems simple, the experimental setup is surprisingly complex and delicate. It is a challenge to adjust the stringency to remove the background while maintaining specific interactions through multiple washing steps. Many factors influence the outcome of co-IP experiments, including buffer conditions, individual handling, and ultimately the quality of the WB analysis. A negative result

in co-IP does not necessarily mean that the investigated proteins are not interacting. The interaction may not be stable enough to be maintained throughout the experiment, or the co-immunoprecipitated protein may not be sufficiently abundant to be detected in the WB analysis.

Generally, the gold standard for co-IP experiments is the use of untagged proteins at their endogenous levels. This is not feasible for experimental setups with LASV L, which is only expressed in cells during LASV infection, which means it would be necessary to perform the experiment under BSL-4 conditions. In addition, the low abundance of LASV L and the lack of specific antibodies prevent the implementation of co-IP experiments under those conditions. Moreover, to test the interaction of LASV L with many different untagged host proteins at endogenous levels, numerous different antibodies against the specific host proteins would have to be used, each of which would have to be validated individually. Therefore, the co-IP experiment was established with an overexpression of tagged proteins. The host proteins and controls were expressed with a myc tag, while LASV L was expressed with a FLAG tag. The myc-tagged proteins were immunoprecipitated, and the presence of FLAG-tagged LASV L in the elution was analyzed by WB.

This way, the interactions of host proteins DDX17, DDX19, DDX24, CCNT1, DDX5, HNRPD, NONO, RBM10, SFPQ, TRIM25, and TUBG1 with LASV L were studied. DDX17, DDX19, and DDX24 were studied in more detail concerning the nucleic acid dependency, enzymatic function, and in the case of DDX17, the importance of the N- and C-terminal domains on the interaction.

5.2.1 Interactions of DDX proteins with the LASV L protein

DDX proteins DDX17, DDX19, and DDX24 showed an interaction with LASV L in co-IP, although the interaction with DDX19 seemed to be comparably weaker in some experiments. As discussed above, it is not possible to conclude whether the observed interactions are direct.

Interactions between proteins can be dependent on many factors, including nucleic acid mediators (214). Since both the LASV L protein and the DDX proteins are RNA-binding proteins, it was investigated whether the observed interactions are nucleic acid-dependent. Therefore, the samples were treated with Benzonase, which degrades all forms of DNA and RNA. This experiment showed that the interactions of DDX17 and DDX24 with LASV L are not dependent on nucleic acids, while for DDX19, the interaction with LASV L could no longer be observed upon Benzonase treatment. This suggests that the interaction may occur indirectly via nucleic acids, i.e., with both proteins binding to the same RNA strand. It is also conceivable that the nucleic acids have structural importance by inducing conformational changes in the proteins. Indeed, both LASV L and DDX19 have been reported to undergo major conformational changes upon RNA binding (65,215). It is

unclear whether Benzonase degrades RNA that is already bound by the proteins. This depends on the affinity of the RNA-protein interaction, how protected the RNA is within the protein, the ionic strength, and the concentration of Benzonase (216,217). Therefore, an involvement of nucleic acids in the interactions of DDX17 and DDX24 with LASV cannot be entirely ruled out, but is unlikely.

DDX proteins bind and hydrolyze ATP to bind and unwind RNA and dissociate RNA-protein complexes (131). In the process, the DDX helicase core undergoes a conformational change from open to closed and back to open (132). For LCMV, Loureiro et al. showed that the ATP binding activity of DDX3 is critical for viral transcription and genome replication (183). Lin et al. demonstrated that the ATP binding activity of DDX3 is important for its interaction with hepatitis E virus (HEV) capsid protein and HEV replication (218). To test the influence of the enzymatic activity of DDX proteins on the interaction with LASV L, ATPase mutants were constructed and tested in co-IP. Therefore, a point mutation of lysine to glutamine in motif I was introduced, which is known to disrupt the binding and hydrolysis of ATP (194,195). For none of the tested DDX proteins, DDX17, DDX19, and DDX24, a difference between the ATPase mutant and the wildtype concerning the interaction with LASV L was observed in co-IP.

The lysine residue in motif I of DDX proteins is necessary for the binding of ATP through the β-phosphate (128). However, there is no consensus in the literature as to whether ATP binding is necessary for RNA binding and the conformational change from open to closed. According to some studies, the combination of ATP and RNA binding, but not ATP or RNA binding alone, leads to the conformational change (219). In some studies, ATP or RNA binding appears to increase the affinity of the DDX proteins for each other. In contrast, it was also reported in other studies that ATP or RNA binding alone can induce at least a partial conformational change (220). It is not clear if those observations can be attributed to functional differences between different DDX proteins or other factors, like the use of different RNAs in the respective experiments. However, there is consensus that ATP and RNA binding are tightly orchestrated in DDX proteins and that ATP binding with subsequent ATP hydrolysis is necessary for the RNA unwinding or remodeling functions and the final release (128).

Given this functional complexity of DDX proteins is not clear if the ATPase mutants are still able to bind RNA with the same affinity as the wildtype or at all. For DDX17, Mao et al. demonstrated that the ATPase mutant still has the ability to bind pregenomic RNA of HBV, but to a lesser extent (195). It is also not clear if a change to closed conformation is still possible for the ATPase mutants. However, certainly, the ATPase mutants can no longer undergo a full helicase cycle of ATP-dependent unwinding and remodeling. Therefore, it can be concluded that the ability of DDX17,

DDX19, and DDX24 to undergo a full helicase cycle does not seem to be important for the interaction with LASV L. For further studies, it would be interesting, especially for DDX19, to test mutants with impaired RNA binding, e.g., through mutating conserved arginine residues in motif V that interact with the phosphate backbone of RNA (133). A mutation in the SAT amino acid sequence in motif III would also be interesting, as it is important in the coordination between the ATP and RNA binding sites and essential for the conformational change (160,221). In addition, it would be interesting to test whether the interactions between LASV L and the DDX17 and DDX24 ATPase mutants might be nucleic acid-dependent, in contrast to the wildtype proteins. Since DDX ATPase mutants may bind RNA with lower affinity and the closed conformation may be inhibited, protection against degradation of bound RNA by nucleases may be reduced.

Many host proteins possess different isoforms, and for some, it is known that only certain isoforms participate in particular protein-protein interactions. One example is ANP32, which is an essential host protein for IAV. Only some isoforms (ANP32A and B, but not E) interact with the IAV polymerase complex, which is required for viral genome replication (222). DDX17 has a shorter isoform DDX17.2, which lacks part of the N-terminal intrinsically disordered region. Differences in the cellular localization and the formation of MLOs were described for the two DDX17 isoforms (223). Therefore, DDX17.2 was tested for its interaction with LASV L in co-IP. Since the N- and C-terminal domains of DDX17 are intrinsically disordered regions, which are often involved in protein-protein interactions (224), it was also tested whether the DDX17 helicase core DDX17.c still interacts with LASV L in co-IP. Since several interaction sites may exist between the two proteins, some of which may depend on nucleic acids, the influence of Benzonase was also tested. The results showed that the interaction between DDX17.2 and LASV L is comparable to DDX17 and also not dependent on nucleic acids. In contrast, DDX17.c showed a weaker interaction with LASV L, independent of Benzonase treatment. Likely, the N- and/or C-terminal domains of DDX17 interact directly with LASV L, resulting in the loss of part of the interaction interface or a second interface for DDX17.c. There is also the possibility that the removal of the N- and/or C-terminal domains has an impact on the structure of the helicase core that mediates the interaction. However, this is rather unlikely, as functional DDX17.c has already been crystallized upon binding to RNA and an ATP analogue (225). Additionally, the helicase core is highly conserved between different DDX proteins and generally functions despite highly variable or absent N- and C-terminal domains. It is also conceivable that the observed influence of the DDX17 N- and/or C-terminal domains is not directly related to an interaction between DDX17 and LASV L. The N- and/or C-terminal domains of DDX17 could also mediate the interaction with another protein to stabilize the interaction between LASV L and DDX17.

5.2.2 Interactions of further host proteins with the LASV L protein

The interaction of further host proteins was tested for interaction with LASV L in co-IP, including CCNT1, DDX5, HNRPD, NONO, RBM10, SFPQ, TRIM25, and TUBG1. These host proteins are a heterogeneous group of proteins that were prioritized based on their occurrence in the different data sets (see Section 4.2).

Of these eight host proteins, CCNT1 and DDX5 showed an interaction with LASV L. No interaction could be validated for HNRPD, NONO, RBM10, SFPQ, TRIM25, and TUBG1. Those were either false positive hits from the combined data set or their potential interaction with LASV L could not be observed under the specific experimental conditions. DDX5 showed an interaction with LASV L similar to its closely related paralog DDX17. The possible consequences of the similarity between DDX5 and DDX17 and their interactions with LASV L are discussed in another section (5.3.2).

CCNT1 showed an interaction with LASV L. CCNT1 is part of the positive transcription elongation factor b, which regulates the elongation phase of transcription by RNA polymerase II (187). Little is known about the role of CCNT1 in viral infections. For IAV, CCNT1 has been shown to interact with the viral polymerase complex, thereby facilitating its association with the cellular RNA polymerase II. The interaction of the viral polymerase complex with the RNA polymerase II in the nucleus is important for the cap-snatching of IAV. Additionally, overexpression of CCNT1 enhances viral transcription activity, while knockdown of CCNT1 inhibits the viral replication of IAV (226). Whether CCNT1 could also have a role in the LASV replication cycle needs to be investigated in further experiments, especially since CCNT1 is mainly a nuclear protein and the LASV replication cycle takes place in the cytoplasm. Despite different cellular localizations, there is generally still the possibility of an interaction between CCNT1 and LASV L. The re-localization of cellular proteins to other compartments for viral hijacking has been widely described (227–232). For example, DDX17 and DDX5 have been shown to re-localize from the nucleus to the cytoplasm in Sindbis virus (SINV) infection, where they interact with viral RNA and capsid protein, which is important for viral replication (233). Additionally, like every protein, CCNT1 is translated in the cytoplasm, where LASV L could theoretically gain access to it.

5.2.3 Interactions of DDX17 with bunyavirus L proteins

Although bunyaviruses are highly diverse in terms of host tropism, viral transmission, and their replication cycle, common strategies include the viral transcription and genome replication in the cytoplasm, which are catalyzed by the L protein. Bunyavirus L proteins share many similarities regarding their modes of function and overall protein architecture. Based on this, it was hypothesized that interactions between bunyavirus L proteins and host proteins may also be conserved.

As it was shown before that LASV L interacts with DDX17, it was tested whether those interactions extend to other bunyavirus L proteins. The class of *Bunyaviricetes* consists of 18 families, five of which contain viruses that can cause severe human disease. Bunyavirus L proteins from the families *Arenaviridae*, *Phenuiviridae,* and *Hantaviridae* were tested for their interaction with DDX17, as they include some of the most important human pathogenic bunyaviruses.

Remarkably, it was shown that DDX17 interacted with all tested bunyavirus L proteins in co-IP, including LASV L, TCRV L, RVFV L, ANDV L, and HTNV L. This is the first evidence for an interaction of DDX17 with bunyavirus L proteins that may be conserved across multiple bunyavirus families. To date, no similarly broad virus-host interaction has been described for the bunyavirus L protein. However, further studies are required to characterize these interactions and their possible role in the bunyavirus replication cycle.

5.2.4 *In vitro* complex formation of DDX proteins and the LASV L protein

To understand the molecular mechanism underlying the interactions between viral and host proteins, it is crucial to determine whether the interactions are direct and which other factors might be involved. The identification of a direct interaction and the characterization of the interface enable the development of small molecule inhibitors for future antiviral therapies. As discussed above, it is not possible to differentiate between direct and indirect interactions with co-IP. Therefore, interaction studies with purified proteins need to be performed outside of the complex cellular environment. Under controlled conditions, it is also possible to study the influence of potential cofactors, such as ions, ATP, or RNA on the stability of the interaction.

The recombinant expression and purification of full-length DDX17 and DDX24 from *E. coli* has not yet been described in the literature and was not successful in previous experiments (186). The successful recombinant expression and purification of shorter DDX17 isoform DDX17.2 from *E. coli* and insect cells was, however, described by Ngo et al. (147). In this work, the purification of DDX17.2 from *E. coli* could not be achieved with the published procedure, and many optimization attempts were also unsuccessful. Reproducing the published procedure was hampered by a lack of

experimental details in the publication. For example, the buffer compositions for each step of the purification were not mentioned; only the final buffer composition was described. Also, details about the tag and the tag position, including possible linkers, were missing. These factors can already have an impact on protein stability. Interestingly, Nelson et al. also reported that they were unable to purify DDX17.2 from *E. coli* (159).

In general, not all human proteins are suitable for protein expression in *E. coli*. This is especially true for larger proteins, as well as proteins that require certain PTMs that are not present in *E. coli* or that rely on mammalian protein processing machineries for correct folding, stability, and function. Both DDX17 and DDX24 have PTMs, which are not present or different in *E. coli*, including phosphorylation, acetylation, and SUMOylation (150,234). Therefore, the expression system was changed to insect cells using a baculovirus expression system, which is more similar to mammalian expression concerning protein processing. This indeed yielded stable and pure full-length DDX17 and DDX24 proteins.

To test if DDX17 and DDX24 are capable of forming complexes with LASV L *in vitro*, mass photometry was employed. Mass photometry is a light scattering-based, single-particle technique that provides information on the relative abundance of molecular species and therefore also enables the study of the stoichiometry of complexes. The results indicated that DDX24 is capable of forming complexes with LASV L and the LASV L dimer *in vitro*, even though the complexes were not highly abundant. For DDX17, no evident complex formation with LASV L was observed. However, subtle increases in counts at expected masses for a complex between DDX17 and LASV L, as well as DDX17 and the LASV L dimer, suggest the presence of a complex with very low abundance that might be of lower affinity or less stable under the tested conditions.

Mass photometry requires only low sample volumes in low concentrations. This can be challenging when studying protein complexes with low binding affinities, as the equilibrium favors the unbound state in low concentrations. Indeed, initial experiments in which DDX17 or DDX24 were incubated with LASV L at a concentration of 500 nM showed no evidence of complex formation. Only when the proteins were incubated at the higher concentration of 5 µM and were diluted to 500 nM shortly before measurement could complexes be observed. This makes it technically challenging to investigate these complexes with mass photometry.

The next step would be to test whether the complexes between DDX proteins and LASV L can be stabilized. Different molar ratios between DDX proteins and LASV L could be tested for the influence on the complex formation. Adding ATP, divalent metal ions, or RNA, which are known cofactors of

DDX and/or LASV L, could lead to conformational changes in the proteins and thereby change the stability of the complex. In addition, different buffer conditions could be tested for their influence on complex stability. For example, varying salt concentrations and pH values could be tested, as those factors generally have a great impact on the stability of protein complexes (235). In theory, testing different buffer conditions and cofactors should be feasible with mass photometry, as this method is reported to be compatible with a wide range of buffers (236). However, the method was found to be very sensitive to precipitates and air bubbles in the buffer, which strongly depend on the buffer composition. Another approach to stabilize the complexes would be cross-linking of the sample at higher concentrations, as the formed complexes would not dissociate upon dilution (237). However, non-specific interactions could be stabilized, especially at higher concentrations, and lead to artificially higher mass species. Therefore, proper controls would be essential.

Low protein concentration seems to be a limitation of mass photometry when studying low-affinity protein-protein interactions. If no improvement in complex stability between DDX proteins and LASV L can be achieved by optimizing the experimental conditions in the future, other methods could be considered. For example, surface plasmon resonance could be tested, which is sensitive enough to measure even weak and transient interactions (238). However, one of the interacting proteins would need to be immobilized, which could influence the interaction.

It is also possible that further proteins are required to stabilize the complex. To identify these, hits from the combined data set could be compared with known interaction partners of the DDX proteins using databases such as STRING (239). Experimental identification of these additional interaction partners would also be feasible. For example, based on the already established co-IP setup, proteins bound to the LASV L-DDX complex could be identified with MS or specific antibodies in WB.

Although optimizations are still required, initial experiments with mass photometry demonstrated the formation of DDX-LASV L complexes, suggesting a direct interaction. The complex formation could also be tested for other bunyavirus L proteins and might enable structural studies via cryo-EM, for example, to characterize the complex and interface at high resolution.

5.2.5 Structural modeling of complexes between host proteins and bunyavirus L proteins

AlphaPulldown was used to predict models of LASV L protein fragments with the host proteins from the combined dataset (180). The model of DDX17 with the LASV L protein fragment (1398 – 1830) achieved an ipTM+pTM score of 0.743, which is above the suggested cutoff of 0.6. While the model was quite confident concerning the LASV L protein fragment, the conserved DDX17 helicase core, and the interaction interface, it could not predict the structure of the N- and C-terminal domains of

DDX17. The N- and C-terminal domains of DDX17 are intrinsically disordered (150), which means they do not fold into defined tertiary structures but adopt an ensemble of different conformations. Those intrinsically disordered regions can have several functions, such as connecting structured domains, mediating protein-protein interactions, and driving LLPS (224). Structural prediction tools like AlphaFold are currently not able to accurately capture the dynamic conformational ensembles of intrinsically disordered regions (240). It is therefore particularly important to integrate experimental data when studying proteins with intrinsically disordered regions. Indeed, the model of DDX17 and the LASV L protein fragment did not show an interaction involving the intrinsically disordered regions of DDX17. However, experimental data of the interaction of full-length DDX17 and DDX17.c with LASV L in co-IP revealed the importance of the N- and/or C-terminal domains for the interaction.

For the interaction between LASV L and DDX24, no model could be predicted using AlphaPulldown. However, this interaction was confirmed experimentally using co-IP and mass photometry. DDX24 also includes intrinsically disordered regions that might be important for the interaction with LASV L protein, but cannot be accurately predicted by AlphaFold.

Furthermore, no interaction between the RVFV L protein fragment and DDX17 was predicted by AlphaFold 3, even though it was observed in co-IP. However, in this case, there is also the possibility that the fragmentation approach is not transferable from LASV L to RVFV L or that the interaction interface with DDX17 is located at a different part of the RVFV L protein.

Four high-confidence hits of the AlphaPulldown *in silico* screen of the combined dataset (CCNT1, DDX5, RBM10, TUBG1) were tested for their interaction with LASV L in co-IP. Only for CCNT1 and DDX5, the interaction could be reliably confirmed in co-IP.

In conclusion, AlphaFold is generally a useful tool for the study of protein-protein interactions. However, it still suffers from limitations, such as the prediction of intrinsically disordered regions as described above. Furthermore, the AlphaFold algorithm was trained using experimentally determined structures from the PDB, in which viral proteins are underrepresented (179). Consequently, its performance on virus-host interaction prediction is limited, as it relies on paired multiple sequence alignments, which are often unavailable due to the rapid evolution of viral proteins, lack of homologous sequences, and asymmetric co-evolution between host and viral proteins (241,242).

5.3 Functional roles of DDX proteins in the bunyavirus replication cycle

5.3.1 The use of minireplicon systems to study virus-host interactions

The L protein plays a central role in the bunyavirus replication cycle by catalyzing the viral transcription and genome replication. Given that DDX proteins have showed an interaction with bunyavirus L proteins, their influence on the processes catalyzed by the L protein were studied. For this, minireplicon systems for LASV and RVFV were utilized (67,68). Minireplicon systems are based on the formation of RNPs, which lead to viral transcription and genome replication of the MG, resulting in reporter gene expression. They allow the study of transcription and genome replication independent from the other parts of the viral replication cycle under BSL-2 conditions. Minireplicon systems are a useful tool to study the roles of L protein residues, by comparing the transcription and genome replication activity of mutated L proteins with the wildtype. Here they were used to test whether minireplicon systems are suitable for studying the effects of knockdown or overexpression of host proteins and, if so, what effect they have.

siRNA-mediated knockdown of DDX17, DDX19, and DDX24 resulted in no apparent effects in both the LASV and RVFV minireplicon systems. WB analysis showed that the knockdown was insufficient. The small effects in reporter activity that were observed, were mostly inconsistent between two different siRNAs targeting the same DDX protein, which could not be traced back to different knockdown efficiencies according to the WB analysis. Generally, the variation within the assays was quite high, especially for the RVFV minireplicon system. Curiously, in previous work, the knockdown of DDX19 led to a significant increase of reporter activity by approximately 35 % in the LASV minireplicon system (Mann-Whitney test; $p = 0.0032$) (186). Even though the protocol was identical and the siRNAs used were the same in both experiments, this could not be reproduced here.

Minireplicon systems generally show higher levels of variation as they depend on many factors, such as cell viability, transfection efficiency, and individual handling during transfection and read-out. In addition, the experiments were performed in Huh7 cells instead of BSR-T7/5 cells, which were originally used to establish the minireplicon systems. The reason for this is that the purchased siRNAs are targeted against human genes and not those of golden hamsters (which are the origin of BSR-T7/5 cells). However, the use of T7-based minireplicon systems in Huh7 cells requires the introduction of T7 RNA polymerase. Therefore, a plasmid carrying T7 RNA polymerase under the control of a CAG promoter was co-transfected with the minireplicon components. In the minireplicon assay, the cells are already transfected with four different plasmids. Adding another plasmid increases the complexity and the total amount of DNA transfected (1260 ng for the LASV and 2010 ng

for the RVFV minireplicon system per well in a 24-well format), which can further increase the variability within the assay.

When studying the effects of siRNA-mediated knockdown of the DDX proteins, further variations are expected. Due to the additional transfection of siRNA, this experimental setup is even more dependent on transfection efficiency and also knockdown efficiency. Varying and generally low knockdown efficiencies likely result in potential effects being rather small and hard to distinguish from the variation of the assay. Therefore, minireplicon systems in this experimental setup do not appear to be suited for investigating the knockdown of host factors.

The minireplicon systems for LASV and RVFV were also used to study the effect of overexpression of DDX17, DDX19, and DDX24 on bunyavirus transcription and genome replication. Pronounced effects were visible when comparing the overexpression of DDX proteins to the transfection of an empty vector control. In the LASV minireplicon system, the reporter activity was decreased, while in the RVFV minireplicon system, the activity was increased. No differences were observed between the DDX ATPase mutants and the wildtypes. Overexpression of unrelated protein MBP was used to control for unspecific effects caused by overexpression, e.g., through saturation of the host translation machinery. MBP originates from *E. coli* and is commonly used as a protein tag to enhance the solubility of a target protein (243). Surprisingly, overexpression of MBP had similar effects as overexpression of the DDX proteins in both the LASV and RVFV minireplicon systems.

This raises the question of which control is appropriate. Overexpression of proteins may generally have an effect, meaning that the observed effects for the DDX proteins are nonspecific. It is also possible that MBP has an unexpected specific effect on the LASV and RVFV minireplicon systems, which is similar to the DDX proteins. Saskia Johanns performed similar experiments in the lab with host protein overexpression in the LASV minireplicon system and also used MBP as a control (244). She could also observe a reduction of reporter activity for all studied host proteins, which were mainly expressed with an N-myc tag in the pDEST vector. However, she did not observe the same effect for the overexpression of MBP. This suggests that MBP is rather unlikely to have an unexpected specific effect. In contrast to the experiments performed here, in which MBP and DDX proteins were expressed with an N-myc tag in the pDEST vector (CMV promoter), Saskia Johanns expressed MBP with the pOPIN-M vector (T7 and CMV promoter) (245). In contrast to the pDEST vector, which is a mammalian expression vector, pOPIN-M is a shuttle vector that allows mammalian, bacterial, and insect expression of target proteins with an MBP tag. It is therefore possible that the observed effects are a result of nonspecific effects caused by the vector backbone or the tag. Further experiments should be performed to test this hypothesis. For example, the DDX proteins could be cloned into the

pDEST vector and a pOPIN vector, with and without N-myc, to see if the effects persist. Without further studies and appropriate controls, no conclusions can be drawn on the possible effects of overexpression of DDX proteins on LASV and RVFV transcription and genome replication.

Taken together, it is questionable whether minireplicon systems are generally suited for the investigation of virus-host interactions in this experimental setup, as high variability may not allow the detection of small effects that are expected for the knockdown of host factors, and overexpression seems to interfere with the system itself.

Bunyavirus minireplicon systems have occasionally been used by other groups to study the effects of knockdown or knockout of host factors on viral transcription and genome replication. For example, Loureiro et al. investigated the effects DDX3 knockout on LCMV transcription and genome replication (183). Reporter activity in DDX3 knockout cells was decreased by approximately 50 %, which was defined as highly significant ($p < 0.001$; Student's t-test). However, normalization of all values to the wildtype cells resulted in one group showing neither variance nor normal distribution, which is a prerequisite for the selected statistical test. Fang et al. investigated the effect of siRNA-mediated knockdown of GSPT-1 on LASV transcription and genome replication (185). Reporter activity was normalized to a non-targeted control and was decreased by approximately 50 %, which was defined as highly significant ($p < 0.001$; Welch's t-test). The experiment was performed in two biological replicates with three technical triplicates, and all six data points were included in the statistical analysis, which fulfills the definition of pseudo-replication and can lead to false statistical significances (246). Although the statistical analysis of the results of both studies could affect the significance of the results, considerable effects were observed. Whether this has biological causes, meaning that it depends on the investigated host factors, or whether the minireplicon systems used produce more stable results and are therefore more suitable for observing smaller effects, is questionable. In the experiments by Fang et al. with the LASV minireplicon system (185), a different cell type, different promoters, and a different MG were used compared to the experimental setup in this work. For future experiments, it might therefore be conceivable to further optimize the experimental conditions in order to achieve a lower variation of the assay and to be able to observe smaller effects.

5.3.2 Effects of DDX gene silencing on the bunyavirus replication cycle

Silencing of host factor genes in infection experiments enables the identification of host factors that are essential for viral replication. To test the influence of DDX17 and DDX24 gene silencing on the bunyavirus replication cycle, first, siRNA-mediated knockdown was tested on RVFV replication. Therefore, Huh7 cells were transfected with siRNA, infected with RVFV, and the viral titers were determined 24 h after infection. Increases of viral titers could be observed upon knockdown of DDX17 and DDX24, but seemed to be within the normal variation of the assay. WB analysis revealed that the knockdown was insufficient.

Comparing the observed effects to the literature, they were within the range that is usually considered as apparent effects. For example, a study by Moy et al. on the influence of DDX17 on RVFV replication showed an increase in the percentage of RVFV-infected cells that were treated with an siRNA against DDX17 of slightly above 1.5-fold compared to a non-targeted control (159). Another study by Balaraman et al. that investigated the effects of host factor knockdown on RVFV replication observed a reduction of viral titers by 56 % upon siRNA-mediated knockdown of host factor WDR7 and a reduction of 96 % upon knockdown of RVFV NP, which served as a positive control (247). In the experiments performed in this work, knockdown of DDX17 in RVFV infection led to a 3-fold increase in viral titers for siRNA DDX17 #1 and a 6-fold increase for siRNA DDX17 #2. Nevertheless, these effects were within the variation of the assay. It was assumed that an improvement of the knockdown efficiency could lead to stronger and more consistent effects. Since the knockdown efficiency of siRNAs strongly depends on transfection efficiency, the stable expression of shRNAs targeting DDX proteins was tested next.

Replication-deficient lentiviral vectors were used for the generation of cell lines with stable shRNA-mediated knockdown of DDX proteins. Huh7 cells with DDX17 or DDX24 knockdown were infected with LASV or RVFV, and the viral titers were determined at different time points. Upon DDX17 knockdown, LASV titers were only slightly increased at 48 h, and RVFV titers were increased at 24 and 48 h after infection. Upon DDX24 knockdown, LASV titers were slightly decreased at 48 and 72 h, while RVFV titer was slightly increased after 24 h. WB analysis confirmed the knockdown in the LASV infection with low knockdown efficiency, while in the RVFV infection the knockdown could not be confirmed. Therefore, the observed effects on RVFV replication might not be the result of DDX17 or DDX24 knockdown in this experimental setup.

It is possible that the shRNA-mediated knockdown of DDX17 and DDX24 was not stable over time despite maintaining the selection pressure. RVFV infection was carried out at a higher cell passage

than LASV infection. Indeed, loss of shRNA expression despite maintaining selection pressure has been previously reported and may be the result of epigenetic silencing of shRNA expression cassettes (248). Alternatively, RVFV infection itself could have led to an increased expression of these proteins. For example, DDX24 is a known ISG and may be upregulated upon viral infections (165). Transcriptomic analysis performed in HEK293 and human small airway epithelial cells infected with RVFV, however, showed no upregulation of DDX24 (249,250). Whether this might be the case in this experimental setup could be tested by analyzing the protein levels of DDX17 and DDX24 in cells infected with RVFV and in uninfected cells. Additionally, shRNA-mediated knockdown of DDX17 might have been less efficient due to its role in the RNAi pathway. DDX17 is a positive regulator of the Drosha/DGCR8 complex, which processes primary miRNAs to precursor miRNAs. These precursor miRNAs are then exported from the nucleus and further cleaved by Dicer to form double-stranded miRNAs. miRNAs are then loaded onto RISC, similar to siRNAs (198). Since shRNAs resemble primary miRNAs, they also require processing by the Drosha/DGCR8 complex. Therefore, shRNA-mediated knockdown of DDX17 may be self-limiting.

Generally, knockdown efficiency did not improve after changing the knockdown strategy from transfecting siRNAs to stable expression of shRNAs. To overcome the problems associated with knockdown, the effect of DDX17 knockout on bunyavirus replication was tested. Infection experiments with a collection of bunyaviruses from three different families (*Arenaviridae*, *Phenuiviridae*, and *Hantaviridae*) were performed, which previously showed an interaction of the L protein with DDX17 in co-IP. Viral titers were determined at different time points to observe the growth kinetics. No effects could be observed for LASV, TCRV, and RVFV infections in DDX17 KO cells compared to the control cells. No effects could be observed for ANDV as well, but ANDV did not seem to grow efficiently on HEK293 cells in general. Consistent with this, a literature search did not reveal studies in which HEK293 cells were used for infection experiments with ANDV. However, an effect was observed for HTNV in the infection experiment performed here, as viral titers were increased at 72 to 144 h after infection in the DDX17 KO cells.

Generally, the DDX17 KO cells showed slower growth compared to the control cells. Since knockout of DDX17 is expected to result in increased viral titers, which was observed for RVFV upon DDX17 knockdown to some extent in this work and in the study by Moy et al. (159), small effects could be compensated for due to a lower cell count. However, as DDX17 was completely depleted compared to the knockdown experiments, it was expected that the effect would be stronger. This raises the question of why a stronger phenotype was not observed. It is possible that the complete knockout of DDX17 led to the upregulation of related genes and thereby phenotype loss. This phenomenon has

been widely described and is referred to as genetic compensation (251). Since some DDX proteins are very similar and show overlapping functions, it is conceivable that another DDX protein takes over the function of DDX17. Indeed, DDX17 and its paralog DDX5 are more closely related than any other member of the DDX family. DDX17 was shown to be upregulated upon DDX5 knockdown, but not the other way around, in HeLa cells (252). Whether the knockout of DDX17 leads to an upregulation of DDX5 in HEK293 cells needs to be tested with specific DDX5 antibodies in the WB analysis of DDX17 KO and control cells in future experiments.

Both protein-specific and redundant roles in viral infections have been described for DDX17 and DDX5. For example, DDX17 but not DDX5 has been described to restrict RVFV infection (159). For HBV, DDX17 and DDX5 have been demonstrated to enhance viral transcriptional read-through, thereby promoting the destabilization of viral RNA (161). For SINV, a synergistic proviral effect of DDX5 and DDX17 was described (233). Taken together, DDX17 and DDX5 can have overlapping or protein-specific effects on viral infection, which can be pro- and anti-viral depending on the virus.

The predominant absence of effects in the bunyavirus infection experiments with the DDX17 KO cells could be explained by redundant roles of DDX17 and DDX5. It is possible that no phenotype of DDX17 knockout could be observed for LASV, TCRV, and RVFV infection, as DDX5 may have taken over its function. Indeed, DDX5 also showed an interaction with LASV L in co-IP. Supporting this hypothesis, structural modeling of DDX17 and DDX5 in complex with LASV L showed the formation of a similar complex, as can be seen in Figure 24 (180).

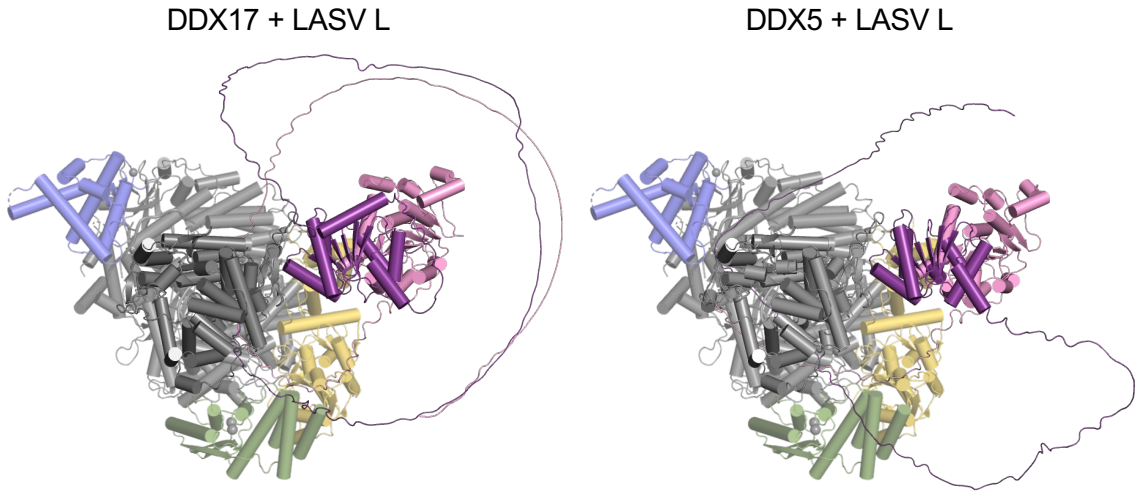

Figure 24: Comparison of the models of DDX17 and DDX5 in complex with LASV L. The complexes of LASV L protein fragment (UniProt ID: O09705; 1398 – 1830) and full-length DDX17 (UniProt ID: Q92841) or DDX5 (UniProt ID: P17844) were predicted by AlphaFold Multimer and are superimposed onto the LASV L structure in elongation state (PDB: 7ojn). DDX17 and DDX5 RecA-like domain 1 and N-terminal domain are colored in pink, RecA-like domain 2 and C-terminal domain in violet, and LASV L fragment in grey. LASV L elongation structure is faded in the background with the EN domain colored in green, the pyramid domain in blue, the C-terminus in yellow, and the rest, including the RdRp, in grey.

To further investigate this hypothesis, an additional siRNA knockdown of DDX5 could be performed in the DDX17 KO cells. If this reveals an effect on the viral titers of the investigated bunyaviruses, it would suggest that DDX5 and DDX17 have synergistic roles.

For HTNV, a distinct phenotype could be observed upon DDX17 knockout, suggesting a stronger dependency on DDX17 compared to the other tested bunyaviruses.

Coming back to the different approaches to investigate the effects of DDX silencing on bunyavirus replication, siRNA-mediated knockdown proved to be the most suitable after all. Firstly, distinct effects on RVFV titers were observed there, which are, at least for DDX17 knockdown, comparable to other studies (159). Additionally, siRNA-mediated knockdown is not dependent on processing by the Drosha/DGCR8 complex, which might lead to self-limitation of shRNA-mediated knockdown of DDX17. Finally, genetic compensation generally does not occur in knockdown compared to knockout (251).

Future experiments could further study the effect of siRNA-mediated knockdown of DDX17 and DDX24 for different bunyaviruses. By increasing the number of biological replicates and observing multiple timepoints, it might be possible to observe effects beyond the variation of the assay. Alternatively, inducible knockout systems, such as the Cre/loxP system or inducible CRISPR/Cas9 approaches could be used to overcome the challenge of genetic compensation by inducing the knockout only shortly before infection (253,254).

5.4 Potential roles of DDX proteins in the bunyavirus replication cycle

This work revealed that DDX proteins interact with bunyavirus L proteins, especially in the cellular context. Complex formation was also detected *in vitro* with purified proteins, but it was a rare event. Functional studies have not provided fully conclusive results yet and require further studies. Therefore, potential functional roles of the interactions between the DDX proteins and the bunyavirus L proteins can only be speculated at present and will need to be investigated in further studies. DDX proteins are multifunctional RNA-binding proteins that play important roles in both host RNA metabolism and innate immune responses (127,128,131,143). Based on their cellular functions and their roles in the replication cycles of other viruses, their functional role in bunyavirus infection can be speculated.

(I) One possibility is that DDX proteins, which act as RNA-RNA remodelers, support the bunyavirus L protein to read the genomic RNA by resolving secondary structures. For example, direct interaction with viral RNA has been shown to support the viral replication cycle for some DDX proteins and viruses, such as DDX6 and DENV (145). Facilitating read-through of secondary structures of the UTRs and other RNA regions could be important for efficient genome replication of bunyaviruses. For some bunyaviruses like the *Arenaviridae,* the genes are arranged in an ambisense orientation and separated by GC-rich IGRs that form stable secondary structures. Termination of transcription occurs at those IGRs that appear to function as physical barriers (60). In genome replication, however, the L proteins can read through those regions. This process could also be regulated by DDX proteins.

(II) As a second hypothesis, a role of DDX proteins in the termination of bunyavirus transcription would also be conceivable. DDX proteins might stabilize and therefore promote the formation of secondary structures in nascent RNA transcripts that exit from the RdRp active site and thereby cause transcript release from the template strand.

(III) Thirdly, it is also conceivable that DDX proteins transiently displace NP from the genomic RNA by acting as RNA-protein remodelers and thereby facilitating translocation of the RNA into the L protein RdRp active site. In line with this, DDX3 has been shown to interact with LASV and LCMV NP and supporting RNA synthesis dependent on the DDX enzymatic function (183).

(IV) Another possibility is that an interaction of the bunyavirus L protein with the DDX proteins could have the purpose of immune evasion, as DDX proteins can act as cytoplasmic sensors to recognize viral RNA and induce the innate immune response. Both DDX17 and DDX24 have been shown to

restrict viral infections by interacting with the RNA of RVFV or mRNAs of KSHV, respectively (159,167).

(V) Related to this, independent of a possible function of DDX proteins as cytoplasmic sensors, many DDX proteins are involved in innate immune signaling. Interactions between the L protein and DDX proteins may therefore positively or negatively regulate RLR signaling, for example.

(VI) Another possible function of DDX proteins could be the recruitment of viral RNPs to sites of transcription and/or replication. Many DDX proteins are predicted to perform LLPS and are involved in the formation, regulation, and breakdown of MLOs (141). Localization studies of NP demonstrated co-localization with P-body resident proteins for some bunyaviruses, such as hantaviruses and RVFV (255,256). P-bodies are MLOs in the cytoplasm, in which cellular mRNAs can be stored or degraded, which might serve as targets for cap snatching (89). Both DDX17 and DDX24 are enriched in P-bodies (142,148).

(VII) Regarding viral cap-snatching, an interaction of bunyavirus L protein with DDX proteins could also mediate the access to cellular mRNAs, as many DDX proteins, such as DDX19, bind to mRNAs (170,257). This idea would be consistent with the nucleic acid dependency of the interaction between DDX19 and LASV L, since an interaction with DDX19 without bound mRNA would not be favorable for the L protein.

(VIII) Furthermore, it is conceivable that DDX proteins modulate the binding of cellular cap-binding proteins to the 5’ cap of cellular mRNAs by acting as RNA-protein remodelers to enable cap-snatching by the L protein.

(IX) DDX19 is also described to be part of the nuclear pore complex and regulates the final step of mRNA export (169). Interaction with bunyavirus L proteins might lead to sequestration of DDX19 in the cytoplasm or inhibition and thereby hinder the export of cellular mRNAs from the nucleus. Many viruses, such as IAV or SARS-CoV-2, have been shown to target the export of cellular mRNAs through a variety of mechanisms to favor viral mRNA translation and/or suppress immune responses (258). In RVFV infections, specific cellular mRNAs have been shown to accumulate in the nucleus, presumably mediated by the NSs protein through an unknown mechanism (250,259).

In summary, many possible roles of DDX proteins in the bunyavirus replication cycle exist. It would be interesting to explore whether one or more of these roles are carried out by different DDX proteins. Overall, the potential roles of DDX proteins in the bunyavirus replication cycle are likely complex and may involve their functions in RNA-RNA and RNA-protein remodelling as well as the modulation of the innate immune response, with both pro- and anti-viral functions being conceivable.

5.5 Conclusion and outlook

In this work, the roles of potential host factors, especially of the DDX family, on bunyavirus replication were investigated, particularly through their interaction with the LASV L protein. The findings suggest that DDX17, DDX19, and DDX24 interact with LASV L in the cellular context, although the interactions differ in their dependence on nucleic acids. DDX17 and DDX24 interactions appeared to be nucleic acid-independent, while DDX19 required nucleic acids, suggesting differing mechanisms of interaction. Additionally, DDX17 showed interactions with L proteins from three bunyavirus families, including LASV L, TCRV L, RVFV L, ANDV L, and HTNV L. Studies with purified proteins revealed the capability of DDX24 and, to some extent, also DDX17 to form complexes with LASV L *in vitro*, although those were of low abundance.

Functional studies provided ambiguous results on whether these interactions are essential for viral replication. Knockdown and knockout experiments of DDX17 and DDX24 showed limited or inconsistent effects on the bunyavirus replication cycle, potentially due to incomplete knockdowns, high variability of the assays, or compensatory mechanisms of the cells (e.g., redundancy with closely related proteins like DDX5 and genetic compensation). It was found that LASV and RVFV minireplicon systems are not suitable for studying the effects of host protein knockdown or overexpression on bunyavirus transcription and genome replication in their current setup. High variability in the assay, incomplete knockdown, and non-specific overexpression effects, which were mirrored by controls, emphasize the need for assessment in infection experiments with full virus.

In summary, this work revealed interactions between LASV L proteins and host proteins, especially from the DDX protein family, but also including CCNT1, and provides indications that a functional relationship may exist. In addition, DDX17 was identified as a conserved interaction partner of bunyavirus L proteins across several families. This is the first description of such a broad virus-host interaction of the bunyavirus L protein. Furthermore, this work forms a methodological basis for future studies, as various assays have been established and evaluated for their feasibility in studying virus-host interactions. This provides a good platform for the identification of new targets for antiviral strategies with broad-spectrum potential in the future. However, further studies are required to characterize these interactions and their possible role in the bunyavirus replication cycle.

REFERENCES

1. SMITHBURN KC, HADDOW AJ, MAHAFFY AF. A neurotropic virus isolated from Aedes mosquitoes caught in the Semliki forest. Am J Trop Med Hyg [Internet]. 1946 Mar 1 [cited 2025 Apr 18];26:189–208. Available from: https://pubmed.ncbi.nlm.nih.gov/21020339/

2. Murphy FA, Harrison AK, Whitfield SG. Bunyaviridae: Morphologic and Morphogenetic Similarities of Bunyamwera Serologic Supergroup Viruses and Several Other Arthropod-Borne Viruses. Intervirology [Internet]. 1973 Apr 1 [cited 2025 Apr 18];1(4):297–316. Available from: https://dx.doi.org/10.1159/000148858

3. Adams MJ, Lefkowitz EJ, Andrew •, King MQ, Harrach B, Robert •, et al. Changes to taxonomy and the International Code of Virus Classification and Nomenclature ratified by the International Committee on Taxonomy of Viruses (2017). [cited 2025 Apr 18]; Available from: http://www.ictv.global/

4. Kuhn JH, Brown K, Adkins S, Torre JC de la, Digiaro M, Ergünay K, et al. Promotion of order Bunyavirales to class Bunyaviricetes to accommodate a rapidly increasing number of related polyploviricotine viruses. J Virol [Internet]. 2024 Oct 22 [cited 2025 Apr 18];98(10):e01069-24. Available from: https://pmc.ncbi.nlm.nih.gov/articles/PMC11494962/

5. International Committee on Taxonomy of Viruses.

6. PATHOGENS PRIORITIZATION A SCIENTIFIC FRAMEWORK FOR EPIDEMIC AND PANDEMIC RESEARCH PREPAREDNESS. 2024;

7. Radoshitzky SR, Buchmeier MJ, Charrel RN, Gonzalez JPJ, Günther S, Hepojoki J, et al. ICTV Virus Taxonomy Profile: Arenaviridae 2023. J Gen Virol [Internet]. 2023 [cited 2025 Apr 19];104(9). Available from: https://pubmed.ncbi.nlm.nih.gov/37698490/

8. Walker DH, McCormick JB, Johnson KM, Webb PA, Komba-Kono G, Elliott LH, et al. Pathologic and virologic study of fatal Lassa fever in man. Am J Pathol. 1982;

9. Günther S, Lenz O. Lassa virus. Critical Reviews in Clinical Laboratory Sciences. 2004.

10. Lendino A, Castellanos AA, Pigott DM, Han BA. A review of emerging health threats from zoonotic New World mammarenaviruses. BMC Microbiol [Internet]. 2024 Dec 1 [cited 2025 Apr 19];24(1):1–9. Available from: https://bmcmicrobiol.biomedcentral.com/articles/10.1186/s12866-024-03257-w

11. Hastie KM, Melnik LI, Cross RW, Klitting RM, Andersen KG, Saphire EO, et al. The

Arenaviridae Family: Knowledge Gaps, Animal Models, Countermeasures, and Prototype Pathogens. J Infect Dis [Internet]. 2023 Oct 15 [cited 2025 Apr 19];228(Suppl 6):S359. Available from: https://pmc.ncbi.nlm.nih.gov/articles/PMC10582522/

12. Briese T, Paweska JT, McMullan LK, Hutchison SK, Street C, Palacios G, et al. Genetic detection and characterization of Lujo virus, a new hemorrhagic fever-associated arenavirus from southern Africa. PLoS Pathog [Internet]. 2009 May [cited 2025 Apr 19];5(5). Available from: https://pubmed.ncbi.nlm.nih.gov/19478873/

13. Dan-Nwafor CC, Ipadeola O, Smout E, Ilori E, Adeyemo A, Umeokonkwo C, et al. A cluster of nosocomial Lassa fever cases in a tertiary health facility in Nigeria: Description and lessons learned, 2018. Int J Infect Dis [Internet]. 2019 Jun 1 [cited 2025 Apr 19];83:88–94. Available from: https://pubmed.ncbi.nlm.nih.gov/30930184/

14. McLay L, Liang Y, Ly H. Comparative analysis of disease pathogenesis and molecular mechanisms of New World and Old World arenavirus infections. J Gen Virol [Internet]. 2014 [cited 2025 Apr 19];95(Pt 1):1. Available from: https://pmc.ncbi.nlm.nih.gov/articles/PMC4093776/

15. Monath TP, Mertens PE, Patton R, Moser CR, Baum JJ, Pinneo L, et al. A hospital epidemic of Lassa fever in Zorzor, Liberia, March-April, 1972. Am J Trop Med Hyg. 1973;

16. Fichet-Calvet E, Rogers DJ. Risk maps of lassa fever in West Africa. PLoS Negl Trop Dis. 2009;

17. Olayemi A, Fichet-Calvet E. Systematics, ecology, and host switching: Attributes affecting emergence of the Lassa virus in rodents across western Africa. Viruses. 2020.

18. Bonwitt J, Sáez AM, Lamin J, Ansumana R, Dawson M, Buanie J, et al. At home with mastomys and rattus: Human-rodent interactions and potential for primary transmission of lassa virus in domestic spaces. Am J Trop Med Hyg. 2017;

19. McCormick JB, Webb PA, Krebs JW, Johnson KM, Smith ES. A Prospective Study of the Epidemiology and Ecology of Lassa Fever. J Infect Dis. 1987;

20. Basinski AJ, Fichet-Calvet E, Sjodin AR, Varrelman TJ, Remien CH, Layman NC, et al. Bridging the gap: Using reservoir ecology and human serosurveys to estimate Lassa virus spillover in West Africa. PLoS Comput Biol. 2021;

21. Asogun DA, Günther S, Akpede GO, Ihekweazu C, Zumla A. Lassa Fever: Epidemiology, Clinical Features, Diagnosis, Management and Prevention. Infectious Disease Clinics of

North America. 2019.

22. Moraz ML, Kunz S. Pathogenesis of arenavirus hemorrhagic fevers. Expert Review of Anti-Infective Therapy. 2011.

23. Casals J, Buckley SM. Lassa Fever, a New Virus Disease of Man from West Africa. Am J Trop Med Hyg. 1970;

24. Yun NE, Walker DH. Pathogenesis of lassa fever. Viruses. 2012.

25. Downs WG, Anderson CR, Spence L, Aitken TH, Greenhall AH. Tacaribe virus, a new agent isolated from Artibeus bats and mosquitoes in Trinidad, West Indies. Am J Trop Med Hyg [Internet]. 1963 [cited 2025 Apr 19];12:640–6. Available from: https://pubmed.ncbi.nlm.nih.gov/22324073/

26. Schountz T. Unraveling the mystery of Tacaribe virus. 2024; Available from: https://doi.org/10.1128/msphere.00520-24

27. Holzerland J, Leske A, Fénéant · Lucie, Garcin D, Kolakofsky D, Groseth · Allison. Complete genome sequence of Tacaribe virus. 2020;165:1899–903. Available from: https://doi.org/10.1007/s00705-020-04681-9

28. Sasaya T, Palacios G, Briese T, Serio F Di, Groschup MH, Neriya Y, et al. ICTV Virus Taxonomy Profile: Phenuiviridae 2023. J Gen Virol. 2023;104(9).

29. Zhou CM, Jiang ZZ, Liu N, Yu XJ. Current insights into human pathogenic phenuiviruses and the host immune system. Virulence [Internet]. 2024 [cited 2025 Apr 24];15(1):2384563. Available from: https://pmc.ncbi.nlm.nih.gov/articles/PMC11290763/

30. Casel MA, Park SJ, Choi YK. Severe fever with thrombocytopenia syndrome virus: emerging novel phlebovirus and their control strategy. Exp Mol Med 2021 535 [Internet]. 2021 May 6 [cited 2025 Apr 24];53(5):713–22. Available from: https://www.nature.com/articles/s12276-021-00610-1

31. McMullan LK, Folk SM, Kelly AJ, MacNeil A, Goldsmith CS, Metcalfe MG, et al. A new phlebovirus associated with severe febrile illness in Missouri. N Engl J Med [Internet]. 2012 Aug 30 [cited 2025 Apr 24];367(9):834–41. Available from: https://pubmed.ncbi.nlm.nih.gov/22931317/

32. Moriconi M, Rugna G, Calzolari M, Bellini R, Albieri A, Angelini P, et al. Phlebotomine sand fly-borne pathogens in the Mediterranean Basin: Human leishmaniasis and phlebovirus

infections. PLoS Negl Trop Dis [Internet]. 2017 Aug 1 [cited 2025 Apr 24];11(8). Available from: https://pubmed.ncbi.nlm.nih.gov/28796786/

33. Gaudreault NN, Indran S V., Balaraman V, Wilson WC, Richt JA. Molecular aspects of Rift Valley fever virus and the emergence of reassortants. Virus Genes [Internet]. 2019 Feb 15 [cited 2025 Apr 24];55(1). Available from: https://pubmed.ncbi.nlm.nih.gov/30426314/

34. Field and laboratory evidence implicating Culex zombaensis and Aedes circumluteolus as vectors of Rift Valley Fever virus in Coastal South Africa (| Enhanced Reader.

35. Pepin M, Bouloy M, Bird BH, Kemp A, Paweska J. Rift Valley fever virus (Bunyaviridae: Phlebovirus): an update on pathogenesis, molecular epidemiology, vectors, diagnostics and prevention. [cited 2025 Apr 24]; Available from: www.vetres.org

36. Nicholas DE, Jacobsen KH, Waters NM. Risk factors associated with human Rift Valley fever infection: systematic review and meta-analysis. Trop Med Int Heal [Internet]. 2014 Dec 1 [cited 2025 Apr 27];19(12):1420–9. Available from: https://onlinelibrary.wiley.com/doi/full/10.1111/tmi.12385

37. Wright D, Kortekaas J, Bowden TA, Warimwe GM. Rift Valley fever: biology and epidemiology. J Gen Virol [Internet]. 2019 [cited 2025 Apr 27];100(8):1187. Available from: https://pmc.ncbi.nlm.nih.gov/articles/PMC7613496/

38. Wichgers Schreur PJ, Van Keulen L, Kant J, Oreshkova N, Moormann RJM, Kortekaas J. Co-housing of Rift Valley fever virus infected lambs with immunocompetent or immunosuppressed lambs does not result in virus transmission. Front Microbiol [Internet]. 2016 Mar 7 [cited 2025 Apr 27];7(MAR):183279. Available from: www.frontiersin.org

39. Adam I, Karsany MS. Case report: Rift Valley Fever with vertical transmission in a pregnant Sudanese woman. J Med Virol [Internet]. 2008 May 1 [cited 2025 Apr 27];80(5):929–929. Available from: https://onlinelibrary.wiley.com/doi/full/10.1002/jmv.21132

40. Antonis AFG, Kortekaas J, Kant J, Vloet RPM, Vogel-Brink A, Stockhofe N, et al. Vertical Transmission of Rift Valley Fever Virus Without Detectable Maternal Viremia. https://home.liebertpub.com/vbz [Internet]. 2013 Aug 9 [cited 2025 Apr 27];13(8):601–6. Available from: https://www.liebertpub.com/doi/10.1089/vbz.2012.1160

41. Dungu B, Lubisi BA, Ikegami T. Rift Valley fever vaccines: current and future needs. Curr Opin Virol. 2018 Apr 1;29:8–15.

42. Chen RX, Gong HY, Wang X, Sun MH, Ji YF, Tan SM, et al. Zoonotic Hantaviridae with

Global Public Health Significance. Viruses [Internet]. 2023 Aug 1 [cited 2025 Apr 19];15(8):1705. Available from: https://pmc.ncbi.nlm.nih.gov/articles/PMC10459939/

43. Kabwe E, Davidyuk Y, Shamsutdinov A, Garanina E, Martynova E, Kitaeva K, et al. Orthohantaviruses, Emerging Zoonotic Pathogens. Pathog (Basel, Switzerland) [Internet]. 2020 Sep 1 [cited 2025 Apr 19];9(9):1–21. Available from: https://pubmed.ncbi.nlm.nih.gov/32971887/

44. Bi Z, Formenty PBH, Roth CE. Hantavirus infection: a review and global update. J Infect Dev Ctries [Internet]. 2008 [cited 2025 Apr 19];2(1):3–23. Available from: https://pubmed.ncbi.nlm.nih.gov/19736383/

45. Afzal S, Ali L, Batool A, Afzal M, Kanwal N, Hassan M, et al. Hantavirus: an overview and advancements in therapeutic approaches for infection. Front Microbiol [Internet]. 2023 [cited 2025 Apr 19];14:1233433. Available from: https://pmc.ncbi.nlm.nih.gov/articles/PMC10601933/

46. Kuhn JH, Schmaljohn CS. A Brief History of Bunyaviral Family Hantaviridae. Diseases [Internet]. 2023 Mar 1 [cited 2025 Apr 19];11(1):38. Available from: https://pmc.ncbi.nlm.nih.gov/articles/PMC10047430/

47. Khaiboullina S, Morzunov S, St. Jeor S. Hantaviruses: molecular biology, evolution and pathogenesis. Curr Mol Med [Internet]. 2005 Nov 29 [cited 2025 Apr 19];5(8):773–90. Available from: https://pubmed.ncbi.nlm.nih.gov/16375712/

48. Lee HW, Lee RW, Johnson KM. Isolation of the etiologic agent of Korean Hemorrhagic fever. J Infect Dis [Internet]. 1978 [cited 2025 Apr 19];137(3):298–308. Available from: https://pubmed.ncbi.nlm.nih.gov/24670/

49. Massari S, Desantis J, Nizi MG, Cecchetti V, Tabarrini O. Inhibition of Influenza Virus Polymerase by Interfering with Its Protein-Protein Interactions. ACS Infectious Diseases. 2021.

50. Noh JY, Jung J, Song JW. Hemorrhagic Fever with Renal Syndrome. Infect Chemother [Internet]. 2019 Dec 1 [cited 2025 Apr 19];51(4):405. Available from: https://pmc.ncbi.nlm.nih.gov/articles/PMC6940369/

51. Liu R, Ma H, Shu J, Zhang Q, Han M, Liu Z, et al. Vaccines and Therapeutics Against Hantaviruses. Front Microbiol [Internet]. 2020 Jan 30 [cited 2025 Apr 19];10. Available from: https://pubmed.ncbi.nlm.nih.gov/32082263/

52. Oloris SCS, Neves VF, Iani FCM, de Oliveira Scarponi CF. Orthohantavirus infections in South America: a systematic review and meta-analysis. Arch Virol [Internet]. 2024 Sep 1 [cited 2025 Apr 19];169(9):1–11. Available from: https://link.springer.com/article/10.1007/s00705-024-06104-5

53. Martinez-Valdebenito C, Calvo M, Vial C, Mansilla R, Marco C, Palma RE, et al. Person-to-person household and nosocomial transmission of andes hantavirus, Southern Chile, 2011. Emerg Infect Dis [Internet]. 2014 Oct 1 [cited 2025 Apr 19];20(10):1629–36. Available from: https://pubmed.ncbi.nlm.nih.gov/25272189/

54. Toledo J, Haby MM, Reveiz L, Sosa Leon L, Angerami R, Aldighieri S. Evidence for Human-to-Human Transmission of Hantavirus: A Systematic Review. J Infect Dis [Internet]. 2022 Oct 15 [cited 2025 Apr 19];226(8):1362–71. Available from: https://pubmed.ncbi.nlm.nih.gov/34515290/

55. Ogbu O. Viruses: Lassa Fever Virus. In: Encyclopedia of Food Safety. 2014.

56. Parvate A, Williams EP, Taylor MK, Chu YK, Lanman J, Saphire EO, et al. Diverse Morphology and Structural Features of Old and New World Hantaviruses. Viruses 2019, Vol 11, Page 862 [Internet]. 2019 Sep 16 [cited 2025 Apr 22];11(9):862. Available from: https://www.mdpi.com/1999-4915/11/9/862/htm

57. Freiberg AN, Sherman MB, Morais MC, Holbrook MR, Watowich SJ. Three-Dimensional Organization of Rift Valley Fever Virus Revealed by Cryoelectron Tomography. J Virol [Internet]. 2008 [cited 2025 Apr 22];82(21):10341–8. Available from: http://cryoem.ucsd.edu/programs.shtm

58. Leventhal SS, Wilson D, Feldmann H, Hawman DW. A Look into Bunyavirales Genomes: Functions of Non-Structural (NS) Proteins. Viruses [Internet]. 2021 Feb 1 [cited 2025 Apr 22];13(2):314. Available from: https://pmc.ncbi.nlm.nih.gov/articles/PMC7922539/

59. Lukasitevicit IS, Stel~iakh TA, Golltbev VP, Stctiesljenok ~ P, Lenesttko NN. Archives of Virology Ribonueleie Acids of Maehupo and Lassa Viruses. Arch Virol. 1984;79:189–203.

60. Auperin DD, Romanowski V, Galinski M, Bishop DH. Sequencing studies of pichinde arenavirus S RNA indicate a novel coding strategy, an ambisense viral S RNA. J Virol. 1984;

61. Barr JN, Wertz GW. Bunyamwera Bunyavirus RNA Synthesis Requires Cooperation of 3-and 5-Terminal Sequences. J Virol [Internet]. 2004 [cited 2025 Apr 22];78(3):1129–38. Available from: https://journals.asm.org/journal/jvi

62. Hass M, Westerkofsky M, Müller S, Becker-Ziaja B, Busch C, Günther S. Mutational Analysis of the Lassa Virus Promoter. J Virol. 2006;

63. Arragain B, Durieux Trouilleton Q, Baudin F, Provaznik J, Azevedo N, Cusack S, et al. Structural snapshots of La Crosse virus polymerase reveal the mechanisms underlying Peribunyaviridae replication and transcription. Nat Commun 2022 131 [Internet]. 2022 Feb 16 [cited 2025 Apr 22];13(1):1–16. Available from: https://www.nature.com/articles/s41467-022-28428-z

64. Williams HM, Thorkelsson SR, Vogel D, Milewski M, Busch C, Cusack S, et al. Structural insights into viral genome replication by the severe fever with thrombocytopenia syndrome virus L protein. Nucleic Acids Res [Internet]. 2023 Feb 22 [cited 2025 Apr 22];51(3):1424–42. Available from: https://pubmed.ncbi.nlm.nih.gov/36651274/

65. Kouba T, Vogel D, Thorkelsson SR, Quemin ERJ, Williams HM, Milewski M, et al. Conformational changes in Lassa virus L protein associated with promoter binding and RNA synthesis activity. Nat Commun. 2021 Dec 2;12(1):7018.

66. Lee KJ, Novella IS, Teng MN, Oldstone MBA, de la Torre JC. NP and L Proteins of Lymphocytic Choriomeningitis Virus (LCMV) Are Sufficient for Efficient Transcription and Replication of LCMV Genomic RNA Analogs. J Virol. 2000;

67. Hass M, Gölnitz U, Müller S, Becker-Ziaja B, Günther S. Replicon System for Lassa Virus. J Virol. 2004;

68. Jérôme H, Rudolf M, Lelke M, Pahlmann M, Busch C, Bockholt S, et al. Rift valley fever virus minigenome system for investigating the role of L protein residues in viral transcription and replication. J Gen Virol [Internet]. 2019 Jul 1 [cited 2025 Feb 4];100(7):1093–8. Available from: https://www.microbiologyresearch.org/content/journal/jgv/10.1099/jgv.0.001281

69. Elliott RM. Orthobunyaviruses: recent genetic and structural insights. Nat Rev Microbiol 2014 1210 [Internet]. 2014 Sep 8 [cited 2025 Apr 22];12(10):673–85. Available from: https://www.nature.com/articles/nrmicro3332

70. Ortiz-Riaño E, Cheng BYH, de la Torre JC, Martínez-Sobrido L. The C-Terminal Region of Lymphocytic Choriomeningitis Virus Nucleoprotein Contains Distinct and Segregable Functional Domains Involved in NP-Z Interaction and Counteraction of the Type I Interferon Response. J Virol [Internet]. 2011 Dec 15 [cited 2025 May 8];85(24):13038–48. Available from: https://journals.asm.org/doi/10.1128/jvi.05834-11

71. Sun Y, Li J, Gao GF, Tien P, Liu W. Bunyavirales ribonucleoproteins: the viral replication and transcription machinery. Crit Rev Microbiol [Internet]. 2018 Sep 3 [cited 2025 Apr 22];44(5):522–40. Available from: https://pubmed.ncbi.nlm.nih.gov/29516765/

72. Arragain B, Reguera J, Desfosses A, Gutsche I, Schoehn G, Malet H. High resolution cryo-em structure of the helical rna-bound hantaan virus nucleocapsid reveals its assembly mechanisms. Elife. 2019 Jan 1;8.

73. Ferron F, Li Z, Danek EI, Luo D, Wong Y, Coutard B, et al. The Hexamer Structure of the Rift Valley Fever Virus Nucleoprotein Suggests a Mechanism for its Assembly into Ribonucleoprotein Complexes. PLOS Pathog [Internet]. 2011 [cited 2025 Apr 22];7(5):e1002030. Available from: https://journals.plos.org/plospathogens/article?id=10.1371/journal.ppat.1002030

74. Lennartz F, Hoenen T, Lehmann M, Groseth A, Garten W. The role of oligomerization for the biological functions of the arenavirus nucleoprotein. Arch Virol. 2013;

75. Hastie KM, Kimberlin CR, Zandonatti MA, MacRae IJ, Saphire EO. Structure of the Lassa virus nucleoprotein reveals a dsRNA-specific 3' to 5' exonuclease activity essential for immune suppression. Proc Natl Acad Sci USA. 2011 Feb 8;108(6):2396–797.

76. Huiskonen JT, Överby AK, Weber F, Grünewald K. Electron cryo-microscopy and single-particle averaging of Rift Valley fever virus: evidence for GN-GC glycoprotein heterodimers. J Virol [Internet]. 2009 Apr 15 [cited 2025 Apr 22];83(8):3762–9. Available from: https://pubmed.ncbi.nlm.nih.gov/19193794/

77. Li S, Rissanen I, Zeltina A, Hepojoki J, Raghwani J, Harlos K, et al. A Molecular-Level Account of the Antigenic Hantaviral Surface. Cell Rep. 2016 May 3;15(5):959–67.

78. Katz M, Weinstein J, Eilon-Ashkenazy M, Gehring K, Cohen-Dvashi H, Elad N, et al. Structure and receptor recognition by the Lassa virus spike complex. Nature [Internet]. 2022 Mar 3 [cited 2025 Apr 22];603(7899):174–9. Available from: https://pubmed.ncbi.nlm.nih.gov/35173332/

79. Hulswit RJG, Paesen GC, Bowden TA, Shi X, Brennan B. Recent Advances in Bunyavirus Glycoprotein Research: Precursor Processing, Receptor Binding and Structure. 2021; Available from: https://doi.org/10.3390/v13020353

80. Vogel D, Rosenthal M, Gogrefe N, Reindl S, Günther S. Biochemical characterization of the Lassa virus L protein. J Biol Chem. 2019;

81. Kranzusch PJ, Whelan SPJ. Arenavirus Z protein controls viral RNA synthesis by locking a polymerase-promoter complex. Proc Natl Acad Sci U S A. 2011;

82. Strecker T, Eichler R, Meulen J ter, Weissenhorn W, Dieter Klenk H, Garten W, et al. Lassa Virus Z Protein Is a Matrix Protein Sufficient for the Release of Virus-Like Particles. J Virol. 2003;

83. Wuerth JD, Weber F. Phleboviruses and the Type I Interferon Response. Viruses 2016, Vol 8, Page 174 [Internet]. 2016 Jun 22 [cited 2025 Apr 22];8(6):174. Available from: https://www.mdpi.com/1999-4915/8/6/174/htm

84. Herath V, Romay G, Urrutia CD, Verchot J. Family Level Phylogenies Reveal Relationships of Plant Viruses within the Order Bunyavirales. Viruses 2020, Vol 12, Page 1010 [Internet]. 2020 Sep 10 [cited 2025 Apr 22];12(9):1010. Available from: https://www.mdpi.com/1999-4915/12/9/1010/htm

85. Vera-Otarola J, Solis L, Soto-Rifo R, Ricci EP, Pino K, Tischler ND, et al. The Andes hantavirus NSs protein is expressed from the viral small mRNA by a leaky scanning mechanism. J Virol [Internet]. 2012 Feb 15 [cited 2025 Apr 22];86(4):2176–87. Available from: https://pubmed.ncbi.nlm.nih.gov/22156529/

86. Jääskeläinen KM, Kaukinen P, Minskaya ES, Plyusnina A, Vapalahti O, Elliott RM, et al. Tula and Puumala hantavirus NSs ORFs are functional and the products inhibit activation of the interferon-beta promoter. J Med Virol [Internet]. 2007 Oct [cited 2025 Apr 22];79(10):1527–36. Available from: https://pubmed.ncbi.nlm.nih.gov/17705180/

87. Crabtree MB, Crockett RJ, Bird BH, Nichol ST, Erickson BR, Biggerstaff BJ, et al. Infection and Transmission of Rift Valley Fever Viruses Lacking the NSs and/or NSm Genes in Mosquitoes: Potential Role for NSm in Mosquito Infection. PLoS Negl Trop Dis [Internet]. 2012 May [cited 2025 Apr 22];6(5):e1639. Available from: https://journals.plos.org/plosntds/article?id=10.1371/journal.pntd.0001639

88. Terhzaz S, Kerrigan D, Almire F, Szemiel AM, Hughes J, Parvy J-P, et al. NSm is a critical determinant for bunyavirus transmission between vertebrate and mosquito hosts. Available from: https://doi.org/10.1038/s41467-024-54809-7

89. Olschewski S, Cusack S, Rosenthal M. The Cap-Snatching Mechanism of Bunyaviruses. Trends in Microbiology. 2020.

90. Wandzik JM, Kouba T, Cusack S. Structure and Function of Influenza Polymerase. Cold

Spring Harb Perspect Med [Internet]. 2021 Sep 1 [cited 2025 Apr 23];11(9). Available from: https://pubmed.ncbi.nlm.nih.gov/32341065/

91. Gogrefe N, Reindl S, Günther S, Rosenthal M. Structure of a functional cap-binding domain in Rift Valley fever virus L protein. PLOS Pathog [Internet]. 2019 May 1 [cited 2025 Apr 23];15(5):e1007829. Available from: https://journals.plos.org/plospathogens/article?id=10.1371/journal.ppat.1007829

92. Jones R, Lessoued S, Meier K, Devignot S, Barata-Garciá S, Mate M, et al. Structure and function of the Toscana virus cap-snatching endonuclease. Nucleic Acids Res [Internet]. 2019 Nov 18 [cited 2025 Apr 23];47(20):10914–30. Available from: https://pubmed.ncbi.nlm.nih.gov/31584100/

93. Reguera J, Weber F, Cusack S. Bunyaviridae RNA polymerases (L-protein) have an N-terminal, influenza-like endonuclease domain, essential for viral cap-dependent transcription. PLoS Pathog [Internet]. 2010 Sep [cited 2025 Apr 23];6(9). Available from: https://pubmed.ncbi.nlm.nih.gov/20862319/

94. Rosenthal M, Gogrefe N, Vogel D, Reguera J, Rauschenberger B, Cusack S, et al. Structural insights into reptarenavirus cap-snatching machinery. [cited 2025 Apr 23]; Available from: https://doi.org/10.1371/journal.ppat.1006400

95. Wallat GD, Huang Q, Wang W, Dong H, Ly H, Liang Y, et al. High-Resolution Structure of the N-Terminal Endonuclease Domain of the Lassa Virus L Polymerase in Complex with Magnesium Ions. PLoS One [Internet]. 2014 Feb 7 [cited 2025 Apr 23];9(2):e87577. Available from: https://journals.plos.org/plosone/article?id=10.1371/journal.pone.0087577

96. Fernández-García Y, Reguera J, Busch C, Witte G, Sánchez-Ramos O, Betzel C, et al. Atomic Structure and Biochemical Characterization of an RNA Endonuclease in the N Terminus of Andes Virus L Protein. PLOS Pathog [Internet]. 2016 Jun 1 [cited 2025 Apr 23];12(6):e1005635. Available from: https://journals.plos.org/plospathogens/article?id=10.1371/journal.ppat.1005635

97. Arragain B, Effantin G, Gerlach P, Reguera J, Schoehn G, Cusack S, et al. Pre-initiation and elongation structures of full-length La Crosse virus polymerase reveal functionally important conformational changes. Nat Commun [Internet]. 2020 Dec 1 [cited 2025 Apr 23];11(1). Available from: https://pubmed.ncbi.nlm.nih.gov/32681014/

98. Peng R, Xu X, Jing J, Wang M, Peng Q, Liu S, et al. Structural insight into arenavirus

replication machinery. Nature [Internet]. 2020 Mar 26 [cited 2025 Apr 23];579(7800):615–9. Available from: https://pubmed.ncbi.nlm.nih.gov/32214249/

99. Meier K, Thorkelsson SR, Trouilleton QD, Vogel D, Yu D, Kosinski J, et al. Structural and functional characterization of the Sin Nombre virus L protein. PLoS Pathog [Internet]. 2023 Aug 1 [cited 2025 Apr 23];19(8). Available from: https://pubmed.ncbi.nlm.nih.gov/37549153/

100. Durieux Trouilleton Q, Barata-García S, Arragain B, Reguera J, Malet H. Structures of active Hantaan virus polymerase uncover the mechanisms of Hantaviridae genome replication. Nat Commun 2023 141 [Internet]. 2023 May 23 [cited 2025 Apr 23];14(1):1–15. Available from: https://www.nature.com/articles/s41467-023-38555-w

101. Williams HM, Thorkelsson SR, Vogel D, Busch C, Milewski M, Cusack S, et al. Structural snapshots of phenuivirus cap-snatching and transcription. Nucleic Acids Res [Internet]. 2024 Jun 10 [cited 2025 Apr 23];52(10):6049–65. Available from: https://dx.doi.org/10.1093/nar/gkae330

102. Wang X, Hu C, Ye W, Wang J, Dong X, Xu J, et al. Structure of Rift Valley Fever Virus RNA-Dependent RNA Polymerase. J Virol [Internet]. 2022 Feb 9 [cited 2025 Apr 5];96(3):1713–34. Available from: https://journals.asm.org/doi/10.1128/jvi.01713-21

103. Amroun A, Priet S, de Lamballerie X, Quérat G. Bunyaviridae RdRps: structure, motifs, and RNA synthesis machinery. Crit Rev Microbiol [Internet]. 2017 Nov 2 [cited 2025 May 8];43(6):753–78. Available from: https://www.tandfonline.com/doi/abs/10.1080/1040841X.2017.1307805

104. Williams HM, Thorkelsson SR, Vogel D, Milewski M, Busch C, Cusack S, et al. Structural insights into viral genome replication by the severe fever with thrombocytopenia syndrome virus L protein. Nucleic Acids Res [Internet]. 2023;51(3):1424–42. Available from: https://doi.org/10.1093/nar/gkac1249

105. Tomas Kouba, Dominik Vogel, Sigurdu Thorkelsson, Emanuelle Quemin, Harry Williams, Morlin Milewski, Carola Busch, Stephan Günther, Kay Grünewald, Maria Rosenthal SC. Conformational changes in Lassa virus L protein associated with promoter binding and RNA synthesis activity. Preprint. 2021;

106. Malet H, Williams HM, Cusack S, Rosenthal M. The mechanism of genome replication and transcription in bunyaviruses. PLoS Pathog [Internet]. 2023 Jan 1 [cited 2025 Apr 23];19(1). Available from: https://pubmed.ncbi.nlm.nih.gov/36634042/

107. Vela EM, Zhang L, Colpitts TM, Davey RA, Aronson JF. Arenavirus entry occurs through a cholesterol-dependent, non-caveolar, clathrin-mediated endocytic mechanism. Virology. 2007 Dec 5;369(1):1–11.

108. Martinez MG, Cordo SM, Candurra NA. Characterization of Junin arenavirus cell entry. J Gen Virol [Internet]. 2007 Jun 1 [cited 2025 Apr 23];88(6):1776–84. Available from: https://www.microbiologyresearch.org/content/journal/jgv/10.1099/vir.0.82808-0

109. Jin M, Park J, Lee S, Park B, Shin J, Song KJ, et al. Hantaan Virus Enters Cells by Clathrin-Dependent Receptor-Mediated Endocytosis. Virology. 2002 Mar 1;294(1):60–9.

110. Oppliger J, Torriani G, Herrador A, Kunz S. Lassa Virus Cell Entry via Dystroglycan Involves an Unusual Pathway of Macropinocytosis. J Virol [Internet]. 2016 Jul 15 [cited 2025 May 8];90(14):6412–29. Available from: https://journals.asm.org/doi/10.1128/jvi.00257-16

111. Chiang CF, Flint M, Lin JMS, Spiropoulou CF. Endocytic Pathways Used by Andes Virus to Enter Primary Human Lung Endothelial Cells. PLoS One [Internet]. 2016 Oct 1 [cited 2025 Apr 23];11(10):e0164768. Available from: https://journals.plos.org/plosone/article?id=10.1371/journal.pone.0164768

112. Harmon B, Schudel BR, Maar D, Kozina C, Ikegami T, Tseng C-TK, et al. Rift Valley Fever Virus Strain MP-12 Enters Mammalian Host Cells via Caveola-Mediated Endocytosis. J Virol [Internet]. 2012 Dec [cited 2025 Apr 23];86(23):12954–70. Available from: https://journals.asm.org/doi/10.1128/jvi.02242-12

113. Lozach PY, Mancini R, Bitto D, Meier R, Oestereich L, Överby AK, et al. Entry of Bunyaviruses into Mammalian Cells. Cell Host Microbe [Internet]. 2010 Jun 17 [cited 2025 Apr 24];7(6):488. Available from: https://pmc.ncbi.nlm.nih.gov/articles/PMC7172475/

114. Reich S, Guilligay D, Pflug A, Malet H, Berger I, Crepin T, et al. Structural insight into cap-snatching and RNA synthesis by influenza polymerase. Nat 2014 5167531 [Internet]. 2014 Nov 19 [cited 2025 Apr 24];516(7531):361–6. Available from: https://www.nature.com/articles/nature14009

115. Mazza C, Ohno M, Segref A, Mattaj IW, Cusack S. Crystal structure of the human nuclear cap binding complex. Mol Cell [Internet]. 2001 Aug 1 [cited 2025 Apr 24];8(2):383–96. Available from: https://www.cell.com/action/showFullText?pii=S1097276501002994

116. Niedzwiecka A, Marcotrigiano J, Stepinski J, Jankowska-Anyszka M, Wyslouch-Cieszynska A, Dadlez M, et al. Biophysical Studies of eIF4E Cap-binding Protein: Recognition of mRNA

5' Cap Structure and Synthetic Fragments of eIF4G and 4E-BP1 Proteins. J Mol Biol. 2002 Jun 7;319(3):615–35.

117. Ferron F, Weber F, de la Torre JC, Reguera J. Transcription and replication mechanisms of Bunyaviridae and Arenaviridae L proteins. Virus Res [Internet]. 2017 Apr 15 [cited 2025 Apr 23];234:118. Available from: https://pmc.ncbi.nlm.nih.gov/articles/PMC7114536/

118. Hepojoki J, Strandin T, Wang H, Vapalahti O, Vaheri A, Lankinen H. Cytoplasmic tails of hantavirus glycoproteins interact with the nucleocapsid protein. J Gen Virol [Internet]. 2010 Sep [cited 2025 Apr 24];91(Pt 9):2341–50. Available from: https://pubmed.ncbi.nlm.nih.gov/20444994/

119. Överby AK, Pettersson RF, Neve EPA. The glycoprotein cytoplasmic tail of Uukuniemi virus (Bunyaviridae) interacts with ribonucleoproteins and is critical for genome packaging. J Virol [Internet]. 2007 Apr [cited 2025 Apr 24];81(7):3198–205. Available from: https://pubmed.ncbi.nlm.nih.gov/17229712/

120. Carnec X, Ermonval M, Kreher F, Flamand M, Bouloy M. Role of the cytosolic tails of Rift Valley fever virus envelope glycoproteins in viral morphogenesis. Virology [Internet]. 2014 Jan 5 [cited 2025 Apr 24];448:1–14. Available from: https://pubmed.ncbi.nlm.nih.gov/24314631/

121. Salanueva IJ, Novoa RR, Cabezas P, López-Iglesias C, Carrascosa JL, Elliott RM, et al. Polymorphism and Structural Maturation of Bunyamwera Virus in Golgi and Post-Golgi Compartments. J Virol [Internet]. 2003 Jan 15 [cited 2025 Apr 24];77(2):1368. Available from: https://pmc.ncbi.nlm.nih.gov/articles/PMC140787/

122. Goldsmith CS, Elliott LH, Peters CJ, Zaki SR. Ultrastructural characteristics of Sin Nombre virus, causative agent of hantavirus pulmonary syndrome. Arch Virol 1995 14012 [Internet]. 1995 Dec [cited 2025 Apr 24];140(12):2107–22. Available from: https://link.springer.com/article/10.1007/BF01323234

123. Sänger L, Williams HM, Yu D, Vogel D, Kosinski J, Rosenthal M, et al. RNA to Rule Them All: Critical Steps in Lassa Virus Ribonucleoparticle Assembly and Recruitment. J Am Chem Soc [Internet]. 2023 Dec 27 [cited 2025 Apr 24];145(51):27958–74. Available from: https://pubmed.ncbi.nlm.nih.gov/38104324/

124. Capul AA, Perez M, Burke E, Kunz S, Buchmeier MJ, de la Torre JC. Arenavirus Z-Glycoprotein Association Requires Z Myristoylation but Not Functional RING or Late

Domains. J Virol [Internet]. 2007 Sep [cited 2025 Apr 24];81(17):9451. Available from: https://pmc.ncbi.nlm.nih.gov/articles/PMC1951451/

125. Wolff S, Ebihara H, Groseth A. Arenavirus budding: A common pathway with mechanistic differences. Viruses. 2013.

126. Linder P, Lasko PF, Ashburner M, Leroy P, Nielsen PJ, Nishi K, et al. Birth of the D-E-A-D box [5]. Nature. 1989.

127. Tanner NK, Linder P. DExD/H box RNA helicases: From generic motors to specific dissociation functions. Molecular Cell. 2001.

128. Linder P, Jankowsky E. From unwinding to clamping ĝ€" the DEAD box RNA helicase family. Nature Reviews Molecular Cell Biology. 2011.

129. Anantharaman V, Koonin E V., Aravind L. Comparative genomics and evolution of proteins involved in RNA metabolism. Nucleic Acids Res [Internet]. 2002 Apr 1 [cited 2025 Apr 25];30(7):1427–64. Available from: https://dx.doi.org/10.1093/nar/30.7.1427

130. Singleton MR, Dillingham MS, Wigley DB. Structure and mechanism of helicases and nucleic acid translocases. Annual Review of Biochemistry. 2007.

131. Jankowsky E. RNA helicases at work: Binding and rearranging. Trends in Biochemical Sciences. 2011.

132. Theissen B, Karow AR, Köhler J, Gubaev A, Klostermeier D. Cooperative binding of ATP and RNA induces a closed conformation in a DEAD box RNA helicase. Proc Natl Acad Sci U S A. 2008;

133. Sengoku T, Nureki O, Nakamura A, Kobayashi S, Yokoyama S. Structural Basis for RNA Unwinding by the DEAD-Box Protein Drosophila Vasa. Cell. 2006;

134. Rogers GW, Komar AA, Merrick WC. eIF4A: The godfather of the DEAD box helicases. Progress in Nucleic Acid Research and Molecular Biology. 2002.

135. Shen L, Pelletier J. General and target-specific DEXD/H RNA helicases in eukaryotic translation initiation. International Journal of Molecular Sciences. 2020.

136. Jarmoskaite I, Russell R. DEAD-box proteins as RNA helicases and chaperones. Wiley Interdiscip Rev RNA [Internet]. 2011 Jan [cited 2025 Apr 26];2(1):135–52. Available from: https://pubmed.ncbi.nlm.nih.gov/21297876/

137. Cordin O, Banroques J, Tanner NK, Linder P. The DEAD-box protein family of RNA helicases.

Gene [Internet]. 2006 Feb 15 [cited 2025 Apr 26];367(1–2):17–37. Available from: https://pubmed.ncbi.nlm.nih.gov/16337753/

138. Rocak S, Linder P. DEAD-box proteins: the driving forces behind RNA metabolism. Nat Rev Mol Cell Biol 2004 53 [Internet]. 2004 Mar [cited 2025 Apr 26];5(3):232–41. Available from: https://www.nature.com/articles/nrm1335

139. Weis K. Dead or alive: DEAD-box ATPases as regulators of ribonucleoprotein complex condensation. Biol Chem [Internet]. 2021 Apr 1 [cited 2025 Apr 26];402(5):653–61. Available from: https://pubmed.ncbi.nlm.nih.gov/33818025/

140. Tauber D, Tauber G, Parker R. Mechanisms and Regulation of RNA Condensation in RNP Granule Formation. Trends Biochem Sci [Internet]. 2020 Sep 1 [cited 2025 Apr 26];45(9):764–78. Available from: https://pubmed.ncbi.nlm.nih.gov/32475683/

141. Overwijn D, Hondele M. DEAD-box ATPases as regulators of biomolecular condensates and membrane-less organelles. Trends Biochem Sci [Internet]. 2023 Mar 1 [cited 2025 Apr 26];48(3):244–58. Available from: https://pubmed.ncbi.nlm.nih.gov/36344372/

142. Dörner K, Hondele M. The Story of RNA Unfolded: The Molecular Function of DEAD- and DExH-Box ATPases and Their Complex Relationship with Membraneless Organelles. Annu Rev Biochem [Internet]. 2024 Aug 1 [cited 2025 Apr 26];93(1):79–108. Available from: https://www.annualreviews.org/content/journals/10.1146/annurev-biochem-052521-121259

143. Rehwinkel J, Gack MU. RIG-I-like receptors: their regulation and roles in RNA sensing. Nat Rev Immunol 2020 209 [Internet]. 2020 Mar 13 [cited 2021 Nov 24];20(9):537–51. Available from: https://www.nature.com/articles/s41577-020-0288-3

144. Tapescu I, Cherry S. DDX RNA helicases: key players in cellular homeostasis and innate antiviral immunity. J Virol [Internet]. 2024 Oct 22 [cited 2025 Apr 26]; Available from: https://journals.asm.org/journal/jvi

145. Ward AM, Bidet K, Yinglin A, Ler SG, Hogue K, Blackstock W, et al. Quantitative mass spectrometry of DENV-2 RNA-interacting proteins reveals that the DEAD-box RNA helicase DDX6 binds the DB1 and DB2 3' UTR structures. RNA Biol [Internet]. 2011 Nov [cited 2025 Apr 26];8(6):1173–86. Available from: https://www.tandfonline.com/doi/abs/10.4161/rna.8.6.17836

146. DDX17 protein expression summary - The Human Protein Atlas [Internet]. [cited 2023 Aug 25]. Available from: https://www.proteinatlas.org/ENSG00000100201-DDX17

147. Ngo TD, Partin AC, Nam Y. RNA Specificity and Autoregulation of DDX17, a Modulator of MicroRNA Biogenesis. Cell Rep [Internet]. 2019;29(12):4024-4035.e5. Available from: https://doi.org/10.1016/j.celrep.2019.11.059

148. The proteome and transcriptome of stress granules and P bodies during human T lymphocyte activation | Enhanced Reader.

149. dePhase [Internet]. [cited 2023 Aug 31]. Available from: https://deephase.ch.cam.ac.uk/

150. DDX17 - Probable ATP-dependent RNA helicase DDX17 - Homo sapiens (Human) | UniProtKB | UniProt [Internet]. [cited 2023 Aug 25]. Available from: https://www.uniprot.org/uniprotkb/Q92841/entry#function

151. Connerty P, Bajan S, Remenyi J, Fuller-Pace F V., Hutvagner G. The miRNA biogenesis factors, p72/DDX17 and KHSRP regulate the protein level of Ago2 in human cells. Biochim Biophys Acta [Internet]. 2016 Oct 1 [cited 2023 Aug 24];1859(10):1299–305. Available from: https://pubmed.ncbi.nlm.nih.gov/27478153/

152. Giraud G, Terrone S, Bourgeois CF. Functions of DEAD box RNA helicases DDX5 and DDX17 in chromatin organization and transcriptional regulation. BMB Rep [Internet]. 2018 Dec 31 [cited 2023 Aug 25];51(12):613–22. Available from: https://www.bmbreports.org/journal/view.html?doi=10.5483/BMBRep.2018.51.12.234

153. Fuller-Pace F V. The DEAD box proteins DDX5 (p68) and DDX17 (p72): Multi-tasking transcriptional regulators. Biochim Biophys Acta - Gene Regul Mech. 2013 Aug 1;1829(8):756–63.

154. Dardenne E, PolayEspinoza M, Fattet L, Germann S, Lambert MP, Neil H, et al. RNA Helicases DDX5 and DDX17 Dynamically Orchestrate Transcription, miRNA, and Splicing Programs in Cell Differentiation. Cell Rep. 2014 Jun 26;7(6):1900–13.

155. Jalal C, Uhlmann-Schiffler H, Stahl H. Redundant role of DEAD box proteins p68 (Ddx5) and p72/p82 (Ddx17) in ribosome biogenesis and cell proliferation. Nucleic Acids Res [Internet]. 2007 [cited 2025 Apr 26];35(11):3590–601. Available from: https://academic.oup.com/nar/article/35/11/3590/2401754

156. Fuller-Pace F V. The DEAD box proteins DDX5 (p68) and DDX17 (p72): Multi-tasking transcriptional regulators ☆. 2013 [cited 2025 Apr 26]; Available from: http://dx.doi.org/10.1016/j.bbagrm.2013.03.004

157. Xu K, Sun S, Yan M, Cui J, Yang Y, Li W, et al. DDX5 and DDX17—multifaceted proteins in

the regulation of tumorigenesis and tumor progression. Front Oncol. 2022 Aug 3;12:943032.

158. Bortz E, Westera L, Maamary J, Steel J, Albrecht RA, Manicassamy B, et al. Host- and strain-specific regulation of influenza virus polymerase activity by interacting cellular proteins. MBio [Internet]. 2011 [cited 2023 Aug 25];2(4). Available from: https://journals.asm.org/journal/mbio

159. Moy RH, Cole BS, Yasunaga A, Gold B, Shankarling G, Varble A, et al. Stem-Loop Recognition by DDX17 Facilitates miRNA Processing and Antiviral Defense. [cited 2023 Aug 24]; Available from: http://dx.doi.org/10.1016/j.cell.2014.06.023

160. Mao R, Dong M, Shen Z, Zhang H, Liu Y, Cai D, et al. RNA Helicase DDX17 Inhibits Hepatitis B Virus Replication by Blocking Viral Pregenomic RNA Encapsidation. J Virol [Internet]. 2021 Sep 9 [cited 2025 Apr 12];95(19). Available from: https://journals.asm.org/doi/10.1128/jvi.00444-21

161. Chapus F, Giraud G, Bourgeois CF, Zoulim F, Correspondence BT, Huchon P, et al. Helicases DDX5 and DDX17 promote heterogeneity in HBV transcription termination in infected human hepatocytes. J Hepatol [Internet]. 2024 [cited 2025 Apr 26];81:609–20. Available from: https://doi.org/10.1016/j.jhep.2024.05.016

162. Dong ML, Wen X, He X, Ren JH, Yu HB, Qin YP, et al. HBx Mediated Increase of DDX17 Contributes to HBV-Related Hepatocellular Carcinoma Tumorigenesis. Front Immunol [Internet]. 2022 Jun 16 [cited 2025 Apr 26];13. Available from: https://pubmed.ncbi.nlm.nih.gov/35784274/

163. DDX24 protein expression summary - The Human Protein Atlas [Internet]. [cited 2025 Apr 27]. Available from: https://www.proteinatlas.org/ENSG00000089737-DDX24

164. Sun S, Jing X, Tong G, Chen C, Xie S, Wang C, et al. Loss of DDX24 inhibits lung cancer progression by stimulating IKBKG splicing-mediated autophagy. Theranostics [Internet]. 2025 [cited 2025 Apr 27];15(5):1879. Available from: https://pmc.ncbi.nlm.nih.gov/articles/PMC11780526/

165. Ma Z, Moore R, Xu X, Barber GN. DDX24 Negatively Regulates Cytosolic RNA-Mediated Innate Immune Signaling. PLoS Pathog. 2013;

166. Ma J, Rong L, Zhou Y, Roy BB, Lu J, Abrahamyan L, et al. The requirement of the DEAD-box protein DDX24 for the packaging of human immunodeficiency virus type 1 RNA. Virology. 2008;

167. Serfecz JC, Hong Y, Gay LA, Shekhar R, Turner PC, Renne R. DExD/H Box Helicases

DDX24 and DDX49 Inhibit Reactivation of Kaposi's Sarcoma Associated Herpesvirus by Interacting with Viral mRNAs. Viruses [Internet]. 2022 Oct 1 [cited 2025 Apr 27];14(10). Available from: https://pubmed.ncbi.nlm.nih.gov/36298642/

168. DDX19A protein expression summary - The Human Protein Atlas [Internet]. [cited 2025 Apr 27]. Available from: https://www.proteinatlas.org/ENSG00000168872-DDX19A

169. Lin DH, Correia AR, Cai SW, Huber FM, Jette CA, Hoelz A. Structural and functional analysis of mRNA export regulation by the nuclear pore complex. Nat Commun 2018 91 [Internet]. 2018 Jun 13 [cited 2025 Apr 27];9(1):1–19. Available from: https://www.nature.com/articles/s41467-018-04459-3

170. Montpetit B, Thomsen ND, Helmke KJ, Seeliger MA, Berger JM, Weis K. A conserved mechanism of DEAD-box ATPase activation by nucleoporins and InsP6 in mRNA export. Nat 2011 4727342 [Internet]. 2011 Mar 27 [cited 2025 Apr 27];472(7342):238–42. Available from: https://www.nature.com/articles/nature09862

171. Collins R, Karlberg T, Lehtiö L, Schütz P, van den Berg S, Dahlgren LG, et al. The DEXD/H-box RNA helicase DDX19 is regulated by an α-helical switch. J Biol Chem [Internet]. 2009 Apr 17 [cited 2025 Apr 27];284(16):10296–300. Available from: https://www.jbc.org/action/showFullText?pii=S0021925820398719

172. Winnard PT, Vesuna F, Raman V. DExD-box RNA helicases in human viral infections: Pro- and anti-viral functions. Antiviral Res. 2025 Mar 1;235:106098.

173. Diot C, Fournier G, Dos Santos M, Magnus J, Komarova A, Van Der Werf S, et al. Influenza A Virus Polymerase Recruits the RNA Helicase DDX19 to Promote the Nuclear Export of Viral mRNAs. Sci Rep. 2016;

174. Refeyn. Mass photometry [Internet]. Available from: https://refeyn.com/about-mass-photometry

175. Beitrag zur kollektiven Behandlung pharmakologischer Reihenversuche | Enhanced Reader.

176. Universitätsklinikum Heidelberg. TCID50 calculator Spearman & Kerber method [Internet]. 17.01.202. 2020 [cited 2025 May 13]. Available from: https://www.klinikum.uni-heidelberg.de/fileadmin/inst_hygiene/molekulare_virologie/Downloads/TCID50_calculator_v2_17-01-20_MB.xlsx

177. Dull T, Zufferey R, Kelly M, Mandel RJ, Nguyen M, Trono D, et al. A Third-Generation Lentivirus Vector with a Conditional Packaging System. J Virol [Internet]. 1998 Nov 1 [cited

2025 Feb 10];72(11):8463. Available from: https://pmc.ncbi.nlm.nih.gov/articles/PMC110254/

178. Weber K, Bartsch U, Stocking C, Fehse B. A multicolor panel of novel lentiviral “gene ontology” (LeGO) vectors for functional gene analysis. Mol Ther [Internet]. 2008 [cited 2025 Feb 10];16(4):698–706. Available from: https://pubmed.ncbi.nlm.nih.gov/18362927/

179. Abramson J, Adler J, Dunger J, Evans R, Green T, Pritzel A, et al. Accurate structure prediction of biomolecular interactions with AlphaFold 3. Nat 2024 6308016 [Internet]. 2024 May 8 [cited 2025 Apr 7];630(8016):493–500. Available from: https://www.nature.com/articles/s41586-024-07487-w

180. Yu D, Chojnowski G, Rosenthal M, Kosinski J. AlphaPulldown—a python package for protein–protein interaction screens using AlphaFold-Multimer. Bioinformatics [Internet]. 2023 Jan 1 [cited 2025 Apr 7];39(1). Available from: https://dx.doi.org/10.1093/bioinformatics/btac749

181. Olschewski S (BNITM). Identifizierung und Charakterisierung essentieller zellulärer Faktoren für die Transkription und Replikation von Arenaviren. 2020;

182. Khamina K, Lercher A, Caldera M, Schliehe C, Vilagos B, Sahin M, et al. Characterization of host proteins interacting with the lymphocytic choriomeningitis virus L protein. PLoS Pathog. 2017;

183. Loureiro ME, Zorzetto-Fernandes AL, Radoshitzky S, Chi X, Dallari S, Marooki N, et al. DDX3 suppresses type I interferons and favors viral replication during Arenavirus infection. PLoS Pathog. 2018;

184. Iwasaki M, Minder P, Caì Y, Kuhn JH, Yates JR, Torbett BE, et al. Interactome analysis of the lymphocytic choriomeningitis virus nucleoprotein in infected cells reveals ATPase Na+/K+transporting subunit Alpha 1 and prohibitin as host-cell factors involved in the life cycle of mammarenaviruses. PLoS Pathog. 2018;

185. Fang J, Pietzsch C, Witwit H, Tsaprailis G, Crynen G, Cho KF, et al. Proximity interactome analysis of Lassa polymerase reveals eRF3a/GSPT1 as a druggable target for host-directed antivirals. 2022;119. Available from: http://www.pnas.org/lookup/suppl/doi:10.1073/pnas.2201208119/-/DCSupplemental.https://doi.org/10.1073/pnas.22012081191of11

186. Krüger S. Investigating potential interactions between Lassa virus L protein and host proteins of the DDX and DHX families. Master thesis. 2021;

187. Fujinaga K, Huang F, Peterlin BM. P-TEFb: The master regulator of transcription elongation.

Mol Cell [Internet]. 2023 Feb 2 [cited 2025 Apr 15];83(3):393–403. Available from: https://pubmed.ncbi.nlm.nih.gov/36599353/

188. White EJF, Matsangos AE, Wilson GM. AUF1 regulation of coding and noncoding RNA. Wiley Interdiscip Rev RNA [Internet]. 2016 Mar 1 [cited 2025 Apr 15];8(2):10.1002/wrna.1393. Available from: https://pmc.ncbi.nlm.nih.gov/articles/PMC5315606/

189. Yu D, Huang CJ, Tucker HO. Established and Evolving Roles of the Multifunctional Non-POU Domain-Containing Octamer-Binding Protein (NonO) and Splicing Factor Proline- and Glutamine-Rich (SFPQ). J Dev Biol 2024, Vol 12, Page 3 [Internet]. 2024 Jan 5 [cited 2025 Apr 15];12(1):3. Available from: https://www.mdpi.com/2221-3759/12/1/3/htm

190. Inoue A. RBM10: Structure, functions, and associated diseases. Gene. 2021 May 30;783:145463.

191. Gack MU, Shin YC, Joo CH, Urano T, Liang C, Sun L, et al. TRIM25 RING-finger E3 ubiquitin ligase is essential for RIG-I-mediated antiviral activity. Nature [Internet]. 2007 Apr 19 [cited 2025 Apr 15];446(7138):916–20. Available from: https://pubmed.ncbi.nlm.nih.gov/17392790/

192. Zheng X, Wang X, Tu F, Wang Q, Fan Z, Gao G. TRIM25 Is Required for the Antiviral Activity of Zinc Finger Antiviral Protein. J Virol. 2017;91(9).

193. Wiese C, Zheng Y. Microtubule nucleation: γ-tubulin and beyond. J Cell Sci [Internet]. 2006 Oct 15 [cited 2025 Apr 15];119(20):4143–53. Available from: https://dx.doi.org/10.1242/jcs.03226

194. Pause A, Sonenberg' N. Mutational analysis of a DEAD box RNA helicase: the mammalian translation initiation factor eIF-4A. EMBO J [Internet]. 1992 Jul [cited 2025 Apr 12];11(7):2643–54. Available from: https://www.embopress.org

195. Mao R, Dong M, Shen Z, Zhang H, Liu Y, Cai D, et al. RNA Helicase DDX17 Inhibits Hepatitis B Virus Replication by Blocking Viral Pregenomic RNA Encapsidation. J Virol [Internet]. 2021 Sep 9 [cited 2023 Nov 27];95(19). Available from: https://journals.asm.org/doi/10.1128/jvi.00444-21

196. Choudhury NR, Heikel G, Trubitsyna M, Kubik P, Nowak JS, Webb S, et al. RNA-binding activity of TRIM25 is mediated by its PRY/SPRY domain and is required for ubiquitination. BMC Biol [Internet]. 2017 Nov 8 [cited 2025 Apr 12];15(1):105. Available from: https://pmc.ncbi.nlm.nih.gov/articles/PMC5678581/

197. Meier K. Structure and function of the bunyavirus L protein. Dr Thesis. 2022;

198. Isenmann M, Stoddart MJ, Schmelzeisen R, Gross C, Della Bella E, Rothweiler RM. Basic Principles of RNA Interference: Nucleic Acid Types and In Vitro Intracellular Delivery Methods. Micromachines [Internet]. 2023 Jul 1 [cited 2025 Apr 13];14(7):1321. Available from: https://pmc.ncbi.nlm.nih.gov/articles/PMC10383872/

199. Balaraman V, Indran S V., Li Y, Meekins DA, Jakkula LUMR, Liu H, et al. Identification of Host Factors for Rift Valley Fever Phlebovirus. Viruses [Internet]. 2023 Nov 1 [cited 2025 Apr 28];15(11):2251. Available from: https://pmc.ncbi.nlm.nih.gov/articles/PMC10675714/

200. Huynh K, Partch CL. Analysis of Protein Stability and Ligand Interactions by Thermal Shift Assay. Curr Protoc Protein Sci [Internet]. 2015 Feb 1 [cited 2025 May 5];79(1):28.9.1-28.9.14. Available from: https://onlinelibrary.wiley.com/doi/full/10.1002/0471140864.ps2809s79

201. Cole D, Young G, Weigel A, Sebesta A, Kukura P. Label-Free Single-Molecule Imaging with Numerical-Aperture-Shaped Interferometric Scattering Microscopy. 2017; Available from: https://pubs.acs.org/sharingguidelines

202. Young G, Hundt N, Cole D, Fineberg A, Andrecka J, Tyler A, et al. Quantitative mass imaging of single molecules. Science [Internet]. 2018 Apr 27 [cited 2025 Apr 9];360(6387):423. Available from: https://pmc.ncbi.nlm.nih.gov/articles/PMC6103225/

203. Ma-Lauer Y, Lei J, Hilgenfeld R, Von Brunn A. Virus–host interactomes — antiviral drug discovery. Curr Opin Virol [Internet]. 2012 [cited 2025 May 11];2(5):614. Available from: https://pmc.ncbi.nlm.nih.gov/articles/PMC7102765/

204. Gu X, Zheng M, Gao Y, Lin S, Zhang X, Chen C, et al. Overview of host-directed antiviral targets for future research and drug development. Acta Pharm Sin B. 2025 Apr 1;15(4):1723–51.

205. Kumar N, Sharma S, Kumar R, Tripathi BN, Barua S, Ly H, et al. Host-Directed Antiviral Therapy. Clin Microbiol Rev [Internet]. 2020 [cited 2025 May 11];33(3):e00168-19. Available from: https://pmc.ncbi.nlm.nih.gov/articles/PMC7227448/

206. Schreiber A, Ludwig S. Host-targeted antivirals against SARS-CoV-2 in clinical development - Prospect or disappointment? Antiviral Res. 2025 Mar 1;235:106101.

207. Jin L, Wang W, Fang G. Targeting protein-protein interaction by small molecules. Annu Rev Pharmacol Toxicol [Internet]. 2014 Jan 6 [cited 2025 May 11];54(Volume 54, 2014):435–56. Available from: https://www.annualreviews.org/content/journals/10.1146/annurev-pharmtox-011613-140028

208. Marković V, Szczepańska A, Berlicki Ł. Antiviral Protein–Protein Interaction Inhibitors. J Med Chem [Internet]. 2024 Mar 14 [cited 2025 May 11];67(5):3205. Available from: https://pmc.ncbi.nlm.nih.gov/articles/PMC10945500/

209. Tan X, Huang Z, Pei H, Jia Z, Zheng J. Molecular glue-mediated targeted protein degradation: A novel strategy in small-molecule drug development. iScience [Internet]. 2024 Sep 20 [cited 2025 May 17];27(9):110712. Available from: https://www.cell.com/action/showFullText?pii=S2589004224019370

210. Vesuna F, Akhrymuk I, Smith A, Winnard PT, Lin SC, Panny L, et al. RK-33, a small molecule inhibitor of host RNA helicase DDX3, suppresses multiple variants of SARS-CoV-2. Front Microbiol. 2022 Aug 25;13:959577.

211. Winnard PT, Vesuna F, Raman V. Targeting host DEAD-box RNA helicase DDX3X for treating viral infections. Antiviral Res [Internet]. 2021 Jan 1 [cited 2025 May 11];185. Available from: https://pubmed.ncbi.nlm.nih.gov/33301755/

212. Paul FE, Hosp F, Selbach M. Analyzing protein–protein interactions by quantitative mass spectrometry. Methods. 2011 Aug 1;54(4):387–95.

213. Mellacheruvu D, Wright Z, Couzens AL, Lambert JP, St-Denis NA, Li T, et al. The CRAPome: A contaminant repository for affinity purification-mass spectrometry data. Nat Methods. 2013;

214. Sanchez de Groot N, Armaos A, Graña-Montes R, Alriquet M, Calloni G, Vabulas RM, et al. RNA structure drives interaction with proteins. Nat Commun 2019 101 [Internet]. 2019 Jul 19 [cited 2025 May 15];10(1):1–13. Available from: https://www.nature.com/articles/s41467-019-10923-5

215. Collins R, Karlberg T, Lehtiö L, Schütz P, van den Berg S, Dahlgren LG, et al. The DEXD/H-box RNA Helicase DDX19 Is Regulated by an α-Helical Switch. J Biol Chem [Internet]. 2009 Apr 17 [cited 2025 May 5];284(16):10296. Available from: https://pmc.ncbi.nlm.nih.gov/articles/PMC2667716/

216. Lohman TM, Von Hippel PH. Kinetics of protein-nucleic acid interactions: use of salt effects to probe mechanisms of interaction. CRC Crit Rev Biochem [Internet]. 1986 [cited 2025 May 5];19(3):191–245. Available from: https://pubmed.ncbi.nlm.nih.gov/3512164/

217. Tabuchi Y, Yang J, Taki M. Relative Nuclease Resistance of a DNA Aptamer Covalently Conjugated to a Target Protein. Int J Mol Sci [Internet]. 2022 Jul 1 [cited 2025 May 5];23(14). Available from: https://pubmed.ncbi.nlm.nih.gov/35887130/

218. Lin S, Sallapalli BT, Chang P, He J, Coyaud E, Pierce BG, et al. RNA Helicase DDX3 Interacts with the Capsid Protein of Hepatitis E Virus and Plays a Vital Role in the Viral Replication. Pathogens [Internet]. 2025 Feb 1 [cited 2025 May 15];14(2):177. Available from: https://pmc.ncbi.nlm.nih.gov/articles/PMC11858535/

219. Theissen B, Karow AR, Köhler J, Gubaev A, Klostermeier D. Cooperative binding of ATP and RNA induces a closed conformation in a DEAD box RNA helicase. Proc Natl Acad Sci U S A [Internet]. 2008 Jan 15 [cited 2025 May 5];105(2):548–53. Available from: https://www.pnas.org/doi/abs/10.1073/pnas.0705488105

220. Putnam AA, Jankowsky E. DEAD-box Helicases as Integrators of RNA, Nucleotide and Protein Binding. Biochim Biophys Acta [Internet]. 2013 Aug [cited 2025 May 5];1829(8):884. Available from: https://pmc.ncbi.nlm.nih.gov/articles/PMC3661757/

221. Hönig A, Auboeuf D, Parker MM, O'Malley BW, Berget SM. Regulation of Alternative Splicing by the ATP-Dependent DEAD-Box RNA Helicase p72. Mol Cell Biol [Internet]. 2002 Aug 1 [cited 2025 May 15];22(16):5698–707. Available from: https://www.tandfonline.com/doi/abs/10.1128/MCB.22.16.5698-5707.2002

222. Arragain B, Krischuns T, Pelosse M, Drncova P, Blackledge M, Naffakh N, et al. Structures of influenza A and B replication complexes give insight into avian to human host adaptation and reveal a role of ANP32 as an electrostatic chaperone for the apo-polymerase. Nat Commun. 2024 Dec 1;15(1).

223. Hirai Y, Domae E, Yoshikawa Y, Tomonaga K. Differential roles of two DDX17 isoforms in the formation of membraneless organelles. J Biochem [Internet]. 2020 Jul 1 [cited 2023 Aug 31];168(1):33–40. Available from: https://dx.doi.org/10.1093/jb/mvaa023

224. Babu MM. The contribution of intrinsically disordered regions to protein function, cellular complexity, and human disease. Biochem Soc Trans [Internet]. 2016 Oct 15 [cited 2025 May 8];44(5):1185. Available from: https://pmc.ncbi.nlm.nih.gov/articles/PMC5095923/

225. Ngo TD, Partin AC, Nam Y. RNA Specificity and Autoregulation of DDX17, a Modulator of MicroRNA Biogenesis. Cell Rep. 2019;

226. Zhang J, Li G, Ye X. Cyclin T1/CDK9 interacts with influenza A virus polymerase and facilitates its association with cellular RNA polymerase II. J Virol [Internet]. 2010 Dec 15 [cited 2025 May 5];84(24):12619–27. Available from: https://pubmed.ncbi.nlm.nih.gov/20943989/

227. Flather D, Nguyen JHC, Semler BL, Gershon PD. Exploitation of nuclear functions by human

rhinovirus, a cytoplasmic RNA virus. PLOS Pathog [Internet]. 2018 Aug 1 [cited 2025 May 15];14(8):e1007277. Available from: https://journals.plos.org/plospathogens/article?id=10.1371/journal.ppat.1007277

228. Waggoner S, Sarnow P. Viral Ribonucleoprotein Complex Formation and Nucleolar-Cytoplasmic Relocalization of Nucleolin in Poliovirus-Infected Cells. J Virol [Internet]. 1998 Aug [cited 2025 May 17];72(8):6699–709. Available from: https://journals.asm.org/doi/10.1128/jvi.72.8.6699-6709.1998

229. Pettit Kneller EL, Connor JH, Lyles DS. hnRNPs Relocalize to the Cytoplasm following Infection with Vesicular Stomatitis Virus. J Virol [Internet]. 2008 Jan 15 [cited 2025 May 17];83(2):770. Available from: https://pmc.ncbi.nlm.nih.gov/articles/PMC2612367/

230. Dhillon P, Tandra VN, Chorghade SG, Namsa ND, Sahoo L, Rao CD. Cytoplasmic Relocalization and Colocalization with Viroplasms of Host Cell Proteins, and Their Role in Rotavirus Infection. J Virol [Internet]. 2018 Aug [cited 2025 May 17];92(15):e00612-18. Available from: https://pmc.ncbi.nlm.nih.gov/articles/PMC6052293/

231. Kamel W, Ruscica V, Embarc-Buh A, de Laurent ZR, Garcia-Moreno M, Demyanenko Y, et al. Alphavirus infection triggers selective cytoplasmic translocation of nuclear RBPs with moonlighting antiviral roles. Mol Cell [Internet]. 2024 Dec 19 [cited 2025 May 17];84(24):4896-4911.e7. Available from: http://www.ncbi.nlm.nih.gov/pubmed/39642884

232. Oh J, Broyles SS. Host Cell Nuclear Proteins Are Recruited to Cytoplasmic Vaccinia Virus Replication Complexes. J Virol [Internet]. 2005 Oct 15 [cited 2025 May 17];79(20):12852–60. Available from: https://journals.asm.org/doi/10.1128/jvi.79.20.12852-12860.2005

233. Messmer M, Pierson L, Pasquier C, Djordjevic N, Chicher J, Hammann P, et al. DEAD box RNA helicase 5 is a new pro-viral host factor for Sindbis virus infection. Virol J [Internet]. 2024 Dec 1 [cited 2025 May 10];21(1):76. Available from: https://pmc.ncbi.nlm.nih.gov/articles/PMC10981342/

234. DDX24 - ATP-dependent RNA helicase DDX24 - Homo sapiens (Human) | UniProtKB | UniProt [Internet]. [cited 2025 May 8]. Available from: https://www.uniprot.org/uniprotkb/Q9GZR7/entry

235. Zhang Z, Witham S, Alexov E. On the role of electrostatics on protein-protein interactions. Phys Biol [Internet]. 2011 [cited 2025 May 15];8(3):035001. Available from: https://pmc.ncbi.nlm.nih.gov/articles/PMC3137121/

236. Wu D, Piszczek G. Standard protocol for mass photometry experiments. Eur Biophys J [Internet]. 2021 May 1 [cited 2025 May 8];50(3–4):403–9. Available from: https://pubmed.ncbi.nlm.nih.gov/33651123/

237. Kluger R, Alagic A. Chemical cross-linking and protein-protein interactions-a review with illustrative protocols. Bioorg Chem [Internet]. 2004 Dec [cited 2025 May 17];32(6):451–72. Available from: https://pubmed.ncbi.nlm.nih.gov/15530987/

238. Zhang X, Oglesbee M. Use of surface plasmon resonance for the measurement of low affinity binding interactions between HSP72 and measles virus nucleocapsid protein. Biol Proced Online [Internet]. 2003 [cited 2025 May 8];5(1):170. Available from: https://pmc.ncbi.nlm.nih.gov/articles/PMC248471/

239. Snel B, Lehmann G, Bork P, Huynen MA. STRING: a web-server to retrieve and display the repeatedly occurring neighbourhood of a gene. Nucleic Acids Res [Internet]. 2000 Sep 15 [cited 2025 May 8];28(18):3442–4. Available from: https://pubmed.ncbi.nlm.nih.gov/10982861/

240. Ruff KM, Pappu R V. AlphaFold and Implications for Intrinsically Disordered Proteins. J Mol Biol. 2021 Oct 1;433(20):167208.

241. Li L, Roy PG, Liu Y, Zhang Z, Xiong D, Savan R, et al. Comprehensive Atomic-Scale 3D Viral-Host Protein Interactomes Enable Dissection of Key Mechanisms and Evolutionary Processes Underlying Viral Pathogenesis. [cited 2025 May 19]; Available from: https://doi.org/10.1101/2025.03.28.645946

242. Gutnik D, Evseev P, Miroshnikov K, Shneider M. Using AlphaFold Predictions in Viral Research. Curr Issues Mol Biol 2023, Vol 45, Pages 3705-3732 [Internet]. 2023 Apr 21 [cited 2025 May 18];45(4):3705–32. Available from: https://www.mdpi.com/1467-3045/45/4/240/htm

243. Fox JD, Waugh DS. Maltose-Binding Protein as a Solubility Enhancer. Methods Mol Biol [Internet]. 2003 [cited 2025 May 9];205:99–117. Available from: https://link.springer.com/protocol/10.1385/1-59259-301-1:99

244. Johanns S. The role of the nucleocytoplasmic mRNA transport pathway in the transcription and genome replication of Lassa virus. Dr Thesis. 2025;

245. Berrow NS, Alderton D, Sainsbury S, Nettleship J, Assenberg R, Rahman N, et al. A versatile ligation-independent cloning method suitable for high-throughput expression screening

applications. Nucleic Acids Res. 2007;

246. Lazic SE, Clarke-Williams CJ, Munafò MR. What exactly is 'N' in cell culture and animal experiments? PLoS Biol [Internet]. 2018 Apr 4 [cited 2025 May 19];16(4):e2005282. Available from: https://pmc.ncbi.nlm.nih.gov/articles/PMC5902037/

247. Balaraman V, Indran S V., Li Y, Meekins DA, Jakkula LUMR, Liu H, et al. Identification of Host Factors for Rift Valley Fever Phlebovirus. Viruses [Internet]. 2023 Nov 1 [cited 2025 May 10];15(11):2251. Available from: https://pmc.ncbi.nlm.nih.gov/articles/PMC10675714/

248. Fish RJ, Kruithof EKO. Short-term cytotoxic effects and long-term instability of RNAi delivered using lentiviral vectors. BMC Mol Biol [Internet]. 2004 Aug 3 [cited 2025 May 9];5:9. Available from: https://pmc.ncbi.nlm.nih.gov/articles/PMC514603/

249. Havranek KE, White LA, Lanchy JM, Lodmell JS. Transcriptome profiling in Rift Valley fever virus infected cells reveals modified transcriptional and alternative splicing programs. PLoS One [Internet]. 2019 May 1 [cited 2025 May 18];14(5):e0217497. Available from: https://pmc.ncbi.nlm.nih.gov/articles/PMC6538246/

250. Pinkham C, Dahal B, De La Fuente CL, Bracci N, Beitzel B, Lindquist M, et al. Alterations in the host transcriptome in vitro following Rift Valley fever virus infection. Sci Reports 2017 71 [Internet]. 2017 Oct 30 [cited 2025 May 19];7(1):1–16. Available from: https://www.nature.com/articles/s41598-017-14800-3

251. El-Brolosy MA, Stainier DYR. Genetic compensation: A phenomenon in search of mechanisms. PLoS Genet [Internet]. 2017 Jul 1 [cited 2025 May 9];13(7):e1006780. Available from: https://pmc.ncbi.nlm.nih.gov/articles/PMC5509088/

252. Jalal C, Uhlmann-Schiffler H, Stahl H. Redundant role of DEAD box proteins p68 (Ddx5) and p72/p82 (Ddx17) in ribosome biogenesis and cell proliferation. Nucleic Acids Res [Internet]. 2007 Jun [cited 2025 May 10];35(11):3590. Available from: https://pmc.ncbi.nlm.nih.gov/articles/PMC1920232/

253. Sun N, Petiwala S, Wang R, Lu C, Hu M, Ghosh S, et al. Development of drug-inducible CRISPR-Cas9 systems for large-scale functional screening. BMC Genomics [Internet]. 2019 Mar 19 [cited 2025 May 19];20(1):1–15. Available from: https://bmcgenomics.biomedcentral.com/articles/10.1186/s12864-019-5601-9

254. Shcholok T, Eftekharpour E. Cre-recombinase systems for induction of neuron-specific knockout models: a guide for biomedical researchers. Neural Regen Res [Internet]. 2022 Feb

1 [cited 2025 May 19];18(2):273. Available from: https://pmc.ncbi.nlm.nih.gov/articles/PMC9396489/

255. Mir MA, Duran WA, Hjelle BL, Ye C, Panganiban AT. Storage of cellular 5' mRNA caps in P bodies for viral cap-snatching. Proc Natl Acad Sci U S A [Internet]. 2008 Dec 9 [cited 2025 May 10];105(49):19294. Available from: https://pmc.ncbi.nlm.nih.gov/articles/PMC2614755/

256. Hopkins KC, McLane LM, Maqbool T, Panda D, Gordesky-Gold B, Cherry S. A genome-wide RNAi screen reveals that mRNA decapping restricts bunyaviral replication by limiting the pools of Dcp2-accessible targets for cap-snatching. Genes Dev [Internet]. 2013 Jul 1 [cited 2025 May 10];27(13):1511–25. Available from: https://pubmed.ncbi.nlm.nih.gov/23824541/

257. Rocak S, Linder P. DEAD-box proteins: the driving forces behind RNA metabolism. Nat Rev Mol Cell Biol 2004 53 [Internet]. 2004 Mar [cited 2025 May 19];5(3):232–41. Available from: https://www.nature.com/articles/nrm1335

258. Guo J, Zhu Y, Ma X, Shang G, Liu B, Zhang K. Virus Infection and mRNA Nuclear Export. Int J Mol Sci [Internet]. 2023 Aug 1 [cited 2025 May 19];24(16):12593. Available from: https://pmc.ncbi.nlm.nih.gov/articles/PMC10454920/

259. Copeland AM, Van Deusen NM, Schmaljohn CS. Rift Valley fever virus NSS gene expression correlates with a defect in nuclear mRNA export. Virology. 2015 Dec 1;486:88–93.

260. Zou W, Zhang DE. The interferon-inducible ubiquitin-protein isopeptide ligase (E3) EFP also functions as an ISG15 E3 ligase. J Biol Chem [Internet]. 2006 Feb 17 [cited 2025 Mar 26];281(7):3989–94. Available from: https://pubmed.ncbi.nlm.nih.gov/16352599/

261. Lahaye X, Gentili M, Silvin A, Conrad C, Picard L, Jouve M, et al. NONO Detects the Nuclear HIV Capsid to Promote cGAS-Mediated Innate Immune Activation. Cell [Internet]. 2018 Oct 4 [cited 2025 Mar 26];175(2):488-501.e22. Available from: https://pubmed.ncbi.nlm.nih.gov/30270045/

262. Poganik JR, Long MJC, Disare MT, Liu X, Chang SH, Hla T, et al. Post-transcriptional regulation of Nrf2-mRNA by the mRNA-binding proteins HuR and AUF1. FASEB J [Internet]. 2019 Dec 1 [cited 2025 Mar 26];33(12):14636–52. Available from: https://pubmed.ncbi.nlm.nih.gov/31665914/

263. Fukuda Y, Pazyra-Murphy MF, Silagi ES, Tasdemir-Yilmaz OE, Li Y, Rose L, et al. Binding and transport of SFPQ-RNA granules by KIF5A/KLC1 motors promotes axon survival. J Cell Biol [Internet]. 2021 Jan 4 [cited 2025 Mar 26];220(1). Available from:

https://pubmed.ncbi.nlm.nih.gov/33284322/

264. Corvaisier M, Zhou J, Malycheva D, Cornella N, Chioureas D, Gustafsson NMS, et al. The γ-tubulin meshwork assists in the recruitment of PCNA to chromatin in mammalian cells. Commun Biol [Internet]. 2021 Dec 1 [cited 2025 Mar 26];4(1). Available from: https://pubmed.ncbi.nlm.nih.gov/34158617/

265. Kim E, Ilic N, Shrestha Y, Zou L, Kamburov A, Zhu C, et al. Systematic Functional Interrogation of Rare Cancer Variants Identifies Oncogenic Alleles. Cancer Discov [Internet]. 2016 Jul 1 [cited 2025 Mar 26];6(7):714–26. Available from: https://pubmed.ncbi.nlm.nih.gov/27147599/

266. Rosenbluh J, Mercer J, Shrestha Y, Oliver R, Tamayo P, Doench JG, et al. Genetic and Proteomic Interrogation of Lower Confidence Candidate Genes Reveals Signaling Networks in β-Catenin-Active Cancers. Cell Syst [Internet]. 2016 Sep 28 [cited 2025 Mar 26];3(3):302-316.e4. Available from: https://pubmed.ncbi.nlm.nih.gov/27684187/

267. Landthaler M, Gaidatzis D, Rothballer A, Chen PY, Soll SJ, Dinic L, et al. Molecular characterization of human Argonaute-containing ribonucleoprotein complexes and their bound target mRNAs. RNA. 2008;

268. McCann JJ, Fleenor DE, Chen J, Lai CH, Bass TE, Kastan MB. Participation of ATM, SMG1, and DDX5 in a DNA Damage-Induced Alternative Splicing Pathway. Radiat Res [Internet]. 2023 Mar 15 [cited 2025 Mar 26];199(4):406–21. Available from: https://pubmed.ncbi.nlm.nih.gov/36921295/

269. Yamauchi T, Nishiyama M, Moroishi T, Yumimoto K, Nakayama KI. MDM2 Mediates Nonproteolytic Polyubiquitylation of the DEAD-Box RNA Helicase DDX24. Mol Cell Biol. 2014;

LIST OF FIGURES

LIST OF TABLES

ANDV	Andes virus
AP-MS	Affinity purification coupled with mass spectrometry
APS	Ammonium persulfate
ATP	Adenosine triphosphate
BNITM	Bernhard-Nocht-Institute for Tropical Medicine
BSL	Biosafety level
BUNV	Bunyamwera virus
C-FLAG	C-terminal FLAG tag
C-StrepII-His	C-terminal StrepII-His tag
CBD	Cap-binding domain
CCNT1	Cyclin T1
Co-IP	Co-immunoprecipitation
CRAPome	Contaminant repository for AP
Cre/loxP	Causes recombination / locus of X-over P1
CRISPR/Cas9	Clustered regularly interspaced short palindromic repeats / CRISPR-associated protein 9
cRNA	Complementary RNA genome
cRNP	Complementary RNP
Cryo-EM	Cryogenic electron microscopy
CTD	C-terminal domain
CV	Column volume
DDX	DEAD-box protein
DDX17 KO cells	DDX17 knockout cells
DDX19	DDX19A
DENV	Dengue virus
DNA	Deoxyribonucleic acid
DTT	1,4-dithiothreitol
E. coli	Escherichia coli
EDTA	Ethylenediaminetetraacetic acid
EIF4E	Eukaryotic initiation factor 4E
EIF4F	Eukaryotic initiation factor 4F
EMA	European Medicines Agency
EMBL	European Molecular Biology Laboratory
EN	Endonuclease
ESCRT	Endosomal sorting complex required for transport
FBS	Fetal bovine serum
FDA	Food and Drug Administration
FFU	Focus forming units
FLAG 407	FLAG tag after amino acid residue 407
FLI	Friedrich Loeffler Institute
FLuc	Firefly Luciferase
FT	Flowthrough
GFP	Green fluorescence protein
GO	Gene Ontology
GP	Glycoprotein
GPC	Glycoprotein precursor
GSPT-1	Eukaryotic peptide chain release factor GTP-binding subunit ERF3A
GST	Glutathione S-transferase
HBV	Hepatitis B virus
HCPS	Hantavirus cardiopulmonary syndrome
HCV	Hepatitis C virus
HEPES	2-Propanol, 4-(2-hydroxyethyl)-1-piperazine ethanesulfonic acid
HEV	Hepatitis E virus
HFRS	Hemorrhagic fever with renal syndrome
HIV	Human immunodeficiency virus
HNRPD	Heterogeneous nuclear ribonucleoprotein D0

HRP	Horseradish peroxidase
HTNV	Hantaan virus
IAV	Influenza A virus
IEC	Ion exchange chromatography
IF	Immunofluorescence
IFA	Immune focus assay
IFN	Interferon
IGR	Intergenic regions
IPTG	Isopropyl-β-D-thiogalacto-pyranoside
iPTM	Interface predicted template modeling
ISG	Interferon stimulated gene
JUNV	Junín virus
KSHV	Kaposi's sarcoma-associated herpesvirus
L	large protein
LASV	Lassa virus
LASV GST-Z	LASV Z with an N-terminal GST tag
LB	Lysogeny broth
LCMV	Lymphocytic choriomeningitis virus
LLPS	Liquid-liquid phase separation
MACV	Machupo virus
MBP	Maltose binding protein
MDA-5	Melanoma differentiation-associated protein 5
MG	Minigenome
min	Minute
miRNA	microRNA
MLO	Membraneless organelle
MOI	Multiplicity of infection
mRNA	Messenger RNA
MW	Molecular weight
N-myc	N-terminal myc tag
NONO	Non-POU domain containing octamer-binding protein
NP	Nucleoprotein
NS	Non-structural protein
NTD	N-terminal domain
Nxf1	Nuclear RNA export factor 1
P-body	Processing body
PA	Acidic polymerase protein
PAE	Predicted aligned error
PB1	Basic polymerase protein 1
PB2	Basic polymerase protein 2
PBS	Phosphate buffered saline
PBST	PBS Tween
PCR	Polymerase chain reaction
PDB	Protein Data Bank
PEI	Branched polyethylenimine
PFU	Plaque forming unit
pLDDT	Predicted local distance difference test
PMSF	Phenylmethylsulfonyl fluoride
pre-mRNA	Precursor mRNA
pTM	Predicted template modeling
RBM10	RNA-binding protein 10
RdRp	RNA-dependent RNA polymerase
RecA	Recombinase A
RIG-I	retinoic acid-inducible gene I
RISC	RNA-induced silencing complex
RKI	Robert Koch Institute
rLASV	Recombinant LASV
rLCMV	Recombinant LCMV
RLR	Rig-I-like receptor
RLU	Relative light units
RLuc	Renilla luciferase
RNA	Ribonucleic acid
RNAi	RNA interference

RNP	Ribonucleoprotein
RSV	Respiratory syncytial virus
RVFV	Rift Valley fever virus
SARS-CoV-2	Severe acute respiratory syndrome coronavirus 2
Scr	Scrambled
SDS	Sodium dodecyl sulphate
SDS-PAGE	SDS polyacrylamide gel electrophoresis
SEC	Size exclusion chromatography
SFPQ	Proline- and glutamine-rich splicing factor
SFTSV	severe fever with thrombocytopenia syndrome virus
SG	Stress granule
shRNA	Small hairpin RNA
siRNA	Small interfering RNA
SN	supernatant
SOC	Super optimal broth with catabolite repression
sRLU	Standardized RLU
SSP	Stable signal peptide
StrepII 407	StrepII tag after residue 407
TAE	Tris-acetate-EDTA
TB	Terrific broth
TCID50	50 % tissue culture infectious dose
TCRV	Tacaribe virus
TEMED	Tetramethylethylenediamine
TRIS	Tris-(hydroxymethyl)-amino methane
TUBG1	Tubulin gamma-1 chain
UTR	Untranslated region
UV	Ultraviolet
vRNA	Viral RNA genome
vRNP	Viral RNP
WB	Western blot
WDR7	WD repeat-containing protein 7
WHO	World Health Organization
WNV	West Nile virus
WT	Wildtype
YFP	Yellow fluorescent protein
Z	Zinc-binding matrix protein
ZAP	Zinc finger antiviral protein
ZIKV	Zika virus

Supplementary Figures

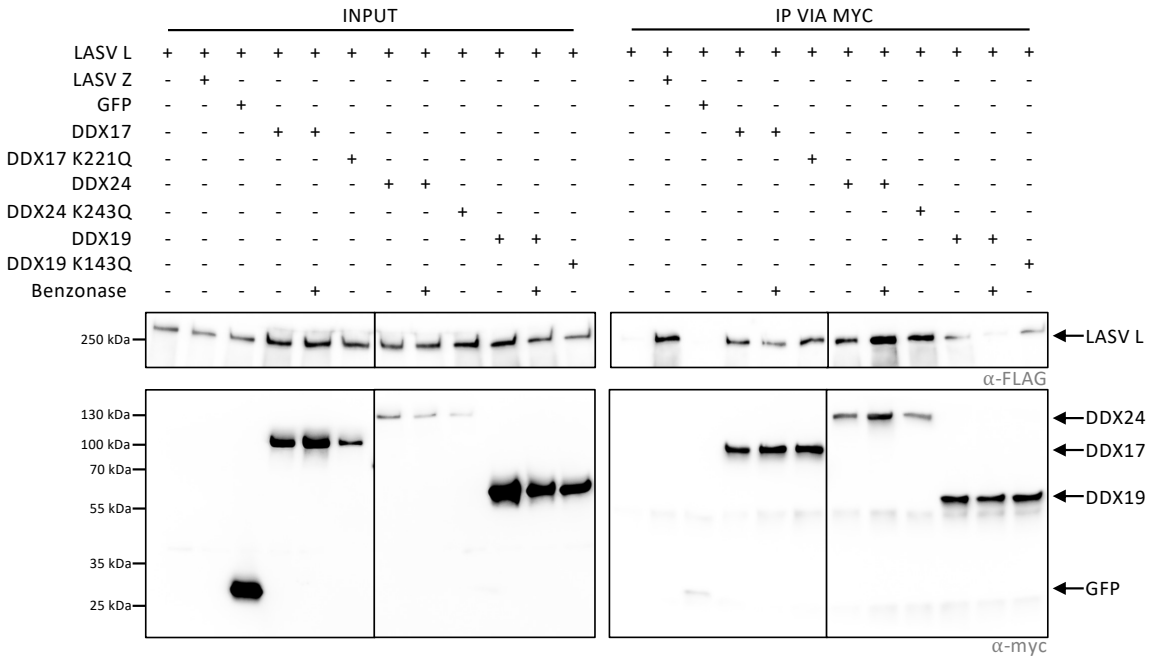

Figure A. 1: Co-IP of DDX17, DDX24, DDX19, and the corresponding ATPase mutants DDX17 K221Q, DDX24 K243Q, and DDX19 K143Q with LASV L with Benzonase treatment. WB analysis of co-IP performed as described in 3.4.10.1. HEK293T cells were transfected with 1 µg LASV L (FLAG 407) and 1 µg DDX, LASV Z or GFP (N-myc) as indicated. 48 h after transfection, cells were lysed with lysis buffer (2.7.2), partially supplemented with 200 U/ml Benzonase and 2 mM $MgCl_2$ as indicated. The insoluble components were removed by centrifugation. The supernatant was incubated with α-myc antibody and protein A sepharose. The sepharose was washed and subsequently eluted with 4x SDS sample buffer. Samples (15 µl) of the supernatant and elution were separated with precast protein gels (BioRad; 15-well; 4 – 15 %) together with 3 µl of Page Ruler Plus protein ladder as a MW marker and blotted according to Section 3.4.8. The membranes were split and stained with HRP-coupled α-FLAG antibody or primary α-myc antibody, followed by secondary HRP-coupled α-mouse antibody. For detection, Clarity (Max) ECL chemiluminescent substrate was applied. Black arrows indicate the bands corresponding to LASV L, DDX17, DDX19, DDX24 and GFP. LASV Z was not detectable in this experiment.

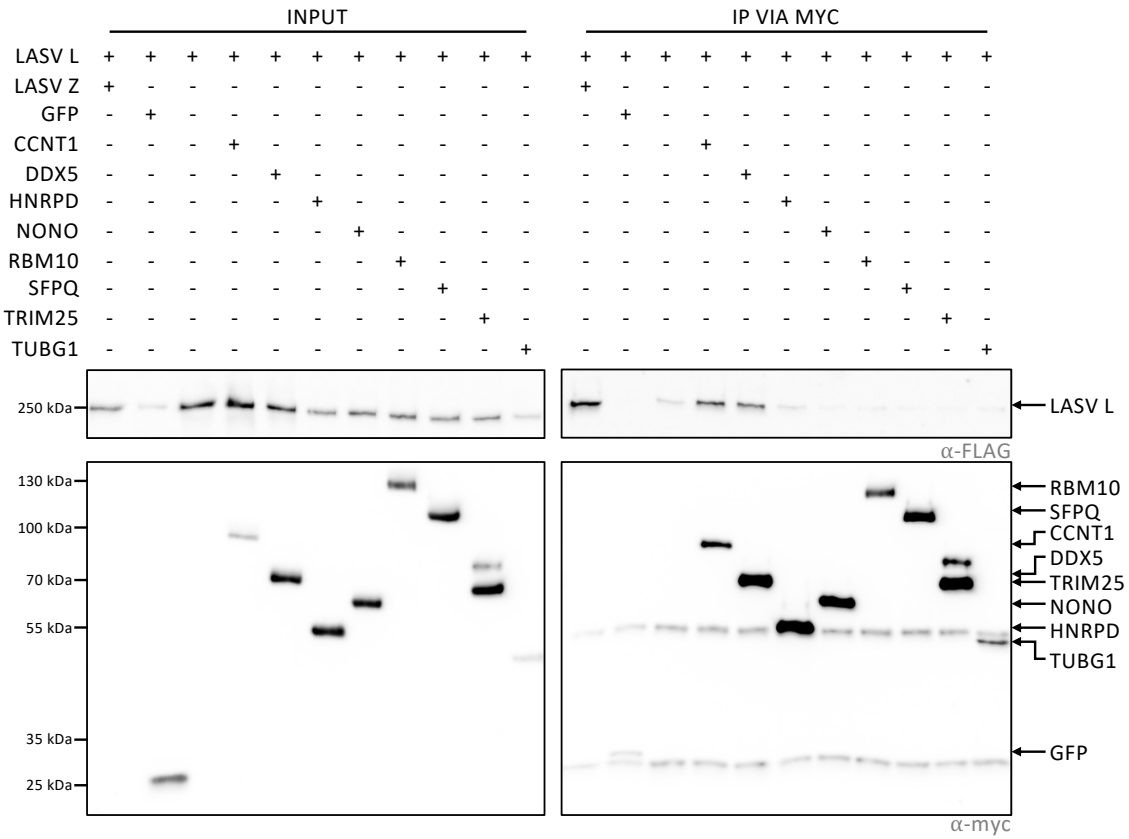

Figure A. 2: Co-IP of CCNT1, DDX5, HNRPD, NONO, RBM10, SFPQ, TRIM25, and TUBG1 with LASV L. WB analysis of co-IP performed as described in 3.4.10.1. HEK293T cells were transfected with 2 µg LASV L (FLAG 407) and 2 µg host protein, LASV Z or GFP (N-myc) as indicated. 48 h after transfection, cells were lysed and the insoluble components were removed by centrifugation. The supernatant was incubated with α-myc antibody and protein A sepharose. The sepharose was washed and subsequently eluted with 4x SDS sample buffer. Samples (15 µl) of the supernatant and elution were separated with 8 % SDS polyacrylamide gels together with 3 µl of Page Ruler Plus protein ladder as a MW marker and blotted according to Section 3.4.8. The membranes were split and stained with HRP-coupled α-FLAG antibody or primary α-myc antibody, followed by secondary HRP-coupled α-mouse antibody. For detection, Clarity (Max) ECL chemiluminescent substrate was applied. Black arrows indicate the bands corresponding to LASV L, CCNT1, DDX5, HNRPD, NONO, RBM10, SFPQ, TRIM25, TUBG1, and GFP. LASV Z was not detectable in this experiment. The data from this figure was generated by Malte Morische.

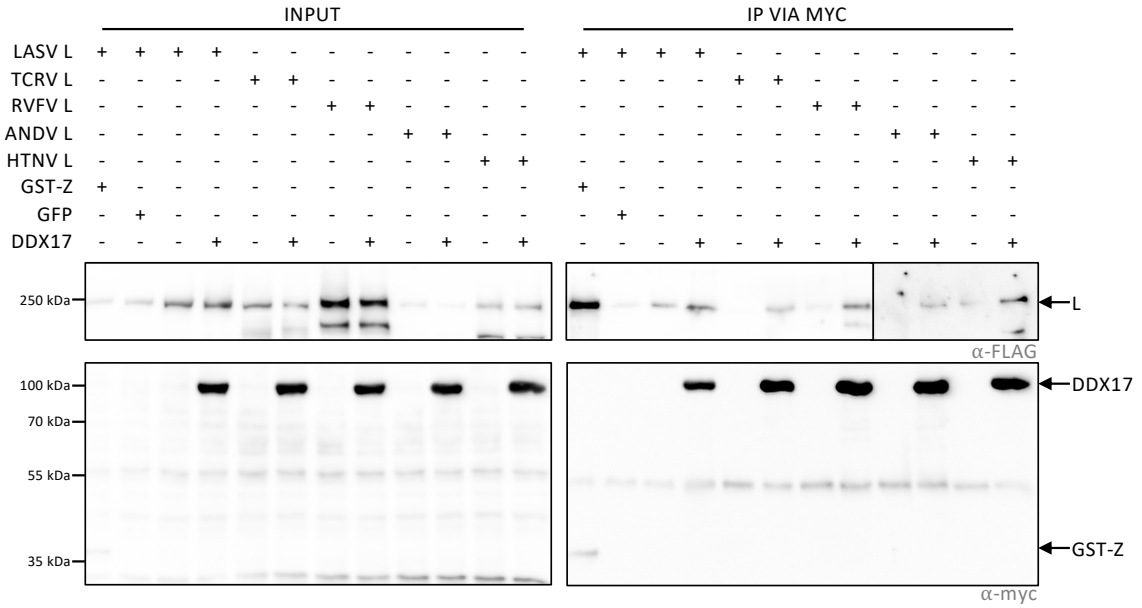

Figure A. 3: Co-IP of DDX17 with LASV L, TCRV L, RVFV L, ANDV L, and HTNV L. WB analysis of co-IP performed as described in 3.4.10.1. HEK293T cells were transfected with 1 µg LASV L (FLAG 407), TCRV L, RVFV L, or 2 µg ANDV L or HTNV L (C-FLAG) and 1 µg DDX17, LASV GST-Z or GFP (N-myc) as indicated. 48 h after transfection, cells were lysed and the insoluble components were removed by centrifugation. The supernatant was incubated with α-myc antibody and protein A sepharose. The sepharose was washed and subsequently eluted with 4x SDS sample buffer. Samples (15 µl) of the supernatant and elution were separated with 8 % SDS polyacrylamide gels together with 3 µl of Page Ruler Plus protein ladder as a MW marker and blotted according to Section 3.4.8. The membranes were split and stained with HRP-coupled α-FLAG antibody or primary α-myc antibody, followed by secondary HRP-coupled α-mouse antibody. For detection, Clarity (Max) ECL chemiluminescent substrate was applied. Black arrows indicate the bands corresponding to L, DDX17, and LASV GST-Z. GFP was not detectable in this experiment as it ran out of the gel during SDS-PAGE.

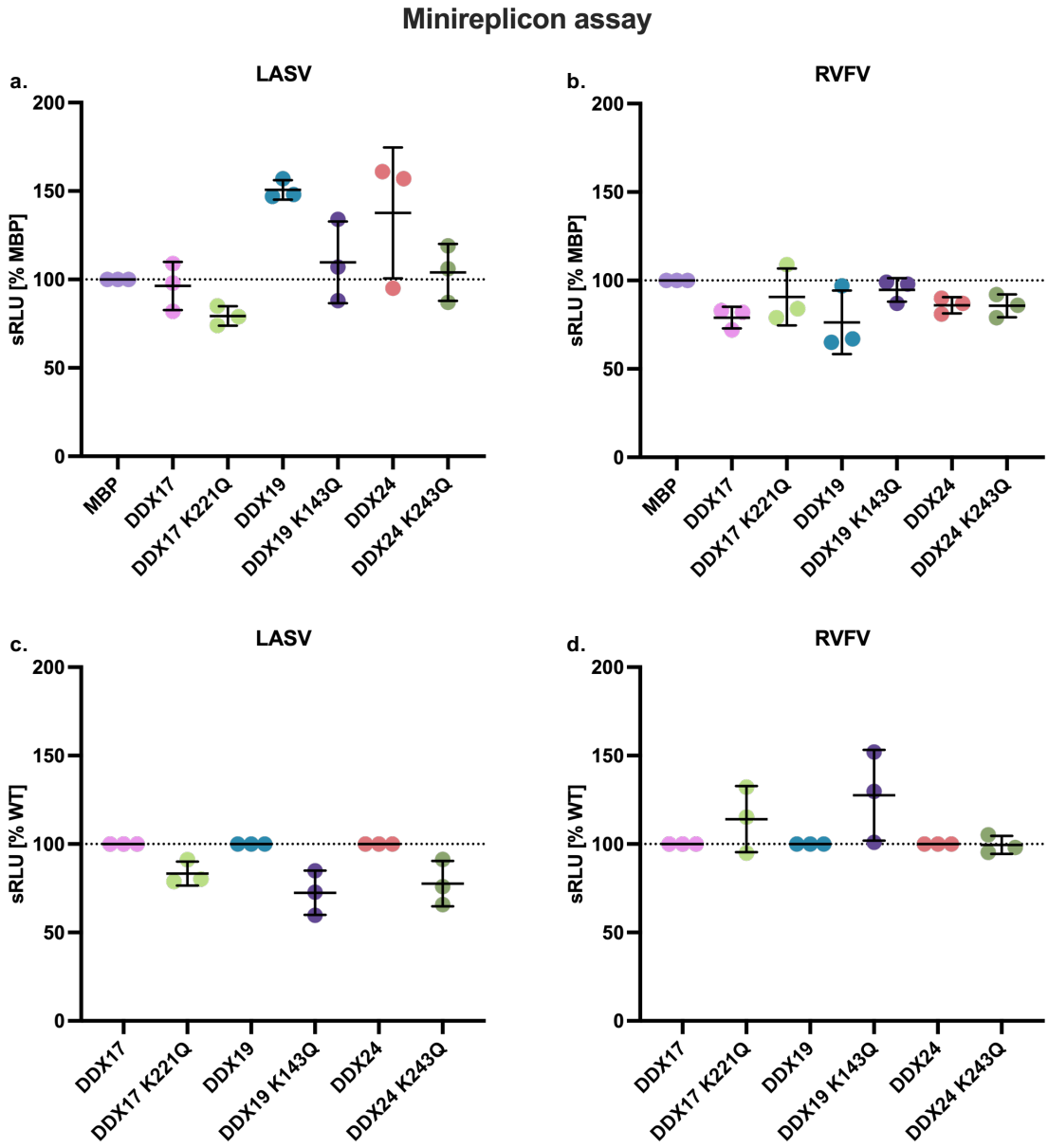

Figure A. 4: Effect of overexpression of DDX17, DDX19, and DDX24 and their respective ATPase mutants on viral transcription and genome replication in the LASV and RVFV minireplicon system. Alternative analysis of the data shown in Figure 14a and b. Huh7 cells were transfected 24 h after seeding with the **a.** LASV minireplicon components or **b.** RVFV minireplicon components together with 250 ng (**a.**) or 100 ng (**b.**) of DDX plasmid (N-myc) according to 3.3.2.1 and 3.4.11. Transfection of an empty vector and MBP (N-myc) served as controls. 48 h after transfection the FLuc and the RLuc activities were measured sequentially with the Dual-Luciferase Reporter Assay System as described in 3.4.11.Rluc activity [RLU] was corrected by dividing by the square root of the FLuc [RLU], resulting in standardized RLU [sRLU]. **a.** and **b.** sRLU were normalized to the MBP control (set to 100 %). **c.** and **d.** sRLU were normalized to the respective wildtype (WT) of the ATPase mutant (set to 100 %). Shown are the individual values, the mean and the standard deviation of three individual experiments.

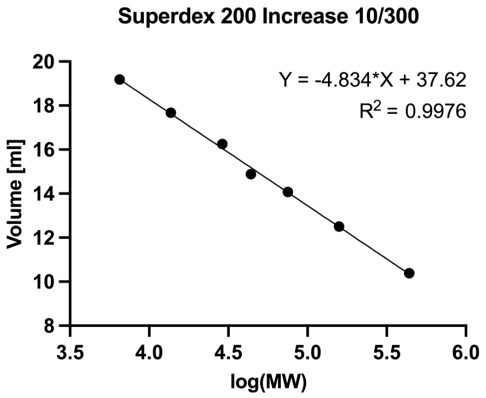

Protein	MW [kDa]	Log(MW)	Volume [ml]
Ferritin	440	5.643	10.38
Aldolase	158	5.199	12.51
Conalbumin	75	4.875	14.07
Ovalbumin	44	4.643	14.88
Carbonic anhydrase	29	4.462	16.25
Ribonuclease A	13.7	4.137	17.67
Aprotinin	6.5	3.813	19.18

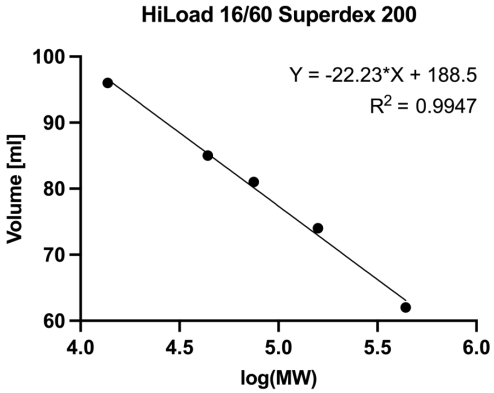

Protein	MW [kDa]	Log(MW)	Volume [ml]
Ferritin	440	5.643	62
Aldolase	158	5.199	74
Conalbumin	75	4.875	81
Ovalbumin	44	4.643	85
Ribonuclease A	13.7	4.137	96

Figure A. 5: Calibration of Superdex 200 Increase 10/300 and HiLoad 16/60 Superdex 200. Graphical presentation of the calibration with indication of the marker protein parameters. The linear dependence of the elution volume on the MW is described by an equation and the coefficient of determination R2 is given below.

Supplementary tables

Table A. 1 List of primers used for cloning.

Name	Sequence (5' to 3')
ANDV_L_C-FLAG_pCAGGS_rev	GGCGCGCCGGCCGGCCGCATGGAAAAGTATAGAGAGATTCATCA
ANDV_L_pCAGGS_fwd	GTCCTTATAGTCTCCGCTCGAGCCATAGAATGTTGATACAGGGTCAC
CCNT1_pDEST_fwd	CCATGGGAACCAATTCAGTAATGGAGGGAGAGAGGAAG
CCNT1_pDEST_rev	GGTCTAGATATCTCGAGTGCTTACTTAGGAAGGGGTGGA
DDX17_K221Q_fwd	GGCTCTGGGCAGACGTTGGCGTATCTCCTGCCTGCAATT
DDX17_K221Q_rev	GCCAACGTCTGCCCAGAGCCAGTCTGAGCAATGCCCA
DDX17_LeGo_rev	CGGAATTTACGTAGC-TCATTTACGTGAAGGAGGAG
DDX17_pDEST_fwd	CCATGGGAACCAATTCAGTAATGCCCACCGGCT
DDX17_pFASTbac_LinkerB_fwd	GGATCTCGGTCCGGCATGCCCACCGGCT
DDX17_pFASTbac_LinkerB_rev	ATGCTTGCCCTCGAGTTTACGTGAAGGAGGAGGA
DDX17.2_pDEST_fwd	CCATGGGAACCAATTCAGTAATGCGCGGAGGAGG
DDX17.2_pDEST_rev	GGTCTAGATATCTCGAGTGCTCATTTACGTGAAGGAGGAGG
DDX17.2_pOPE_fwd	TACAATCAAAGGAGATATACATGCGCGGAGGAG
DDX17.2_pOPINF_fwd	AGTTCTGTTTCAGGGTCCCATGCCCACCGGCTT
DDX17.2_pOPINF_rev	CAAACTGGTCTAGAAAGCTTCATTTACGTGAAGGAGGAGG
DDX17.2_pOPJ_fwd	AAGTTCTGTTTCAGGGCCCGATGCGCGGAGGAG
DDX17.2_pOPJ_rev	TTAAACTGGTCTAGAAAGCTTTTACGTGAAGGAGGAGG
DDX17.c_pDEST_fwd	CCATGGGAACCAATTCAGTAGGTAATCCTGGGGAGC
DDX17.c_pDEST_rev	GGTCTAGATATCTCGAGTGCTTATCCTCTGTGGTCCACAA
DDX19A_K143Q_pDEST_fwd	GGTACTGGTCAAACAGCTGCCTTCGTGCTGGCCAT
DDX19A_K143Q_pDEST_rev	GCAGCTGTTTGACCAGTACCAGACTGAGATTGGGCAATTA
DDX19A_pDEST_fwd	CCATGGGAACCAATTCAGTAATGGCCACCGACTCG
DDX19A_pDEST_rev	GGTCTAGATATCTCGAGTGCTCACTCAATCTCGTCCAAATC
DDX24_ K243Q_pDEST_fwd	GGAAGTGGGCAAACTCTTGCCTTTGCCATCCCAATG

Name	Sequence (5' to 3')
DDX24_ K243Q_pDEST_rev	GCAAGAGTTTGCCCACTTCCTGTCTCAGCAGCCCC
DDX24_LeGO_rev	CGGAATTTACGTAGC-TTAATTTGCACTTGTACTTGGC
DDX24_pDEST_fwd	CCATGGGAACCAATTCAGTAATGAAGTTGAAGGACACAAAATC
DDX24_pDEST_rev	GGTCTAGATATCTCGAGTGCTTAATTTGCACTTGTACTTGGC
DDX24_pFASTbac_LinkerB_fwd	GGATCTCGGTCCGGCATGAAGTTGAAGGACACAAAAT
DDX24_pFASTbac_LinkerB_rev	ATGCTTGCCCTCGAGATTTGCACTTGTACTTGGCT
DDX5_pDEST_fwd	CCATGGGAACCAATTCAGTAATGTCGGGTTATTCGAGTG
DDX5_pDEST_rev	GGTCTAGATATCTCGAGTGCTTATTGGGAATATCCTGTTGG
GDP_pDEST_fwd	CCATGGGAACCAATTCAGTAATGGTGAGCAAGGGC
GFP_pDEST_rev	GGTCTAGATATCTCGAGTGCTTACTTGTACAGCTCGTCCATG
GST-DDX17.2_pOPE_fwd	TACAATCAAAGGAGATATACATGTCCCCTATACTAGGTTATTGG
HNRPD_pDEST_fwd	CCATGGGAACCAATTCAGTAATGTCGGAGGAGCAGTTC
HNRPD_pDEST_rev	GGTCTAGATATCTCGAGTGCTTAGTATGGTTTGTAGCTATTTTGATG
HS_RVFV_L_pCAGGS_fwd	AGGCGGCTCGAGCGGAGACTATAAGGACCATGATGGTG
HS_RVFV_L_pCAGGS_rev	AGGCGGCTCGAGCGGAGACTATAAGGACCATGATGGTG
HTNV_L_C-FLAG_pCAGGS_rev	GTCCTTATAGTCTCCGCTCGAGCCATAGAAAGATGAAATAGAATCCTGTG
HTNV_L_pCAGGS_fwd	GGCGCGCCGGCCGGCCGCATGGATAAATATAGAGAAATTCACAGC
LASV_GST_Z_pDEST_fwd	CCATGGGAACCAATTCAGTAATGTCCCCTATACTAGGTTATTGG
LASV_GST_Z_pDEST_rev	GGTCTAGATATCTCGAGTGCTTAGGGTGTGTATGGCG
LASV_Z_pDEST_fwd	CCATGGGAACCAATTCAGTAATGGGCAACAGGCAGA
LASV_Z_pDEST_rev	GGTCTAGATATCTCGAGTGCTCAGGGGCTGTATGGTG
MBP_pDEST_fwd	CCATGGGAACCAATTCAGTAATGAAAATCGAAGAAGGTAAACTG
MBP_pDEST_rev	GGTCTAGATATCTCGAGTGCTCAAGTCTGCGCGTCTTTCA
myc_LeGO_fwd	GTGTGGTGGTACGGG-ATGGAACAAAAACTTATTTCTGAAG
NONO_pDEST_fwd	CCATGGGAACCAATTCAGTAATGCAGAGTAATAAAACTTTTAACTTG
NONO_pDEST_rev	GGTCTAGATATCTCGAGTGCTTAGTATCGGCGACGTTT

Name	Sequence (5’ to 3’)
RBM10_pDEST_fwd	CCATGGGAACCAATTCAGTAATGGAGTATGAAAGACGTGG
RBM10_pDEST_rev	GGTCTAGATATCTCGAGTGCTCACTGGGCCTCGTT
SFPQ_pDEST_fwd	CCATGGGAACCAATTCAGTAATGTCTCGGGATCGGT
SFPQ_pDEST_rev	GGTCTAGATATCTCGAGTGCCTAAAATCGGGGTTTTTTGT
TCRV_L_C-FLAG_pCAGGS_rev	GTCCTTATAGTCTCCGCTCGAGCCCTCAATGTCCTCCACTGTG
TCRV_L_pCAGGS_fwd	GGCGCGCCGGCCGGCCGCATGGATGAAACTGTGTCTGAA
TRIM25_pDEST_fwd	CCATGGGAACCAATTCAGTAATGGCAGAGCTGTGCC
TRIM25_pDEST_rev	GGTCTAGATATCTCGAGTGCCTACTTGGGGGAGCAGATG
TUBG1_pDEST_fwd	CCATGGGAACCAATTCAGTAATGCCGAGGGAAATCA
TUBG1_pDEST_rev	GGTCTAGATATCTCGAGTGCTCACTGCTCCTGGGTG
VS_RVFV_L_pCAGGS_fwd	GCGCCGGCCGGCCGCGGCCGCATGGATTCTATATTATCAAAACAGC
VS_RVFV_L_pCAGGS_rev	AGTCTCCGCTCGAGCCGCCTAGCATGTCATCCG

Table A. 2 List of plasmids used.

Plasmid name	Source
pFLAGCMV2-EFP	Addgene #12449; Dong-Er Zhang (260)
pcDNA3.1-HA-NONO	Addgene #127655; Nicolas Manel (261)
pET28a His6Flag2AUF1	Addgene #135942; Yimon Aye (262)
HA-SFPQ	Addgene #166959; Rosalind Segal (263)
pGEX2T-TUBG1	Addgene #171967; Maria Alvarado-Kristensson (264)
pNIC28-Bsa4 DDX19A	Addgene #42419; Nicola Burgess-Brown
pDONR223_RBM10_WT	Addgene #81771; J.Boehm, W. Hahn, D. Root (265)
CCNT1_pLX307	Addgene #98328; William Hahn, Sefi Rosenbluh (266)
DDX17 pDEST-myc	Addgene #19876; Thomas Tuschl (267)
DDX5 WT V5	Agggene #199576; Michael Kastan (268)
T7 pCAGGS	BNITM
TCRV L (11573)	BNITM
pRVFV MG (ZH501-BNI)	BNITM, Hanna Jérôme (68)
RVFV L (ZH501-BNI) pCITE	BNITM, Hanna Jérôme (68)
RVFV NP (ZH501-BNI) pCITE	BNITM, Hanna Jérôme (68)
RVFV inactive L mutant D1133N (ZH501-BNI) pCITE	BNITM, Janna Scherf
ANDV L K44A (9717869)	BNITM, Kristina Meier
pFASTbac HTNV L D97L (Q32)	BNITM, Kristina Meier
LASV Z (AV) pOPIN-J	BNITM, Lennart Säger
LASV Inactive L mutant D1331A (Ba366) pCITE	BNITM, Lisa Oestereich
LASV L (Ba366) pCITE	BNITM, Lisa Oestereich
LASV Z (Ba366) pCITE	BNITM, Lisa Oestereich
pCAGGS	BNITM, Lisa Oestereich
eGFP-C2	BNITM, Maria Rosenthal
FLuc pCITE	BNITM, Meike Pahlmann (67)
LASV NP (Ba366) pCITE	BNITM, Meike Pahlmann (67)

Plasmid name	Source
pLAS MG	BNITM, Meike Pahlmann (67)
LASV L (Ba366) C-FLAG pCAGGS	BNITM, Silke Olschewski
LASV L (Ba366) FLAG 407 pCAGGS	BNITM, Silke Olschewski
pFASTBac™HTB	Invitrogen
pcDNA3-FLAG-DDX24	Kyushu University, Keiichi Nakayama (269)
Mission® pLKO.1 DDX17 shRNA TRCN00000287045	Merck
Mission® pLKO.1 DDX24 shRNA TRCN0000050314	Merck
Mission® pLKO.1 non-targeted shRNA SHC016	Merck
pOPIN-E, pOPIN-F, pOPIN-J	Oxford Expression Facility (245)
ANDV L (9717869) C-FLAG pCAGGS	This work
DDX17.2 pOPIN-E	This work
DDX17.2 pOPIN-F	This work
DDX17.2 pOPIN-J	This work
GST-DDX17.2 pOPIN-E	This work
HTNV L D97L (Q32) C-FLAG pCAGGS	This work
LeGO-iG2 Puro+ DDX17	This work
LeGO-iG2 Puro+ DDX24	This work
CCNT1 pDEST-myc	This work
DDX17 K221Q pDEST-myc	This work
DDX17.2 pDEST-myc	This work
DDX17.c pDEST-myc	This work
DDX19A pDEST-myc	This work
DDX19A K143Q pDEST-myc	This work
DDX24 pDEST-myc	This work
DDX24 K243Q pDEST-myc	This work
DDX5 pDEST-myc	This work

Plasmid name	Source
HNRPD pDEST-myc	This work
LASV (AV) GST Z pDEST-myc	This work
LASV (Ba366) Z pDEST-myc	This work
MBP pDEST-myc	This work
NONO pDEST-myc	This work
RBM10 pDEST-myc	This work
SFPQ pDEST-myc	This work
TRIM 25 pDEST-myc	This work
TUBG1 pDEST-myc	This work
DDX17 pFASTbac	This work
DDX24 pFASTbac	This work
RVFV L (ZH501-BNI) C-FLAG pCAGGS	This work
TCRV L (11573) C-FLAG pCAGGS	This work
LeGO-iG2 Puro+	UKE, Kristoffer Riecken
phCMV-vsv-G	UKE, Kristoffer Riecken
pMDLg/pRRE	UKE, Kristoffer Riecken
pRSV-Rev	UKE, Kristoffer Riecken

Table A. 3: Overview of the selected host proteins with details on their appearance in different datasets (indicated with +) and their involvement in the top 20 biological processes.

	Appearance in different datasets											
	CCNT1	DDX17	DDX19	DDX24	DDX5	HNRPD	NONO	RBM10	SFPQ	TRIM25	TUBG1
L	+	+	+	+	+	+	+	+	+	+	+
rLASV						+	+				
KO		+		(+)	(+)		(+)				
rLCMV		+			+	+	+	+	+		
L prox		(+)		(+)	+	(+)	(+)		(+)	(+)	(+)
α-PD	+	+			+			+			+
Chromosome segregation (GO:0007059)	+								+		+
DNA conformation change (GO:0071103)							+		+		
DNA repair (GO:0006281)							+		+	+	
DNA-templated transcription elongation (GO:0006354)	+										
Mitotic Prometaphase (R-HSA-68877)											+
mRNA processing (GO:0006397)	+	+			+	+	+	+	+		
Nuclear transport (GO:0051169)	+		+						+		
Regulation of chromosome organization (GO:0033044)						+			+		
Regulation of mRNA metabolic process (GO:1903311)	+	+			+	+	+	+	+	+	+
Regulation of mRNA processing (GO:0050684)	+	+			+			+	+		
Regulation of translation (GO:0006417)						+					
Ribonucleoprotein complex biogenesis (GO:0022613)		+									

TUBG1	TRIM25	SFPQ	RBM10	NONO	HNRPD	DDX5	DDX24	DDX19	DDX17	CCNT1	
									+	+	Ribosome biogenesis (GO:0042254)
			+		+	+				+	RNA catabolic process (GO:0006401)
	+					+			+		Transport of mature mRNAs from intronless transcript (R-HSA-159234)
+											Vesicle-mediated transport (R-HSA-5653656)
	+					+				+	Viral life cycle (GO:0019058)

L: Identified in AP-MS screens with purified LASV and LCMV L. rLASV: Identified in AP-MS screens with rLASV. KO: Identified in genetic knockout screen. rLCMV: Identified in rLCMV interactome. L prox: Identified in proximity-based AP-MS screen. α-PD: Identified as a high confidence hit in the AlphaPulldown screen of LASV L.

Table A. 4: List of models and scores of the DDX17 and LASV L complex predicted with AlphaFold Multimer.

Model	ipTM + pTM
LASV L (1398 - 1830) and DDX17	0.743
LASV L (1830 - 2217) and DDX17	0.483
LASV L (290 - 1398) and DDX17	0.308
LASV L (196 – 279 + 700 - 1398) and DDX17	0.264
LASV L (700 - 1398) and DDX17	0.260
LASV L (1 – 200) and DDX17	0.249
LASV L (1904 - 2077) and DDX17	0.246
LASV L (290 - 711) and DDX17	0.228

Table A. 5: List of models and scores of the DDX24 and LASV L complex predicted with AlphaFold Multimer.

Model	ipTM + pTM
LASV L (700 - 1398) and DDX24	0.303
LASV L (290 - 1398) and DDX24	0.300
LASV L (1830 - 2217) and DDX24	0.288
LASV L (196 – 279 + 700 - 1398) and DDX24	0.279
LASV L (1 – 200) and DDX24	0.248
LASV L (1398 - 1830) and DDX24	0.244
LASV L (1904 - 2077) and DDX24	0.232
LASV L (290 - 711) and DDX24	0.228

Table A. 6: List of residues of the interaction interface of the AlphaFold Multimer model of the DDX17 and LASV L fragment (1398 – 1830) complex generated by PDBsum.

Type of bond	Residue on LASV L	Residue on DDX17
Hydrogen bond	R1467	R440
Hydrogen bond	R1724	R440
Salt bridge	R1467	D441
Salt bridge	D1724	R439
Non-bonded contact	R1467	R440
Non-bonded contact	F1715	E441
Non-bonded contact	F1717	A415
Non-bonded contact	F1718	P444
Non-bonded contact	Y1725	R439
Non-bonded contact	F1726	R439
Non-bonded contact	F1726	R440
Non-bonded contact	L1728	R440
Non-bonded contact	T1731	R440
Non-bonded contact	L1817	R440
Non-bonded contact	L1817	D441
Non-bonded contact	L1817	G442
Non-bonded contact	R1818	D441
Non-bonded contact	R1818	G442
Non-bonded contact	R1818	W443

EIDESSTATTLICHE ERKLÄRUNG - AFFIDAVIT

Hiermit versichere ich an Eides statt, die vorliegende Dissertationsschrift selbst verfasst und keine anderen als die angegebenen Hilfsmittel und Quellen benutzt zu haben. Sofern im Zuge der Erstellung der vorliegenden Dissertationsschrift generative Künstliche Intelligenz (gKI) basierte elektronische Hilfsmittel verwendet wurden, versichere ich, dass meine eigene Leistung im Vordergrund stand und dass eine vollständige Dokumentation aller verwendeten Hilfsmittel gemäß der Guten wissenschaftlichen Praxis vorliegt. Ich trage die Verantwortung für eventuell durch die gKI generierte fehlerhafte oder verzerrte Inhalte, fehlerhafte Referenzen, Verstöße gegen das Datenschutz- und Urheberrecht oder Plagiate.

Ich versichere, dass dieses gebundene Exemplar der Dissertation und das in elektronischer Form eingereichte Dissertationsexemplar (über den Docata-Upload) und das bei der Fakultät (zuständiges Studienbüro bzw. Promotionsbüro Physik) zur Archivierung eingereichte gedruckte gebundene Exemplar der Dissertationsschrift identisch sind.

I hereby declare and affirm that this doctoral dissertation is my own work and that I have not used any aids and sources other than those indicated. If electronic resources based on generative artificial intelligence (gAI) were used in the course of writing this dissertation, I confirm that my own work was the main and value-adding contribution and that complete documentation of all resources used is available in accordance with good scientific practice. I am responsible for any erroneous or distorted content, incorrect references, violations of data protection and copyright law or plagiarism that may have been generated by the gAI.

I, the undersigned, declare that this bound copy of the dissertation and the dissertation submitted in electronic form (via the Docata upload) and the printed bound copy of the dissertation submitted to the faculty (responsible Academic Office or the Doctoral Office Physics) for archiving are identical.

Hamburg, den 21.05.2025 _____

Selina Karoline Krüger

ACKNOWLEDGEMENTS

First of all, I would like to thank Dr. Maria Rosenthal for giving me the opportunity to pursue my PhD in the Structural Virology group in the Department of Virology at the BNITM. Her professional guidance and personal support throughout this time have been invaluable.

I would also like to thank Prof. Dr. Esther Schnettler for her great support and for reviewing my thesis.

A big thank you goes out to all members of the Virology Department, especially the Structural Virology group, for their help in the lab, their advice, and the great working environment.

A special mention goes to my fellow PhD students Saskia, Janna, Lennart, Kristina, Annika R., Gabriele, and Solvej for making this time so memorable. I would also like to thank Morlin, Carola, Annika K., Kerstin, and Steffi for their invaluable support in the lab, as well as Harry, Dominik, and Claire for their helpful advice. Furthermore, I would like to thank my star interns Malte and Yasmin for their help on my project. Special thanks also go out to Silke for her support and thoughtful feedback from afar.

Thank you to our cooperation partners at the EMBL Heidelberg, Dr. Jan Kosinski and Dingquan Yu, for their bioinformatical support.

Finally, I would like to thank my family and friends, especially Timm, for their endless support, encouragement, and patience. It would not have been possible without you.

And last but not least - a thank you goes out to my dogs, whose companionship helped me stay grounded throughout this journey.